Teesside University

SCHOOL OF COMPUTING, ENGINEERING & DIGITAL TECHNOLOGIES

CONTROLLING EXPOSURE TO HEXAVALENT CHROMIUM IN WELDING FUME

by

VISHAL VATS

A thesis submitted in partial fulfilment of the requirements of Teesside University
for the degree of Doctor of Philosophy

This research was carried out in collaboration with the National Structural Integrity Research Centre (NSIRC) Cambridge and TWI ltd Cambridge

February 2023

Author Declaration

I, Vishal Vats, declare that the work present in this thesis is entirely my own and has at no time, to my knowledge, been submitted for another degree.

Vishal Vats

Acknowledgements

I am beyond thankful for the opportunity to have been guided and supported by my supervisors, Dr Venkatesan V. Krishnan, Geoff Melton, and Prof Meez Islam, during my PhD journey at Teesside University. Their expertise, encouragement, and guidance have been invaluable to me, and my appreciation for their mentorship will never end.

I would also like to extend my heartfelt appreciation to all the technicians and project leaders, especially Sally Day and the welding technicians at TWI, for their insights, support and guidance with welding and collecting fumes. I know that without their help, my research would not have been possible.

I am deeply humbled by the opportunity given to me by Teesside University, TWI Ltd and National Structural Integrity Research Centre (NSIRC) for allowing me to undertake my PhD and for hosting me during my research.

I would like to express my sincere gratitude to Dr Qarib Ullah and Dr Kamal Elyasi Gomari for their help and support throughout my time at Teesside University. I am also thankful to the administrative staff at TWI and NSIRC for their support.

Lastly, I would like to express my deepest appreciation and love to my father, mother, sister, and my loving fiancé Surabhi. Their unwavering support and belief in me have been an invaluable source of motivation and inspiration. This PhD is dedicated to them, with my heartfelt thanks.

Vishal Vats

Abstract

Classified as an Occupational Hazard, welding fumes pose a threat due to the presence of Cr(VI), a known carcinogen. To effectively address this issue, it's crucial to comprehend the elemental form and mechanism of Cr(VI) formation in welding fumes. In this research, the formation of Cr(VI) in welding fumes was studied to understand the potential health hazards it poses to welders. FTIR was utilized to identify Cr(VI) species by analysing the vibrational peaks of various bonds in the compounds. FTIR proved useful in identifying Cr(VI) compounds by detecting the anti-symmetric vibrations of Cr-O-Cr, the symmetric stretching of CrO_4 tetrahedra, and the stretching vibrations of the planar CrO_3 structure of chromium trioxide. However, the study in quantifying the amount of Cr(VI) in welding fumes using FTIR and electrochemistry required further refinement and will be part of ongoing research.

As part of another study, in order to understand the mechanism of Cr(VI) formation in welding fumes using shielding gases, the composition of Cr(VI) in welding fumes was found to depend on the type of shielding gas used. The oxidation index of the shielding gas played a crucial role, with the lowest levels of Cr(VI) observed when using argon. Other important factors included the arc stability and ionization potential of the shielding gas. The combination of CO_2 and O_2 was found to provide the most stable arc and the lowest levels of Cr(VI), despite having the highest oxygen index. It was also observed that fluxes containing Alkali metals (Na, K, in particular) had the highest propensity for forming Cr(VI) fumes; in cases where Cr(VI) concentrations were very less, the K, Na levels were very less in the fumes, but were detected in the welding slag.

The main scope of this study is to enhance the knowledge of Chromium (VI) in welding fumes by addressing the problems in Chromium (VI) analysis, investigating the chemical forms of Chromium (VI) in different welding fumes, identifying factors affecting Chromium (VI) formation in welding fumes, and discussing the mitigation methods of Chromium (VI) in welding fumes.

Contents

List of figures

List of tables

List of abbreviations and/or acronyms

As Low as Reasonably Practicable	ALARP
Attenuated Total Reflectance	ATR
Cyclic Voltammetry	CV
Contact Tip to Work Distance	CTWD
Diphenyl Carbazide	DPC
Deoxyribonucleic Acid	DNA
Energy- Dispersive X-Ray	EDX
Field Emission Gun Scanning Electron Microscope	FEG-SEM
Flux-Cored Arc Welding	FCAW
Fourier Transform Infrared Spectroscopy	FTIR
Fume Formation Rate	FFR
Health and Safety Executives	HSE
Hexavalent Chromium	Cr (VI)
Inductively Coupled Plasma -Mass Spectroscopy	ICP-MS
Infrared Red	IR
International Agency for Research on Cancer	IARC
International Institute of Welding	IIW
International Organization for Standardization	ISO
Ion Chromatography	IC
Local Exhaust Ventilation	LEV

Manual Metal Arc Welding	MMA
Metal Inert/Active Gas Welding	MIG/ MAG
Partial Least Squares	PLS
Personal Protective Equipment	PPE
Principal Component Analysis	PCA
Respiratory Protective Equipment	RPE
Scanning Electron Microscopy	SEM
Short Term Exposure Limits	STEL
Standard Calomel Electrode	SCE
Stainless Steel	SS
Time Weighted Average	TWA
Tungsten Inert Gas Arc Welding	TIG
Ultraviolet	UV
Workplace Exposure Limits	WEL
X-Ray Diffraction	XRD

List of symbols

K	Kelvin
C	Celsius
°	Degree
V	Volts
A	Amps
%	Percentage
Nm	Nanometre
Mm	Micrometre
D	Diameter
mm	Millimetre
min	Minutes
Mg	Milligram
M	Meters
Cm	Centimetre
Nm	Nanometre
A_{Si}	Absorbance intensity of silica
A_{Cr}	Absorbance intensity of Cr (VI)
Λ	concentration constant
mA	Milliamps

R	Pearson’s correlation coefficients
V_d	Volume of drop
V_w	Wire velocity
P	Pressure
P	Density
F	Force

Other symbols are explained in the thesis where they are mentioned.

Chapter I : Introduction

Arc welding is a widely used method among all welding processes for metal fabrication. Many welders still prefer arc welding for certain mass production applications because it is more versatile and requires simpler equipment. While, arc welding has also witnessed the recent introduction of robots, most of the arc-welding is performed manually, which, in turn, poses significant health and safety risks to a large number of workers in various industries. Hazards associated with welding include intense heat, light, ultraviolet radiation, risk of fire and electrocution, and exposure to toxic or asphyxiating gases and particulate fumes and electromagnetic fields. The use of Personal Protective Equipment (PPE) such as gauntlets, appropriate clothing, and face shields can minimize the effects of heat, light, and ultraviolet radiation and reduce the risk of fires and electrocution. However, protecting welders from exposure to gases and respirable fumes is more challenging.

Occupational safety and health are crucial issue in the modern world, and exposure to hazardous chemicals, asbestos, painting solvents, gases, fumes, or other risks in confined spaces is a significant concern. Industrial processes such as welding, thermal spraying, casting, chemical manufacturing, and fossil fuel combustion generate a significant number of fumes and dust particles, which can contain contributions from multiple sources such as:

(a) vaporization of the wire, rod, or metallic/ alloying coatings. This can occur when the heat from the welding arc causes the metal to vaporize and release fumes into the air.

(b) decomposition and vaporization of the flux materials. The flux materials used in some welding processes can also release fumes when heated and decomposed.

(c) spatter from the arc region and weld pool. During the welding process, small droplets of molten metal can be expelled from the weld pool, creating spatter that can release fumes.

(d) evaporation from the molten weld metal. As the weld metal cools, it can release fumes through evaporation.

The impact of welding fumes on human health is extremely dangerous. Welding fumes are classified as carcinogens and pose significant hazards to workers who are exposed to them. Exposure to these welding fumes can lead to various health hazards, including the development of occupational asthma, cancer, respiratory tract irritation, metal fume fever, and pneumonia. According to the Health and Safety Executive (HSE), the national regulator for workplace

health and safety in Britain, new scientific evidence has emerged showing that exposure to all types of welding fumes, including mild steel welding fumes, can cause lung cancer. Additionally, there is limited evidence linking welding fumes to kidney cancer.

The legal limits for exposure to welding fumes and their constituents are clearly defined by Workplace Exposure Limits (WELs) and Short-Term Exposure Limits (STELs) and should not be exceeded. Due to the classification of all welding fumes as carcinogenic, exposure to them should be reduced as much as is reasonably possible. It's worth noting that there is no single WEL for welding fumes, as welding fumes can contain various different metal oxide compounds and gases. The Health and Safety Executive (HSE) document EH40 outlines the WELs for the various metal, metalloid compounds and gases that can be found in welding fumes. Employers are responsible for ensuring that the exposure of their employees to welding fumes does not exceed these limits and that the appropriate control measures are in place to protect their health. Exposure limits of different gases and elements generated during welding is shown in table no 1.1.

Substance	**WEL**	**Notes**
Aluminium fume particles	10 mg/m^3	Aluminium metal and oxides have both inhalable and respirable WEL of 10 mg/m^3inhalable and 4 respirable (most applicable to welding fumes).
Chromium fume particles	0.5 mg/m^3	
Iron (as oxides of Iron)	4 mg/m^3 10 mg/m^3 STEL	10 inhalable and 4 respirable
Manganese - Inhalable Fraction - Respirable Fraction	 0.2 mg/m^3 0.05 mg/m^3	
Titanium (as TiO_2)	10 mg/m^3	
Nitrogen Oxide	2.5 mg/m^3	
Nitrogen Dioxide	0.955 mg/m^3, 1.91 mg/m^3 STEL	
Copper fumes particles	0.2 mg/m^3	
Nickel fume particles	0.1 mg/m^3 soluble Ni compounds	In welding fumes, it is assumed most of them are insoluble.

	0.5mg/m3 insoluble Ni Compounds	
Ozone	0.4 mg/m^3 STEL	
Chromium VI (process generated e.g.: During welding)	0.025 mg/m^3	

Table 1.1 : Exposure limits of different gases and elements generated during welding. (HSE document EH40)

The WELs are based on an average 8-hour Time Weighted Average (TWA) of exposure. This means that for workers who are carrying out welding, it is possible that they may be exposed to a short-term, moderately high concentration of fumes, but when averaged over an 8-hour shift, the exposure is considered low. However, some substances have Short-Term Exposure Limits (STELs) that must not be exceeded over a 15-minute period, regardless of the 8-hour TWA. This is to ensure that workers are not exposed to dangerous, immediately harmful concentrations of certain substances. It is important to note that The STEL values shall not be exceeded any time during the working day. Exposure above Threshold limit value (TLV) up to the STEL should be less than 15 minutes and should occur no more than 4 times a day and there should be at least 60 minutes between successive exposures in this range. Employers should monitor the workers' exposure to welding fumes to ensure that the 8-hour TWA and STELs are not exceeded and take appropriate control measures if required. Welding fumes are a complex mixture of airborne gases and fine particles, including Nitrous Oxide, Ozone, metals (such as Chromium, Iron, Zinc, Aluminium, Sodium, and Potassium). Among these, Chromium (VI) is a known carcinogen commonly found in welding fumes generated from the welding of stainless steels. The amount of exposure to Chromium (VI) is related to the generation of fumes, which in turn, depends on the type of welding and the process conditions. Therefore, it is crucial to accurately analyse the composition of welding fumes and closely monitor the exposure of welders to the fumes and its component Chromium (VI).

Due to health concerns, the exposure limit for Chromium (VI) is regularly revised and regulated by governing bodies. The EU, USA, and UK have stringent exposure limits in place, but some countries still do not have strict reduced limits in force, or none at all. Currently, in the UK, the exposure limit for process generated hexavalent chromium is 0.025 mg/m^3 for the 8-hour time-

weighted average (TWA) exposure and it is proposed to further reduce it to 0.005 mg/m3 after 2025. As a result of these regulations, there is a need to understand the Chromium (VI) chemistry and the different forms that exist in welding fumes in order to facilitate mitigation and compliance.

The main scope of this thesis is to enhance the knowledge of Chromium (VI) in welding fumes by addressing the problems in Chromium (VI) analysis, investigating the chemical forms of Chromium (VI) in different welding fumes, identifying factors affecting Chromium (VI) formation in welding fumes, and discussing the mitigation methods of Chromium (VI) in welding fumes. The thesis is organized and divided into the following 8 chapters.

- **Chapter I :** an introduction to the thesis.
- **Chapter II :** an introduction to arc welding, welding fumes, the process of welding fume generation during welding, health effects of welding fumes and Cr(VI) generation in welding fumes along with literature review.
- **Chapter III :** the methodology of welding fumes collection and sampling.
- **Chapter IV :** an in-depth look at the problems in analytical methods of Cr(VI) measurements and discussing the role of FTIR to address these problems and developing FTIR for a convenient tool for detecting and identifying airborne Cr(VI) compounds arising from arc welding.
- **Chapter V :** exploring possibilities of developing FTIR and Electrochemical analysis for quantification of Cr(VI) in welding fumes.
- **Chapter VI :** an in-depth study and discussion of the role of shielding gases in Cr(VI) generation in MIG/MAG and FCAW welding.
- **Chapter VII :** mathematical approaches to describing fume formation during welding.
- **Chapter VIII :** the main conclusions from the thesis.

Chapter II : Literature Review

2.1 Introduction to Welding

Welding is a technique that combines materials by applying heat, pressure, or a combination of both, to create a connection. It is commonly used to join metal and thermoplastics but can also be used to join wood. There are over 80 different types of welding processes, including Manual Metal Arc welding (MMA or SMAW), Metal Inert/Active Gas welding (MIG/MAG), Tungsten Inert Gas arc welding (TIG), and Flux-Cored Arc Welding (FCAW)[1]. Different type of welding processes is shown in detail in fig 2.1.

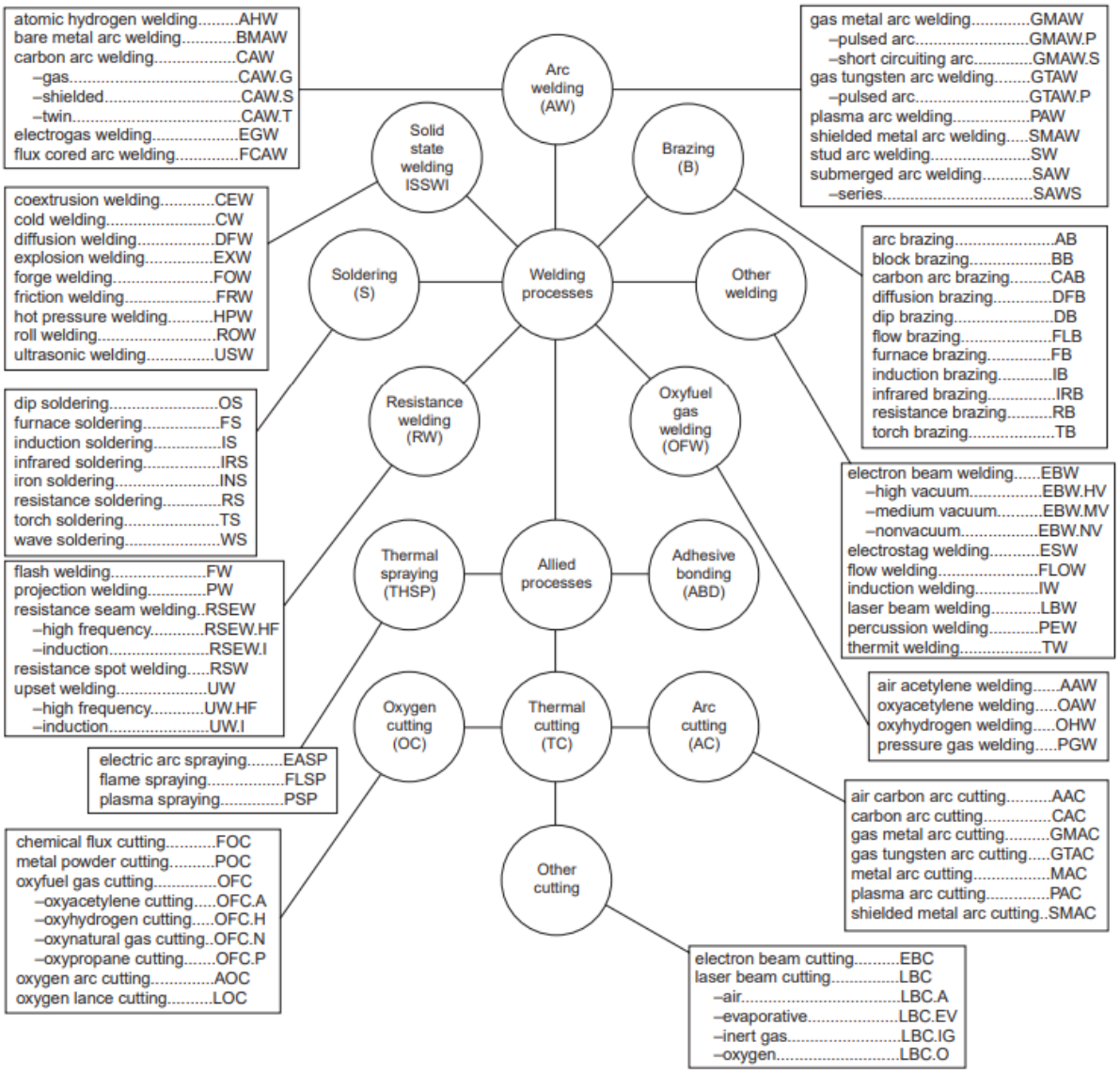

Figure 2.1 : Welding and Allied processes (From: Welding science and technology by M Ibrahim Khan) [1]

2.1.1 Arc Welding Processes

Electric arc welding is a process in which an electric arc is used to join metals together. The arc generates high heat to melt the metal at the point of welding, and a filler metal is added to the molten area to create the weld. This area is known as the weld pool. Electric arc welding can be divided into two categories: those that use consumable electrodes and those that use non-consumable electrodes. Tungsten Inert Gas (TIG) welding is an example of arc welding that uses a non-consumable electrode. In this process, the tungsten is the cathode and the base plate or metal piece to be welded is the anode of the arc. To prevent oxidation, which can weaken the weld strength, the arc column and weld pool are bathed in an inert gas such as argon, which is passed through a welding gun and flows down the tungsten rod.

Consumable electrode processes can be divided into two main categories: Manual Metal Arc (MMA) and Metal Inert Gas/ Metal Active Gas (MIG/MAG). MMA welding is a process in which a flux-coated metal stick is used as one electrode and the base plate is the other electrode. The polarity of the electrodes in this case typically depends on the type of metal to be welded. In this case, the metal stick acts as a consumable as it melts and serves as the filler metal. The flux, which is coated around the metal stick, becomes molten and floats over the weld, forming a bead that protects the weld from contamination and oxidation. These fluxes, in flux-coated wires and flux-cored wires, also contain compounds that melt to provide a shield between the molten metal and the atmosphere by releasing gases such as CO_2. Fluxes also offer other advantages such as improving the electrical properties of the wire, improving the mechanical properties of the weld, and increasing deposition rates [2]. Figure (2.2) shows the typical schematic of a Manual Metal Arc (MMA) welding process.

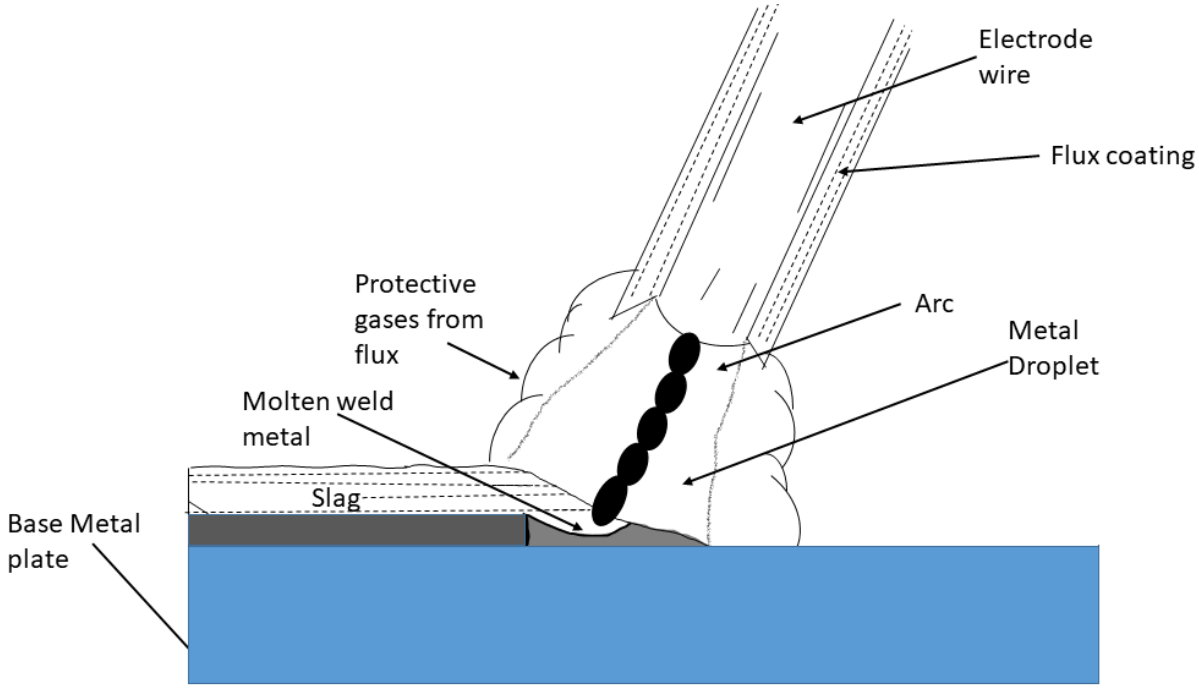

Figure 2.2 : Schematic of a Manual Metal Arc (MMA) welding process

The Metal Inert Gas/Metal Active Gas (MIG/MAG) process is an automated process that uses a continuously fed wire as one electrode and the base plate as the other electrode. The wire is fed from the reel into the welding torch and is shielded by either an inert gas, such as argon, or an active gas, such as CO_2 or O_2. The wire is fed continuously, and the arc is struck between the base plate and the wire. The wire and base plate melt and form a weld pool that is protected by the shielding gases coming from the welding torch along with the wire. The consumable wire can be either solid metal or hollow metal filled with fluxes. The wires filled with fluxes can sometimes be used without the shielding gases.

2.2 Electric Arc Physics

An arc is defined by Milner et al. as the result of passage of electricity through a gas between two electrodes [3]. When an electric current is passed through a gas between two electrodes the arc is formed. When the arc is formed the electrons are generated at cathode and they move towards the anode by the applied electric field to gain energy. Part of their energy is lost during this phenomenon by the collision with the atoms or molecules of the gas in the arc column. Due to this collision and energy loss the temperature of the gas raises between 5,000-50,000

K, at which the thermal ionisation of atoms, and or dissociation and ionisation of the molecules occurs.

In 1954 Busz conducted some experiments to measure the temperature in front of the cathode of the argon arc and it was to be around 30,000°C [4]. At this temperature they estimated the collision frequency to be $4x10^{11}$/sec, and the electron mean free path length to be $3x10^{-4}$cm. Milner in 1960 concluded from his research that the temperature of the welding arcs is considerably higher than the required temperature for welding. [3].

Due to the cooling effects of the electrodes, the gas does not exist at high temperatures in the immediate vicinity of the electrodes. In order to maintain a high current, a high potential drop is required between the anode and cathode regions. The electrons in the column flow from the cathode to the anode, but as they approach the anode, the temperature decreases and therefore the density of the positive ions (which are produced by thermal ionization) also decreases. This creates an anode potential drop due to the negatively charged space. Under these conditions of the potential drop between the anode and cathode, the electrons accelerate, resulting in gaining kinetic energy which is later lost by collision with the anode. The ions travel towards the cathode similarly by gaining kinetic energy, until they collide with the cathode surface where they become neutralized and give up their energy of recombination.

2.2.1 Electric Arc Physics in welding and Arc Temperature

In an electric arc, the currents are several hundred amperes and the potential difference between the electrodes is just a few tens of volts. At this small voltage, it's difficult to strike an arc spontaneously if there is a gap between the electrodes. To overcome this, the electrodes are brought into contact with each other to cause local electrical resistance heating. Then, upon separation of the electrodes, a spark is generated which is a self-sufficient arc if the power input is sufficient to cause thermal ionization of the gas in the arc column. After this, the arc physics is similar: the electrons are generated and then they accelerate and collide, resulting in a high arc temperature.

The arc conditions and the electrode material govern the mechanism of electron emission. For non-consumable electrodes such as tungsten electrode, the electron emissions are thermionic which is provided by the counter-flowing positive electrons upon neutralisation[5]. For

consumable electrodes such as stainless steel electrodes, the electrons are emitted as a result of the intense electric field which is in result of the cathode drop at the electrode surface [5].

The temperature of the unconstructed arc depends highly on the nature of the gases in the arc column. In free burning, unconstructed arcs of pure argon, the column temperatures reaches between approximate value of 8000-22000K [6]. In welding arc which contains large quantities of evaporated metal, the temperatures are found to be considerably low [5]. The core arc temperatures of the pure alkali metal vapour is reported to be around 4000K and for transition metal vapour arc to be around 6000K [5]. However, research conducted by Acinger et al. shows the temperature for MIG welding arc with Iron electrodes and argon shielding gas to be around 8000 K. They also found that the arc column consists of only 10% metal vapours [7]. It was also reported that the arc temperatures near the electrodes were lowered due to conductive heat loss to the metal [7].

Alloys of iron such as stainless steels contain relatively volatile elements such as manganese and chromium. Due to this, the arc of stainless steel MIG welding will contains more metal vapours at lower temperatures. Howden estimated the anode temperature of the TIG arc to be approximately at 2500K [8]. However, his research concluded that the rate of metal evaporation from the anode surface was consistent with the surface temperature close to metal melting point, which in case of iron is 3,135K [9].

2.2.2 Components of the electric arc

- **Heat Transfer**: Heat transfer during welding occurs in and electric arc. Electric arc is used to provide heat to both the workpiece and the electrode in order to form a weld pool. This heat is supplied in two ways: Firstly, by conduction and convection from the arc column and secondly, by condensation of the stream of electrons entering from the anode.

- **Mass Transfer**: The arc is also an area for mass transfer as in welding arc chemical reactions between the high temperature gases of the arc atmosphere, the molten metal droplets and weld pool occurs. These reactions form the main components of the welding fumes.

- **Metal Transfer**: The molten metal droplet travels through the arc column and forms the weld pool, this occurs in electric arc and contributes to fume formation.

- **Arc stability:** The maintenance of a continuous arc of constant size and characteristics is required to get a good weld. The stability of the arc has a significant effect on the formation of fumes.

2.2.3 Electromagnetic forces in electric arc

When the electric current is passed along the arc column during welding, it generates an electric field, which causes the phenomenon of force generation upon the moving charge carriers (electrons and ions) towards the axis of the column. As a result of this 'magnetic pinch' (magnetic force), the gas pressure at the centre of arc column increases by an amount inversely proportional to the cross-sectional area of the arc. Milner et al, calculated that the pressure increase of 900 pascal for 200amps current flowing through an arc of 2.4mm diameter[3]. These electromagnetic forces determine the shape of the arc. With a small diameter electrode, of either polarity forms a conical shape arc, unless the electrode spot on the workpiece is very small. These electromagnetic forces directed along the arc axis in the direction of increasing cross-sectional area are called as Lorentz forces.

These electromagnetic forces may introduce a very high jet flow resulting in arc plasma, which are responsible for majority of the heat transfer to the workpiece [10] and also the important force in the metal transfer from consumable electrode to the work piece [11].

2.4 Metal transfer in consumable electrode welding

The way of transferring the molten metal from the consumable to the work piece is called as the metal transfer mode and this can determine the suitability of the process for metal fabrication. The transfer of the molten metal is determined by various factors, such as the surface tension, gravity, electromagnetic and hydrodynamic forces[8, 12, 13]. When a droplet is formed at the tip of the consumable, it is held in position by the surface tension. In case of vertically positioned electrode over the weld pool, and if the hydrodynamic forces and the electromagnetic forces at the tip of electrode are very week(as in case of low currents), then

the droplet continues to grow until the gravity overcomes the surface tension ,causing the droplet to detach from the consumable tip and deposit at the weld pool[14]. At this point, a short circuit occurs, extinguishes the arc. The electromagnetic forces come into effect after the droplet is detached, drawing it into the weld pool. This detachment causes the arc to restrike, and the cycle is repeated again. A Plasma jet may also exert force on the droplet, whether it is attached or in free flight in the arc column[5]. There are mainly three modes of metal transfer.

- Dip transfer
- Globular transfer
- Spray transfer

2.4.1 Dip transfer

Dip transfer is observed at lower voltage ranges, typically around 12-16 volts, depending on the electrode wire type and size[15]. Dip transfer is characterized by alternating periods of arcing and short-circuiting, which is explained in the above paragraph[13]. When the droplet appears to dip into the weld pool, the arc extinguishes, which results in the evaporation of the heated wires and weld pool[15]. The vapours generated during this time are rich in volatile elements of the weld. When the short circuit breaks and the arc strikes, it leads to an increase in temperature and thus resulting in increased vaporization from the electrodes and from the droplet in the arc column. The process of alternating short-circuiting and arcing is observed many times per second. At high voltages, dip transfer tends to slow down and eventually, globular transfer is observed[15].

2.4.2 Globular transfer

Globular transfer is typically observed at higher voltage than dip transfer. It is characterized by an increase in spatter rate and arc time[15]. During globular transfer, the melting of wire is observed in the welding arc, forming a droplet, which grows in size as the wire is fed in. When the size of the droplet becomes very large, the force of gravity becomes sufficient to detach the droplet, and the droplet falls into the weld pool due to its size and gravitational force. Fractioned vapours are formed by the evaporation of elements from the wire tip, weld pool, and the droplets in the arc[16]. Unfractionated vapours are generated from the vaporization at the base of the arc and from explosive vaporization at the neck of the droplet as it detaches[15]. This explosion accounts for a large amount of spatter formation when the droplet detaches itself.

Spatter can contribute to a large amount of fumes, which can be even more if oxidizing shielding gases such as CO_2 are used [17].

2.4.3 Spray Transfer

Spray transfer is observed at much higher voltages than both globular and dip transfer. It is usually observed at 30-32 volts[15]. In spray transfer, there is little or no short-circuiting of the arc. The size of the droplets in spray is very tiny and they are accelerated axially from the tip of the welding wire to the weld pool[18]. Spray transfer observes very small amounts of spatter, as a result, most of the fumes are produced within the arc region[15]. In spray transfer, the fumes may contain large amounts of more volatile components such as chromium and manganese relative to less volatile components such as iron, nickel, and molybdenum due to the fact that in spray transfer, the detachment of the metal droplet is less volatile, and a reduced level of spatter formation occurs compared to other transfer modes[16].

2.5 The Hazards of Welding [19]

- Electrical burns and electrocution due to high electric currents during welding.
- Risk of fire due to high temperatures and electrical faults.
- Risk of burns due to exposure to high temperatures of the weld and the spatter particles.
- Exposure to ultraviolet, infrared, and visible radiations
- Heat stress problems due to heavy PPEs to protect from high temperatures.
- Exposure of toxic gases such as ozone and nitrous oxides produced during welding.
- Exposure to welding fumes.
- Exposure to electromagnetic fields (EMF) due to the high currents generated by a power source flowing through a power cable into your torch and electrode.

During welding, Personal Protective Equipment (PPEs) such as masks, eye shields, and protective clothing are very effective in protecting against radiation, burns, and hot metals. Hazards from electrocution are minimized by the safe design of welding equipment and training. However, protecting welders from exposure to fumes and gases remains challenging, even with the use of local exhaust ventilation (LEVs) and masks. There are several ways to reduce this risk, such as.

- **Automation or robots:** The best way to protect welders from exposure to fumes is by using automation and robotic arms. However, this process cannot be widely implemented due to higher production costs and the fact that complicated structures cannot be welded using this method.

- **Welding enclosures**: In some cases, welders can carry out welding inside a glove box or other enclosure device to protect themselves from exposure to fumes and gases. This process has some drawbacks, such as reduced ease of working and slower speed, and is generally limited to small welding tasks.

- **Respiratory protective equipment:** The most widely accepted and used method in industry to protect welders from fumes and gases is the use of respiratory protective equipment (RPE). RPE filters out contaminants from the air before it is breathed in by welders or by supplying fresh air from outside the contaminated area. However, these types of equipment can be uncomfortable to wear and restrictive in movement.

- **General ventilation :** General ventilation of welding workshops to control the overall concentrations of fume. This method does very little to none to control the concentrations of fume around welders breathing zone.

- **Local exhaust ventilation (LEVs)** : LEVs installed in the welding bays can be used to control fume at source. However, protection from the use of LEVs highly depends on the positioning of the welding operations. This can restrict the work and in some cases is impractical, particularly when welding in confined spaces.

- **Process modification**: the best way of controlling exposure of welding fumes is by process modification, this requires understanding of the mechanism of fume formation and requires knowledge of the factors that governs the rate of fume formation and the composition of fumes.

2.5.1 Emissions from the Arc welding process and their effects

During arc welding we observe lot of different types of emissions[19]. They are the results of high arc temperature and the arc column. Major emissions from arc welding processes are shown in Table 2.1

Emissions	Type	Origin
Radiation	UV	Arc column
	Visible	
	Infrared	
Gases	NO_x	Reaction between heat and atmosphere
	O_3	Reaction of O2 with UV
	Co_x	Reaction of shielding gases because of high temperatures
Fumes	Metal oxides including: Cr, Cr(VI), Ni, Fe,	Approximately 90% welding wires and 10% base plate(depends on weld conditions electrode materials
	Chromates, Dichromates, Carbonates, Fluorides	Fluxes of the electrodes

Table 2.1 : The health hazards associated with welding radiations, gases, and fumes.

2.5.2 Effects of radiations

The non-ionising electromagnetic radiations emitted during the welding process can damage the eyes and skin of the welders. These are produced in the ultra-violet, visible and infrared regions of the spectra. To protect welders from this harmful radiation welders should use protective face shields and protective clothing during welding[19].

UV rays radiation exposure is known for causing ‘arc welders flash’ disease which is characterised by conjunctivitis and keratitis [20]. Short and intensive exposure to visible and near infrared radiation (400-1400 nm) can cause thermal retinal damage, and the blue light between 400-500 nm wavelength can cause photochemical retinal injury referred to as a ‘blue

light hazard' [21]. The long term exposure to infrared radiations below wavenumber 1400 nm can cause lenticular cataracts which may take up to 10-15 years to develop [22].

Exposure of skin to UV radiations from arc welding can also cause reddening of the skin due to the dilation and inflammation of minute blood vessels in the dermis layer of the skin. In some cases, continuing exposure to UV (between 270 and 320nm spectra) has been shown to be the cause of skin cancer [23].

2.5.3 Effects of gases associated with the arc welding process.

Ozone, nitrogen oxides, carbon monoxide and carbon dioxide are the major gases formed during welding. Carbon dioxide and carbon monoxide can be dangerous to welders if the welding is taking place in a closed workshop without proper ventilation[24]. However, they are required to be present in relatively high concentrations to cause adverse health effects.

Ozone exposure can result in cough, substernal pain, shortness of breath, chest tightness, dry throat, wheezing, dyspnoea, and changes in lung function[24]. Studies on several animals have shown that chronic exposure to ozone can cause chronic bronchiolitis with bronchiolar fibrosis, pneumonitis, emphysema and epithelial lesion in the trachea and major bronchi[25]. Ozone can also cause dryness and irritation to the eyes.

Oxides of nitrogen can cause irritation of the eyes and mucous membranes and can also cause irritation in the lungs if inhaled[26]. High-concentration exposures to NO_2 can cause pulmonary irritation and exposure to NO can cause methemoglobinemia[26]. The most severe and dangerous effect of NO_x inhalation is pulmonary oedema which can be fatal.

2.5.4 Effects of welding fumes

Welding fumes have very adverse effects on the welder's health, the effects from welding fumes may either be acute and/or chronic[27]. The effects of welding fumes depend on the nature of the substance in welding fumes, exposure time to the welding fumes and quantity of the welding fumes[27, 28]. The exposure to the welding fumes is mainly through inhalation but in some cases, it can also be through ingestion. As the majority of welding fumes are less

than 1 μm, they can easily enter the respiratory track and can be Hazardous to welders. When the welding fumes enter the body, they can follow different ways through/out of the body.

- They can be exhaled.
- They can be absorbed by the respiratory tract or the lungs and then can be transferred to the rest part of the body by the blood.
- They can be transferred to the gastrointestinal tract after being absorbed by the mucus in the respiratory tract.
- It can later be transferred to the other body parts by blood when absorbed from the gastrointestinal tract.
- The way fumes affect the body highly depends on the individual components of the welding fumes.

As described earlier, welding fume aerosol refers to a mixture of gases and fine metal and flux dust originating from both the base metal and consumables used in arc welding. The term "dust" here considers the aerodynamic diameter of small solid particles, which can vary in size and shape and have the potential to enter different parts of the respiratory tract depending on these characteristics[29]. The welding fume contains metal oxide nanoparticulate vapours derived from the consumables and weld pool, which subsequently condense and aggregate into compounds[16]. These nanoparticle agglomerates can range from 0.005 to 20 μm in size, and their deposition in the respiratory tract varies accordingly[30]. Larger particles tend to deposit between the entry points (mouth and nose) and the larynx, while the smallest particles can penetrate as far as the alveolar region.

Regarding airborne dust sampling, researchers have categorized three groups of particulate fractions to represent the aerodynamic diameter of particles and their likely deposition regions within the respiratory tract. The particulate fraction of PM (Particulate Matter) is classified based on its size range, and each fraction has different implications for the respiratory tract involvement [EN481 and ISO 7708]:

Note: The size range for the particulate fractions are taken from the EN481 standard document which is currently under revision while writing the thesis. It would be revised and published soon.

Inhalable fraction: Particle size range is 0.5 μm ≤ aerodynamic diameter (dae) ≤ 100 μm. This fraction is capable of reaching and depositing in the upper respiratory tract, including the

mouth, nose, and throat. These larger particles are generally filtered out by the upper respiratory system and do not penetrate deep into the lungs.

Thoracic fraction: Particle size range is $0.5\ \mu m \leq dae \leq 40\ \mu m$. This fraction consists of smaller particles that can penetrate into the lower respiratory tract. These particles can reach the bronchi and bronchioles, posing potential health risks to the lungs and respiratory system.

Respirable fraction: Particle size is $0.5\ \mu m \leq dae \leq 15\ \mu m$. This fraction contains the smallest particles, often referred to as nanoparticles. Due to their extremely small size, these particles can penetrate deep into the distal respiratory tract, reaching the alveolar region of the lungs. Inhalation of these ultrafine particles poses the greatest risk to respiratory health, as they can cause severe health effects and may have systemic implications.

MMA welding is known to produce a higher amount of fume compared to MIG/MAG welding, and FCAW (Flux-Cored Arc Welding) generates the highest level of UPF (Ultrafine Particle) mass concentration[31]. In enclosed spaces, fumes tend to accumulate unless proper measures are taken, such as employing local exhaust ventilation systems to remove them or using air-fed helmets to supply the welder with clean and fume-free air. The fume generated during mild- or carbon-steel welding primarily contains iron (80–95%) and manganese (1–15%), but other metals, inorganic compounds, organic carbon, and elemental carbon may also be present. Gases like CO (Carbon Monoxide), O_3 (Ozone), and NO_x (Nitrogen Oxides) are produced during welding and can locally reach high concentrations, but their potential health hazards have not been widely studied in this context. The particles found in welding fume are predominantly in the Ultrafine Particle (UFP) size range, and there is a strong correlation between ultrafine and total particle concentrations[32-38]. Turbulence resulting from heat generation at the arc encourages the aggregation of primary particles into longer chains, though it remains uncertain whether these longer chains dissociate into primary ultrafine particles upon inhalation and interaction with pulmonary cells and lung lining fluid[39].

2.5.5 Acute Effects of welding fumes

- **Toxic damage:** Welding fumes consist of components that can affect the respiratory system directly, while others may travel through the lymphatic and circulatory system,

reaching various parts of the body, and can have toxic effects when combined with the blood. For instance, ozone and NO_2 can cause irritation in the respiratory tract and lead to pulmonary oedema following acute exposure. On the other hand, carbon monoxide, when inhaled, binds with haemoglobin, resulting in anoxia during high exposures.[27, 28].

- **Irritation:** It is the most common and obvious effect of welding fumes[28]. Due to welding fumes, irritation in the upper and lower respiratory tracts, mild or severe can be felt. Restrictions to sinus drainage or mucous membrane can also be seen as the response to irritants in the welding fumes.

- **Metal Fume Fever:** Metal fume fever is considered one of the common industrial diseases caused by the inhalation of the oxides of metals such as magnesium, iron, copper etc[40]. Welding fumes also contain a large number of metal oxides hence welders also experience metal fume fever. The symptoms of metal fume fever include a sweet or metallic taste, nausea, muscle and joint pains, fever, and chills. It takes 4 to 12 hours for symptoms to appear after exposure to high levels of fume (around $5mg/m^3$)[41]. The symptoms may last for 24-48 hours and are more common with zinc oxide metal particles[41].

2.5.6 Chronic Health Effects of welding fumes

- **Asthma:** Asthma is characterised as the obstruction in the airways and causes chest tightness, wheezing and shortness of breath in response to some external stimuli. Occupational asthma (which has an occupational origin) has been reported as the highest incidence of any other single respiratory disease of occupational origin[42-44]. There are many chemicals which are associated with occupational asthma and welding fumes are one of them. Health and safety executive UK (HSE) have listed chromium and nickel in stainless steel welding fume as capable of causing occupational asthma and categorise them as asthmagens.

- **Bronchitis:** Bronchitis is also a respiratory disease caused by the infection of the main airways of the lungs (bronchi). The main symptom is a cough, which may

bring up yellow-grey mucus (phlegm). Bronchitis may also cause a sore throat and wheezing Study conducted by Growth et.al has shown that welders display higher occurrences of chronic bronchitis[45].

- **Pneumoconiosis:** Pneumoconiosis is the deposition of a significant amount of particulate matter in the lungs. It has been observed in the welders since world war I. Iron oxide in welding fumes is considered the cause of pneumoconiosis in welders lungs [46].

- **Lung Cancer:** For a long time, there was a debate regarding the linking of welding fumes to cancer, but recently in Feb 2019, Health and Safety Executive in the UK endorsed and reclassified all welding fumes(including mild steel welding fume) as a human carcinogen. This decision came into enforce after considering the past research and recommendations by the International Agency for Research on Cancer(IARC). The old epidemiological studies have suggested that welders when compared to the normal population have a slightly higher risk of developing lung cancer [47-49]. These studies were questioned because of the problems associated with the variability and quantity of exposure to welding fumes, low occurrence, and incidence of lung cancer in general, and the slow development of the disease. Many factors such as the smoking history of welders were not accounted for in these studies. In 1990 IARC classified welding fumes as Possibly carcinogenic(Group 2B) to humans[50].

Numerous case reports dating back to the late 19th and early-to-mid-20th centuries raised concerns about the potential cancer risks faced by workers exposed to Cr(VI) compounds in various industries, including chromate production, chromate pigment production, and chromium plating[50-53]. To investigate these concerns, cohort mortality studies were conducted from the mid-20th century onwards, involving industries like ferrochromium or stainless-steel production, welding, leather tanning, among others, where potential exposure to chromium compounds existed. By the 1980s, substantial evidence had accumulated regarding the cancer risks posed to Cr(VI)-exposed workers, leading to the classification of Cr(VI) compounds as human carcinogens by IARC (1990)[50]. The informative cohort studies pointed to an excess risk of lung cancer among workers exposed to Cr(VI), particularly in chromate production, chromate pigment production[54-56], and chromium electroplating industries[57,

58]. Studies of chromate production workers consistently demonstrated elevated lung cancer risks, while those of chromate pigment production workers tended to show similar patterns, though not always statistically significant. Chromium electroplating workers also showed excess risks of lung cancer. In other industries, such as stainless-steel welding, ferrochromium production, and leather tanning, where Cr(VI) exposure levels might have been lower, the evidence was less conclusive[59, 60]. In some studies, high-quality smoking histories were collected and considered in the analysis, revealing elevated risks independent of smoking. However, for most studies with partial or representative smoking data, confounding effects from smoking patterns were unlikely to significantly impact the main results[59, 60].
A review of cohort studies estimated a mean standardized mortality ratio (SMR) for lung cancer of 278 among chromate production workers, chromate pigment production workers, and chromium platers. A recent meta-analysis reported an overall SMR of 141 for lung cancer among 47 studies of workers with possible Cr(VI) exposure[59, 60]. Regarding specific Cr(VI) compounds, workers in chromate production were likely exposed to mixtures of sodium, potassium, calcium, and ammonium chromates and dichromates, showing the highest and most consistent excess risks. Similarly, workers in chromate pigment production and spray painting were likely exposed to zinc and/or lead chromates, also resulting in high risks. On the other hand, workers in steel smelting and welding, possibly exposed to alkaline chromates, presented less distinct risks compared to the chromate and chromate pigment producers[59, 60].

IARC's conclusion in 2012 reaffirmed the association between Cr(VI) exposure and an increased risk of lung cancer, particularly in certain industrial settings with high exposure levels to specific Cr(VI) compounds.

However, in 1992 after scientific reviews and scientific commentary undertaken by the International Institute of Welding(IIW) Commission VIII (international welding community concerned with health and safety issues in welding and allied processes) published a statement stating that welders show a higher risk of getting lungs cancer from welding fumes compared to the general population.

In 2018, IARC published a new Monograph 118, in which they evaluated and reclassified welding fumes as Group 1 (carcinogenic to humans). This reclassification was based on epidemiological excess risk for lung cancer and the suppressive effect on the immune system

caused by welding fumes. The main reason for classifying welding fumes as lung cancer causing substances, is due to the presence of Hexavalent Chromium [Cr(VI)].

2.6 Fume Formation Mechanism

Welding fumes are ultrafine particles with varied shapes, sizes, structures, and compositions; hence all the particles cannot be formed by a single mechanism. Welding fumes can originate from several mechanisms. The major contributor to welding fumes is the filler electrode(more than 90% particles)[61] . Welding fumes particles are formed when the vapour condenses. Haidar et al. have reported that about 1% of the electrodes condenses into metal oxide nanoparticles and they aggregate together to form particle agglomerates[62]. Welding fume particle size highly depends on the mechanism by which they are formed. Particles less than 20nm are usually the result of vapour condensation, aggregates are formed by the collision of primary particles.

The fume particles are divided into three groups ultrafine ($0.01 \leq d \leq 0.1 \mu m$), fine($0.1 \leq d \leq 2.5 \mu m$) and coarse ($d > 2.5\ \mu m$)[30]. The main phases or steps in fume formation are.

- Metal droplet Expulsion
- Vaporisation
- Condensation
- Oxidation (fractionated and unfractionated)
- Agglomeration

The mechanism of welding fumes is categorised and explained as follows:

- **Evaporation followed by condensation, with or without oxidation:**
  Large molten metal droplets partially evaporate. Volatile components such as Manganese become more concentrated in the fume resulting in what is called fractionated fume[16]. This process also occurs from the surface of the weld pool. Small metal droplets may evaporate completely resulting in a fume of the same composition as the droplet. This is called unfractionated fume. If the evaporation rate is extremely high this could result in the depletion of more volatile components at the surface and lead to a fume similar in composition to the droplet[16].

- **Oxidation enhanced evaporation followed by condensation of an oxide fume:**
  Here the oxidation of metal vapour near the surface of the molten metal results in the removal of metal vapour and enhancement of the evaporation rate. It is debatable whether this operates in the welding arc as the oxides of the metals may well be dissociated at the temperature of the interface[63]. Droplet temperature lies somewhere between the melting point and boiling point of the alloy which for mild steel is somewhere between about 1800 K and 3100 K. The interface temperature between the droplet and the arc will be higher than this since the arc is at 6000K to 20000 K or higher. FeO has a boiling point of 2700 K and decomposes at 3400 K. In support of oxidation enhanced evaporation occurring in welding is the work of Corderoy et al (1980). They examined the composition of forming droplets in GMAW with shield gases of different oxygen contents. With oxygen contents, up to 10%, no surface depletion of Mn and Si was measured. For 20%, oxygen, there was surface depletion for Si and Mn. Si and Mn loss rates increased as the C>2 content of shield increased as did the overall loss of Si and Mn from the droplets[64].

- **Chemically enhanced evaporation:**
  One example of this is the formation of SiO at the metal surface. SiO is more volatile than Si hence Si is lost more rapidly in an oxidising atmosphere than might be expected[65].

- **Heterogeneous combustion:**
  If the rate of diffusion of oxygen to the metal surface is sufficiently high the hot metal, as opposed to the metal vapour, will be oxidised. This is an exothermic process and is effectively combustion[66]. It is often accompanied by copious fume formation by both evaporative and physical mechanisms[66].

- **Physical mechanisms:**
  These involve the ejection of particles in the aerosol size range, typically, 1 μm to 20μm, giving rise to unfractionated fume. One such mechanism is a gas eruption from molten droplets[67]. Gas or vapour production can result from the decomposition of a component of the material, for example, a carbonate, the presence of a volatile

component such as water or the formation of a volatile substance or gas[67-69]. This last source includes the oxidation of carbon contained in the molten metal. This is an exothermic reaction resulting in the production of CO, which erupts as bubbles from the surface forming minute particles of metal at the same time. Another mechanism is the explosive detachment of particles from the tip of the electrode. Droplets about to detach from the electrode tip are connected by a thin neck of molten metal. The current density can be extremely high in the neck and can result in an explosive rupture. In globular and spray transfer the current density is not likely to result in explosive detachment as there is an established arc carrying current. The arc can be displaced from the droplet to the tip of the wire being fed in so largely bypassing the narrow neck. The process of explosive rupture is particularly prevalent in MIG/MAG dip transfer where the arc has been extinguished and the neck formed as the wire melts must carry the full current[2, 67, 69].

Flux components also give rise to fume through some of the physical and evaporative mechanisms described above. Spatter is molten metal droplets ejected from the arc. Large spatter can be 2mm or more in diameter and produces fume in similar ways to those described above. As spatter is ejected from the shielded area around the arc it meets the much higher oxygen concentration in the external atmosphere. Figure 2.3 shows the graphical representation of the fume formation mechanism.

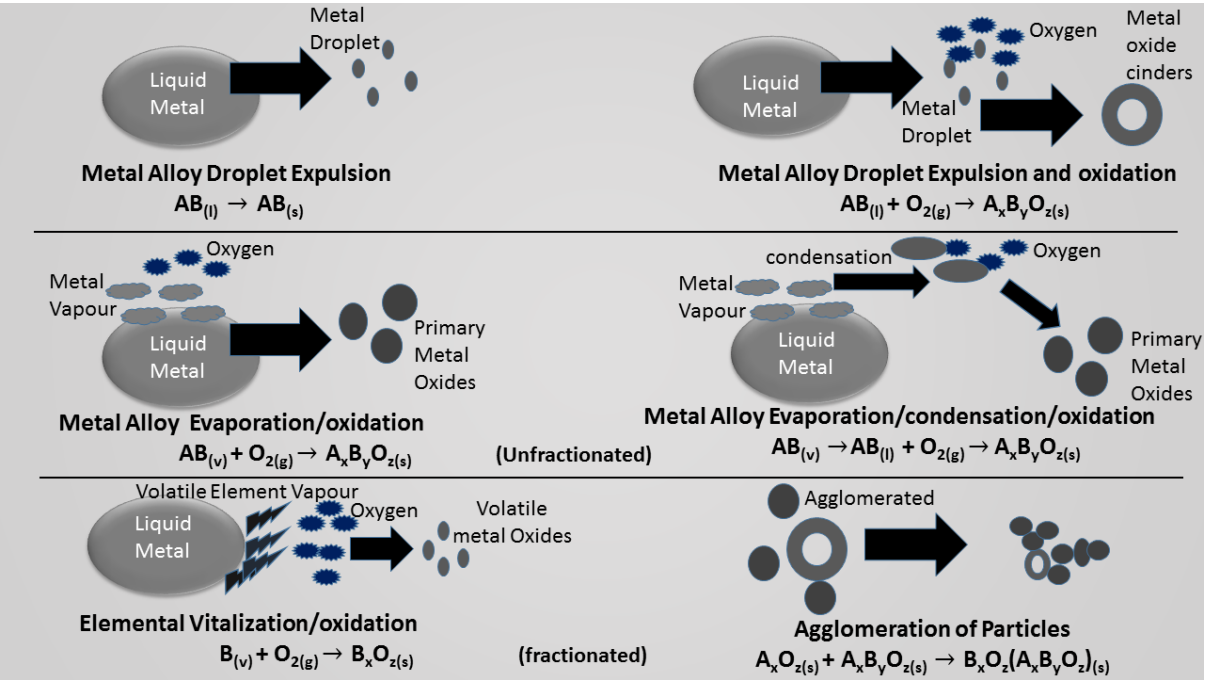

Figure 2.3 : Graphical representation of the fume formation mechanism

2.6.1 Mechanism of Cr (VI) formation in welding fumes

Welding fumes are generated during welding processes at high temperatures by the processes of vaporisation, oxidation, and condensation. In welding fumes, the main form of chromium is chromium spinel, chromic oxides, metallic chromium.

The consumables with fluxes used for welding stainless steel are rich in chromium and alkali earth metals and when the welding arc strikes, chromium and the alkali elements present in the consumable react with each other to form the alkaline chromates and dichromates via the reaction (2.1) and (2.2) pathways[28, 70].

$$2Na^{+} + Cr + 2O_2 + 2e \rightarrow Na_2CrO_4 \quad (2.1)$$

$$2K^{+} + Cr + 2O_2 + 2e \rightarrow K_2CrO_4 \quad (2.2)$$

This mechanism of Cr(VI) formation is true for flux electrodes but does not justify the formation of Cr(VI) in solid stainless-steel electrodes. Understanding the formation of Cr(VI) in solid stainless steel wire electrodes is one of the objectives of this thesis and is discussed later in detail in Chapter V of this thesis.

A study by Dennis et al. shows that ozone plays some role in oxidising Cr (III) to Cr (VI) compounds [71]. In his work, he concludes, that due to high temperatures in arc welding, UV emissions occur which photo chemically converts O_2 to O_3 which react with Cr(III) and oxidises it to Cr(VI) compounds. While his work talks about Metal Inert Gas(MIG) welding, it does not show the relation of UV and Cr (VI) generation in other welding wires and is, therefore, an interesting area for investigation.

Table 2.2 shows the possible Cr(VI) species with their thermal stabilities, which may be formed in the MIG/MAG welding fumes.

Cr(VI) species	Formula	Thermal stability
Ferric dichromate	$Fe_2(Cr_2O_7)_3$	Decomposes at 410 K

Chromic dichromate	$Cr_2(Cr_2O_7)_3$	
Nickel dichromate	$NiCr_2O_7$	
Manganese dichromate	$MnCr_2O_7$	
Molybdenum dichromate	$Mo(Cr_2O_7)_3$	
Chromium trioxide	CrO_3	Decomposes at 600 K
Nickel chromate	NiCrO4	
Manganese chromate	MnCrO4	

Table 2.2 : Cr(VI) species which may occur in stainless steel MIG/ MAG welding fumes [72].

2.6.2 Welding parameters and their effect on Cr (VI) generation

A large amount of work has been carried out on the effect of changing welding parameters on welding fumes, but there is a limited amount of literature existing on how the welding parameters affect the Cr(VI) formation during welding. Work by many researchers shows that there is a direct connection between welding parameters and Cr(VI) generation[12, 73, 74].

- **Welding Voltage:** The arc welding voltage affects many other parameters of the arc welding such as energy input into the arc, mode of metal transfer, the evaporation system, heat transfer, etc[12]. The fume formation changes with the mode of metal transfer, e.g., when the voltage is low there is less fume formation during dip metal transfer, but it increases with the increase in voltage in globular mode and is highest in the spray mode this may be explained by the factors such as the heat input increases with the voltage and the change in the mode of metal transfer also changes the formation of spatter. There is more spatter in spray mode than in dip transfer mode. Although there is no direct effect of voltage on Cr (VI) generation explained in the literature, but

it can be linked to the formation of more fumes and spatter and as result, there is high Cr (VI) formation with the increase in welding voltage[2, 75].

- **Welding Current:** In a general aspect, if there is an increase in current then the increase in Fume Formation Rate (FFR), since an increase in current increases the voltage as there is a direct relation between voltage and current, but after a certain point when the current has increased the reduction in FFR is being observed[75]. . Some researchers have reported the decrease in FFR at the transition point between globular and spray transfer, but others have not found a direct impact of current and FFE so it's hard to predict the relationship between Cr (VI) generation with the welding current.

- **Shielding gas:** Shielding gases play an important role in protecting the weld pool and metal droplets from getting oxidized due to atmospheric oxygen[14, 76]. There is no doubt about the role of shielding gases in reducing fume formation in welding. But there is a research gap in understanding the role of shielding gases in Cr(VI) formation in welding. Exploring this research gap is one of the main objectives of my thesis which is later discussed in detail in chapter VI.

- **Shielding gas flow rate:** With the increase in the flow rate of shielding gases the decrease in fume formation is being observed as it helps in reducing the possibility of oxygen entrainment into the region of the gas shield and thereby reduces the rate of both evaporation and spatter ejection from this region[69].

2.6.3 Methods of Cr (VI) reduction in welding fumes:

The research in the field of Cr (VI) mitigation is yet not being accepted in the industry with the open arms either because they have some cost issues, issues with the quality of weld attached with them or other health and safety related issues. The methods of Cr (VI) mitigation can be categorised as follows:

- **Composition of welding wires:** A large group of researchers blame sodium and potassium for Cr (VI) generation in welding fumes so their focus was to reduce the content of these elements as if these elements are not present then they will not react

with Cr from the stainless-steel wire electrode and hence the amount of Cr (VI) generation can be easily reduced. The addition of lithium and zinc in place of potassium has shown positive results as it reduces the possibility of alkaline chromates and dichromate formation [77]. There is one more advantage of using lithium and zinc in welding wire as they also help in reducing the O_3 formation during welding[77]. Some researchers have used nanotechnology to find a way of reducing Cr (VI). Vishnu et al. used nano TiO_2 and nano Al_2O_3 coatings on the welding wire to reduce the Cr (VI) [78]. These Nano particles help stabilising the welding arc by providing high oxidising potential hence resulting in less FFR due to less spattering and stable arc which results in less Cr (VI) than the standard electrode wire [78].

- **Composition of shielding gases**: Shielding gases are used to protect the weld pool from oxidation hence different compositions and mixtures are studied by researchers to reduce the Cr (VI) content in welding fumes. The addition of reducing agents in the shielding gases has a positive impact in reducing Cr (VI) content hence use of NO and C_2H_4 along with conventional shielding gases are studied by Dennis et al. and their results show a reduction in Cr (VI) content in the fumes [71]. Double shroud delivery of silica precursor is also studied, and it also shows the positive impact on Cr (VI) reduction. In this method, the silica precursor reacts with the oxygen present in the arc and hence Cr does not react in large amounts with the oxygen and hence Cr (VI) generation is impacted [79].

- **Arc Stabilising:** Arc stabilising helps in the reduction of spatter formation which eventually helps in fewer fume generation hence helping in reducing Cr (VI) concentration in welding fumes. Schwemmer et al. added FeO and CaO in the flux to improve arc stability, as FeO and CaO can be easily ionized and thus help in arc stabilising[80].

- **Controlling Ozone formation:** The UV emissions from the welding arc are responsible for the formation of Ozone in the welding Arc. Ozone is formed by the photochemical process of converting O_2. Ozone contributes to Cr (VI) formation by oxidising metal fumes and reducing the formation of Ozone can eventually help in the reduction of Cr (VI) formation in welding fumes.

- **Replacing Cr with other elements in the welding electrode:** Cr is added to the stainless steel to protect steel from getting easily oxidised, but it has led to the Cr (VI) in welding fumes. Sowards et al. have produced a welding electrode that is based on the Ni-Cu-Ru system and generated less Cr (VI) in welding fume[81]

2.7 Motivation and objectives of the research

The main scope of this study is to enhance the knowledge of Chromium (VI) in welding fumes by addressing the problems in Chromium (VI) analysis, investigating the chemical forms of Chromium (VI) in different welding fumes, identifying factors affecting Chromium (VI) formation in welding fumes, and discussing the mitigation methods of Chromium (VI) in welding fumes. . Welding is a common practice in multiple industries, and a large group of workers are exposed to the fumes on a daily basis. Despite the known impact of Cr(VI) on welders' life expectancy and quality of life, there is still a significant research gap in understanding the mechanisms of Cr(VI) formation in welding fumes.
Based upon this, the objectives of this research are therefore to:

- Understand the mechanism of Cr(VI) formation in solid stainless-steel wires.

- Developing fast and reliable technique to identify/quantify the Cr(VI) compounds in welding fumes.

- Developing a mathematical model to understand the effect of different parameters on weld droplet temperature and its effect on different chromium compounds known to be found in welding fumes.

- Study the influence of shielding gases on Cr(VI) formation on arc welding fumes.

Chapter III: Materials and Methods

In this chapter, a comprehensive overview of the experimental methods and apparatus employed in this research will be presented. It is crucial to note that prior to conducting the primary experiments, a thorough development process had to be undertaken in order to establish standardized procedures and calibrate the equipment to ensure accurate and precise results. This included determining the most appropriate methodology and selecting the necessary apparatus, as well as fine-tuning and testing the equipment to ensure that it met the necessary specifications and standards. Additionally, the procedures were optimized to minimize any sources of error and to maximize the accuracy and precision of the data collected. This process is essential in order to ensure that the results obtained are reliable and can be used to draw meaningful conclusions. In this chapter the following will be explained:

- Welding equipment and Consumables.
- Fume collection apparatus.
- Extraction of fume samples for analysis.
- Methods of analysis fume composition and hexavalent Chromium.
    - Ion Chromatography (IC)
    - Inductively Coupled Plasma -Mass Spectroscopy (ICP-MS)
    - Fourier Transform Infrared Spectroscopy (FTIR)
- Other Characterisation techniques for welding fumes
    - X-Ray Diffraction (XRD)
    - Scanning Electron Microscopy (SEM)
    - Energy- Dispersive X-ray Spectroscopy(EDX)

3.1 Welding Equipment and Consumables

Before beginning the process of collecting and analysing the fumes produced during welding, a series of welding trials were conducted in order to establish the optimal welding parameters for achieving ideal weld conditions. These trials were performed using an inverter MIG/MAG power source that operated in the open arc transfer mode, which is commonly used for MIG/MAG welding. The welding conditions were manually set on the power source, and a standard swan neck welding torch was connected and securely held in place above a moving traverse. The torch nozzle was positioned at a 90-degree angle to the vertical, and the welding

progressed in a "push" direction. To collect the welding fumes, a fume hood, as specified in ISO 15011-1:2009 [82] , was suspended above the welding torch to capture the fumes produced during the process. This hood was designed to meet industry standards and ensure the fumes were effectively collected for analysis. Setup for fume collection is shown in figure 3.1.

The welding parameters which were set during trails were:

- Shielding gas flow rate: Gas flow rate was set up at 20 ml/min.
- Voltage: It varied by the process and the type of shielding gas used
- Welding torch nozzle angle: It was kept 90 degrees to the work piece.
- Welding speed : It was different for different welding processes.
- Welding wire feed rate: It was different for different welding processes.
- CTWD(contact tip to work distance): It was kept 20mm.

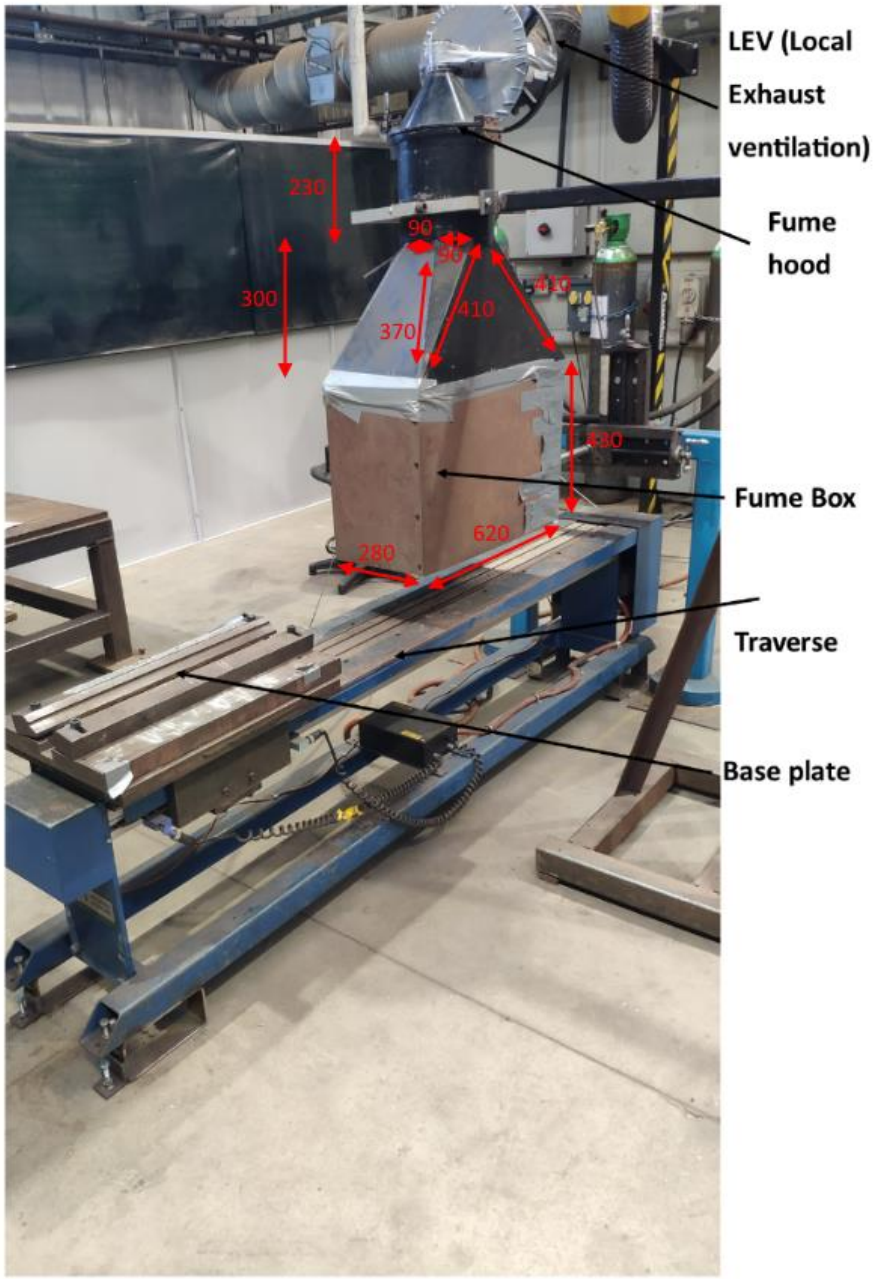

Figure 3.1 : Welding setup for collecting fume samples via MIG/MAG welding.

Details regarding the specific welding parameters used in this research are discussed in later chapters as they were highly dependent on the type of welding process and the type of shielding gas used. The welding trials were conducted on 304SS plates that measured 500 X 50 X 10 mm, which were securely clamped in a fixture on the traverse. The welding progressed by moving the plate under a stationary welding torch, and the traverse travel speed was set at 300mm/min. For MMA welding trials, they were carried out by an experienced welder who kept the fume hood above the welding table instead of traverse. The welding fumes were effectively captured by the fume hood and collected on cellulose filter paper that was placed

on the top of the hood. Particle retention sizes for the filter paper was > 8 μm. After the welding process was completed, the fumes were brushed off from the filter paper, and further analysis of the fumes was carried out to gain insights on the chemical composition and other properties of the fumes produced. In our study, special care was taken to ensure accurate analysis by using a paint brush to gently brush off the top layer of fumes from the filter papers before further examination. There is a possibility that the fumes which form the lower layer on the filter paper may be reduced, but the subsequent layers above do not experience the reduction.

Welding consumables which were used in for this work are :

- Manual Metal Arc (Rutile Electrode)
- Manual Metal Arc (Basic Electrode)
- Flux cored Wire electrode
- Solid stainless steel wire electrode
- Carbon/Mild steel wire electrode

The composition of the electrodes used in this research is discussed in detail in later chapters.

3.2 Fume hood and collection of welding samples

The fume hood used in this research was designed in accordance with the specifications outlined in the ISO 15011-1-2009 standard [82]. The fume collection process was carried out by placing filter paper on the top of the fume hood, which was attached to an extraction unit. The welding process was conducted under the fume hood, where the fumes produced during welding were effectively drawn to the filter paper and settled on it. After 2-3 welding passes, the filter paper was removed from the fume hood, and the fume samples were carefully brushed off and stored in airtight glass vials. These fume samples were subsequently analysed using a variety of analytical methods, which are discussed in later chapters. These methods include various chemical, physical, and analytical techniques to determine the composition, properties, and safety hazards of the fumes produced during the welding process.

3.3 Characterisation of Welding fume particles

3.3.1 Inductively Coupled Plasma - Mass Spectroscopy (ICP-MS) and Ion Chromatography (IC)

The elemental composition of the welding fumes was determined using Inductively Coupled Plasma-Mass Spectrometry (ICP-MS) technique. This technique is particularly useful for measuring the total Cr content in the welding fumes. To determine the Cr(VI) composition specifically in the welding fumes, Ion Chromatography (IC) was used. Both these analyses were carried out in accordance with **ISO 16740:2005** standard.

Ion Chromatography is a technique used to separate ions based on their interactions with the stationary phase (resin) and the mobile phase (eluent). Depending on the ion, the column could be an anion column (attracting anions) or a cation column (attracting cations). The speed at which ions move through the columns is determined by their affinity for the resin, and their separation is based on differences in charge and size. The eluted ions are then detected by an electrical conductivity detector, which produces a graph, called a chromatogram, that plots conductivity over time. Each ion produces a peak, the height of which depends on the ion's concentration in the sample. To avoid interference from ions in the mobile phase, a suppressor may be used to remove unwanted electrolytes before the conductivity measurement.

For the IC analysis, the fume samples were first isolated from other chemical species present in the welding fumes. This was achieved by adding 2% NaOH/ 3% Na2CO3 solution, followed by hot plate extraction in which the sample was heated on a hotplate at 135°C with occasional swirling between 45 min to 60 min to avoid the solution boiling or evaporating. The sample was then cooled to room temperature and post-column derivatization was carried out by using 2 mM 1, 5-diphenyl carbazide (DPC) / 10% methanol/ 1M H_2SO_4.

3.3.2. Scanning Electron Microscopy (SEM) and Energy Dispersive X-ray spectroscopy (EDX)

Particle size and elemental composition of the welding fumes were investigated by Scanning Electron Microscopy (SEM) and Energy Dispersive X-ray spectroscopy (EDX). SEM images were taken by Zeiss ∑igma FEGSEM attached with EDX spectroscopy. EDX was performed on the particles by Oxford Instruments X-Max2 silicon drift detector.

3.3.3 X-ray diffraction analysis (XRD)

The phase analysis and crystal structure of the welding fume particles were analysed by X-ray diffraction analysis (XRD) using Siemens D501 Diffractometer.

XRD, or X-ray diffraction, is a technique used to determine the crystal structure of a material by analysing the way in which X-rays are scattered by the atoms in the material. It is commonly used in fields such as materials science, chemistry, and mineralogy. The principle of XRD is based on the fact that X-rays interact with the electrons in the atoms of a crystal lattice, causing them to scatter in different directions. The scattered X-rays will have different wavelengths and phases, and when they are detected and recorded, they form a diffraction pattern. By analysing the diffraction pattern, it is possible to determine the crystal symmetry, lattice parameters, and the positions of the atoms in the crystal lattice. In XRD, the sample is placed in a beam of X-rays, and the diffraction pattern is recorded using a detector such as a film or a detector array. The diffraction pattern can be analysed using software to determine the crystal structure of the sample.

3.3.4 Fourier Transform Infra-red Spectroscopy (FTIR)

Fourier Transform Infra-red Spectroscopy (FTIR) is a well-established analytical technique for qualitative analysis, with the mid-infra-red (IR) region (4000 cm−1 to 400 cm−1) being rich in information about the presence of the functional groups. FTIR can also be used quantitatively, as the energy absorbed at a particular wavelength is in proportion to the number of bonds absorbing the associated quanta of energy, so with larger concentrations of analyte more of the energy will be absorbed.

The attenuated total reflectance (ATR) attachment for FTIR, allows direct measurement of the sample with minimal preparation, and the potential for re-usability, if required. ATR-FTIR is a reflectance method with the incident infra-red radiation, undergoing total internal reflection in the ATR crystal, resulting in an evanescent wave at the crystal surface which penetrates the sample.

FTIR was performed using a Thermo Fisher iS5 attached with an Attenuated Total Reflectance (ATR) accessory (ID7). The FTIR spectra were obtained after 128 scans with 2cm-1 resolution in the transmission mode. The background was measured for each sample and subtracted from the final spectra.

Chapter IV: FTIR Spectroscopy as a convenient tool for detection and identification of airborne Cr(VI) compounds arising from arc welding fumes.

4.1 Introduction

As already discussed in previous chapters that, welding is the backbone of the modern industrial world as it is performed in large number of industries such as shipbuilding, aerospace, automobile, construction, power generation etc. [1, 83, 84]. Welders and all personnel employed in these industries are exposed to welding fumes and risk contracting lung cancer significantly more than other people [85-87]. This is primarily due to the presence of hexavalent chromium [Cr(VI)], a known carcinogen found in arc welding fumes generated from the welding of stainless steels [27, 54, 70, 85, 88]. Amongst all the other type of welding processes, arc welding is the most common and widely used method of all welding processes because it is versatile, and uses simple equipment [1] – due to its widespread usage, it impacts the health and safety of a very large number of workers who involved regularly in these industries. Exposure to Cr(VI) is due to fume generation which in turn, depends on the type of welding and process conditions [89, 90]. Therefore, it becomes more important to analyse accurately the composition of welding fumes and keep a close eye on the exposure of welders to the welding fumes and its component Cr(VI).

Due to health concerns, the exposure limit for Cr(VI) is revised on a regular basis and regulated by governing bodies. The EU, USA and UK have stringent exposure limits in place, but some countries still don't have such reduced limits in force, or none at all. Currently, in UK for welding fumes the exposure limit is 0.025 mg/m^3 for the 8-hour time-weighted average (TWA) exposure and it is proposed to further reduce it to 0.005 mg/m^3 after 2025. As a result of these regulations, there is need to understand the Cr(VI) chemistry and the different forms that exist in welding fumes in order to facilitate mitigation and compliance.

As mentioned before, airborne hexavalent chromium compounds, generated during arc welding are known human carcinogens [highly toxic due to its ability to oxidize biomolecules, notably DNA] whilst Cr(III) is not harmful, because it is usually in the condensed phase [27, 28, 70,

86, 87, 91]. Sodium (Na) and Potassium (K) ions present in welding electrodes are known for forming Cr(VI) compounds during welding via the reaction (4.1) and (4.2) pathways [28, 70].

$$2Na^{+} + Cr + 2O_2 + 2e \rightarrow Na_2CrO_4 \quad (4.1)$$

$$2K^{+} + Cr + 2O_2 + 2e \rightarrow K_2CrO_4 \quad (4.2)$$

The presence of both $^{+}3$ and $^{+}6$ oxidation states of chromium in welding fumes makes it difficult to analyse the correct amount of Cr(VI) [70]. The current analytical methods for determining Cr(VI) percentage in welding fumes are being challenged for inaccuracies, as these methods involve wet chemistry, thus introducing errors in analysis due to Cr-redox chemistry, which is strongly pH dependant[70]. The most common existing procedure for Cr(VI) analysis is via extraction of air filtered particulate samples using sulfuric or nitric acid. Extraction is followed by spectrophotometric analysis of the magenta chromogen (at λ_{max} = 540 nm) which is formed by the reaction of Cr(VI) with 1, 5-diphenyl carbazide (DPC) in a strongly acidic solution[22, 70, 92]. Another widely accepted way of detecting and measuring hexavalent chromium in welding fumes is, by Ion Chromatography (IC). To extract Cr(VI) and isolate it from other chemical species present in welding fume samples, the sample is extracted by adding 2% NaOH/ 3% Na_2CO_3 solution followed by hot plate extraction in which sample is heated on hotplate at 135°C with occasional swirling between 45 min to 60 min to avoid the solution boiling or evaporating and then cooling to room temperature and then post column derivatization is carried out by 2 mM 1, 5-diphenyl carbazide (DPC) / 10% methanol/ 1M H_2SO_4 [22].

During the analysis, there are chances of redox pathways between Cr(III) to Cr(VI), as follows:[70]

$$Cr^{3+} + 3OH^{-} \rightleftarrows Cr(OH)_3 \quad (4.3)$$

$$Cr(OH)_3 + OH^{-} \rightleftarrows [Cr(OH)_4]^{-} \quad (4.4)$$

$$4[Cr(OH)_4]^{-} + 3O_2 + 4OH^{-} \rightarrow 4CrO_4^{2-} + 10H_2O \quad (4.5)$$

Additionally, the divalent iron [Fe(II)], which is most likely present in the welding fumes, works as a reducing agent for Cr(VI). Also, the manganese dioxide which is likely to be present in welding fumes may react with Cr(III) and oxidise it to Cr(VI) during hot alkaline extraction of insoluble Cr(VI) compounds in welding fumes[93]. The effect of pH on the distribution of

chromium between trivalent and hexavalent oxidation states in presence of iron is described by the equation below[70].

$Cr(OH)_3$ (Trivalent Cr) + $5OH^-$ + $3Fe^{3+}$ ⇄ CrO_4^{2-} (Hexavalent Cr) + $4H_2O$ + $3Fe^{2+}$ (4.6)

To avoid these redox reactions during the analysis of Cr(VI) new methods to analyse Cr(VI) in welding fumes are being sought after and continually explored.

An interesting possibility is the direct usage of Fourier Transform Infrared Spectroscopy (FT-IR) to analyse the welding fume samples. FT-IR does not involve any wet chemistry so there are no chances of redox reactions due to pH variations, and the analysis reflects 'as-received' samples (directly from the filter paper).

Fourier Transform Infrared Spectroscopy (FTIR) is a well-established analytical technique for qualitative analysis, with the mid-infrared red (IR) region (4000 cm^{-1} to 400 cm^{-1}) being rich in information about the presence of the functional groups. FTIR can also be used quantitatively, as the energy absorbed at a particular wavelength is in proportion to the number of bonds absorbing the associated quanta of energy, so with larger concentrations of analyte more of the energy will be absorbed.

The attenuated total reflectance (ATR) attachment for FTIR, allows direct measurement of the sample with minimal preparation, and the potential for re-usability, if required. ATR-FTIR is a reflectance method with the incident infrared radiation, undergoing total internal reflection in the ATR crystal, resulting in an evanescent wave at the crystal surface which penetrates the sample.

Currently FTIR technique has not been widely used in the analysis of welding fumes, due to the complexity in assigning characteristic peaks for the different elements, given the presence of several compounds being all together in one sample. However, there are instances in related areas, where FTIR is being used to quantify the components present in mixtures, such as a study by Reigh et al., in which they used a constant ratio method to quantify calcium carbonate and silica (quartz) in geological samples using FTIR [94]. Researchers have also used sophisticated methodologies such as principal component analysis (PCA) or partial least squares (PLS) for quantification of mixtures using FTIR [95]. Therefore, there is a huge

opportunity to develop FTIR (with ATR) for – firstly, qualitative detection and establishment of the various compounds in the welding fumes, including Cr(VI), which is presented in this work, and secondly, quantification of these species, which will be a subject of another paper to be submitted very soon. Also, in this work, the fumes generated from Manual Metal Arc welding (MMA), Flux Cored Arc welding (FCAW), and Single Wire or Metal Inert Gas welding/ Metal Active Gas Welding (MIG/ MAG) are the primary subjects of investigation, as they have been known to release Cr(VI) at levels that are above the threshold of occupational hazard.

4.2 Materials and Methods

4.2.1 Materials and welding methods

Three types of arc welding processes were investigated in this work. For MMA and FCAW, the base plate used was stainless steel (SS) 304 (500 X 50 X 10 mm) along with SS electrodes (with flux material). For Metal Inert Gas/ Metal Active Gas (MIG/ MAG) welding, carbon steel base plates were used with Carbon Steel electrodes, and for a SS304 base plate, SS electrodes (no flux materials) were used. Composition of welding consumables and base plates are shown in table 4.1 MMA welding was carried out manually (as the name suggests) and FCAW and MIG/ MAG welding was carried out on an automated welding table by welding technicians. All the welding was carried out inside a fume hood in accordance with International Organization for Standardization (ISO) 15011-1:2009 specifications which states that the welding fumes should be collected inside fume box using cellulose filter paper, as it is an inert medium, and would not contaminate the fume sample. Samples can also be easily brushed off from these filter paper. All electrodes for MMA have a diameter of 4 mm, and welding was carried out at a current of 145 A - 150 A (90% of max current). Fumes during these experiments were collected on cellulose filters and then brushed off and stored in glass vials. For manual metal arc (MMA) welding, rutile and basic electrodes were both used. While the details of the commercial electrodes and their flux materials are not revealed, it is known that rutile electrodes are rich in titania (titanium dioxide) whereas basic electrodes are rich in calcium carbonate and calcium fluoride. Welding fumes from basic electrodes are designated as M1 and M2. M1 and M2 are two samples of the same electrodes, and as such welding conditions were identical. Welding fumes from rutile electrode are designated as M3 and M4 and there are no differences in welding conditions for M3 and M4, either. Welding fumes generated

during flux cored arc welding (FCAW) were designated as FC1, FC2, FC3 and FC4 – these were 4 different samples of the same material, and the welding conditions were the same for each of them samples. Shielding gases used for all FCAW samples were mixtures of CO_2 and O_2. MIG/ MAG welding was carried out using combinations of CO_2, O_2, He and Ar as shielding gases, and stainless-steel and carbon steel wires were the consumables.

	C (%W/ W)	**Mn (%W/ W)**	**Si (%W/ W)**	**Cr (%W/ W)**	**Ni (%W/ W)**	**Cu (%W/ W)**	**S (%W/ W)**
Base Plate (SS 304)	0.08	2.0	0.75	18.0 - 20.0	8.0 - 10.5	-	-
Base Plate (Carbon Steel)	0.18 - 0.20	1.50	-	-	-	0.55	0.030
Manual Metal Arc Electrode (Basic)	0.03	0.9	1	19	10	-	0.01
Manual Metal Arc Electrode (Rutile)	0.03	0.8	0.8	19.8	10.2	-	0.025
Flux cored wire consumable	0.06	1.3	0.50	19.3	9.5	-	-
Solid stainless steel wire consumable	0.02	1.7	0.90	20	10	-	-
Carbon Steel Electrode	0.1	1.3	0.8	-	-	-	-

Table 4.1: Elemental composition of welding consumables and base plates.

4.2.2 Characterisation of welding fume particles

Particle size and elemental composition of the welding fumes were investigated by Scanning Electron Microscopy (SEM) and Energy Dispersive X-ray spectroscopy (EDX). SEM images were taken by Zeiss ∑igma FEGSEM attached with EDX spectroscopy. EDX was performed on the particles by Oxford Instruments X-Max^2 silicon drift detector. The phase analysis and crystal structure of the welding fume particles were analysed by X-ray diffraction analysis (XRD) using Siemens D501 Diffractometer.

FTIR was performed using a Thermo Fisher iS5 attached with an Attenuated Total Reflectance (ATR) accessory (ID7). The FTIR spectra were obtained after 128 scans with 2cm^{-1} resolution in the transmission mode. The background was measured for each sample and subtracted from the final spectra. Typically, 3-4 samples of the same fume/ compound were examined – the technique is such that the absolute intensities are not reproducible. The reason why the peak intensities are not reproducible is, due to use small differences in sample thickness, in spatial arrangement, and lack of precisely the same alignment with the ATR (Reflectance signal). However, the relative peak intensities of the various vibrational modes were constant, for different samples of the same compound. Hence, in future, all quantification of FTIR spectra is to be done on the basis of ratios of various components in the welding fume. The development of this method will be discussed in another paper which will be submitted shortly. In addition to FTIR, elemental analysis of the welding fumes using Inductively Coupled Plasma – Mass Spectrometry (ICP-MS), and Cr(VI) estimation, by Ion Chromatography (IC) data were done at HSE Science and Research Centre at Buxton.

4.3 Results and Discussions

4.3.1 ICP-MS, IC, and Fourier Transform Infrared Spectroscopy (FTIR) Data

4.3.1.1 Manual Metal Arc (MMA) welding fumes

Welding fumes from MMA (described earlier) were sent to HSE for ICP-MS for the elemental composition of these fumes. Simultaneously using another batch of the sample, ion chromatography (IC) was carried with the purpose of measurement of Cr(VI) in the welding

fume (also at HSE). Table 4.2 shows the elemental composition of welding fumes (ICP-MS, and IC, for Cr(VI)) from these samples.

Elements	M1 (%m/m)	M2 (%m/m)	M3 (%m/m)	M4 (%m/m)
Al	0.5	0.1	1.6	1.5
Bi	<0.1	<0.1	6.3	6.1
Ca	9.0	10.3	0.7	0.7
Total Cr	0.5	0.5	5.1	5.3
Cr(VI)	0.4	0.4	4.8	4.7
Fe	18.1	19.7	5.7	6.0
K	18.6	13.3	21.7	21.7
Mn	3.9	4.9	3.2	3.2
Na	2.7	5.3	4.8	4.7
Ni	0.1	0.1	0.7	0.7
Si	2.4	2.8	8.5	9.1
Ti	0.5	1.1	2.2	2.1
F	23.7	19.0	18.6	17.7

Table 4.2: Elemental composition of welding fumes from MMA welding electrode

There is evidence of considerable Cr(VI) in the rutile electrodes, relative to the basic ones, as shown in Table 4.2. However, there is uncertainty in the Cr(VI) due to the numerous digestion processes which are part of the sample preparation procedure (discussed earlier in the introduction section).

Finally, the remaining quantities of the above samples was sent for FTIR, as discussed in the following sections.

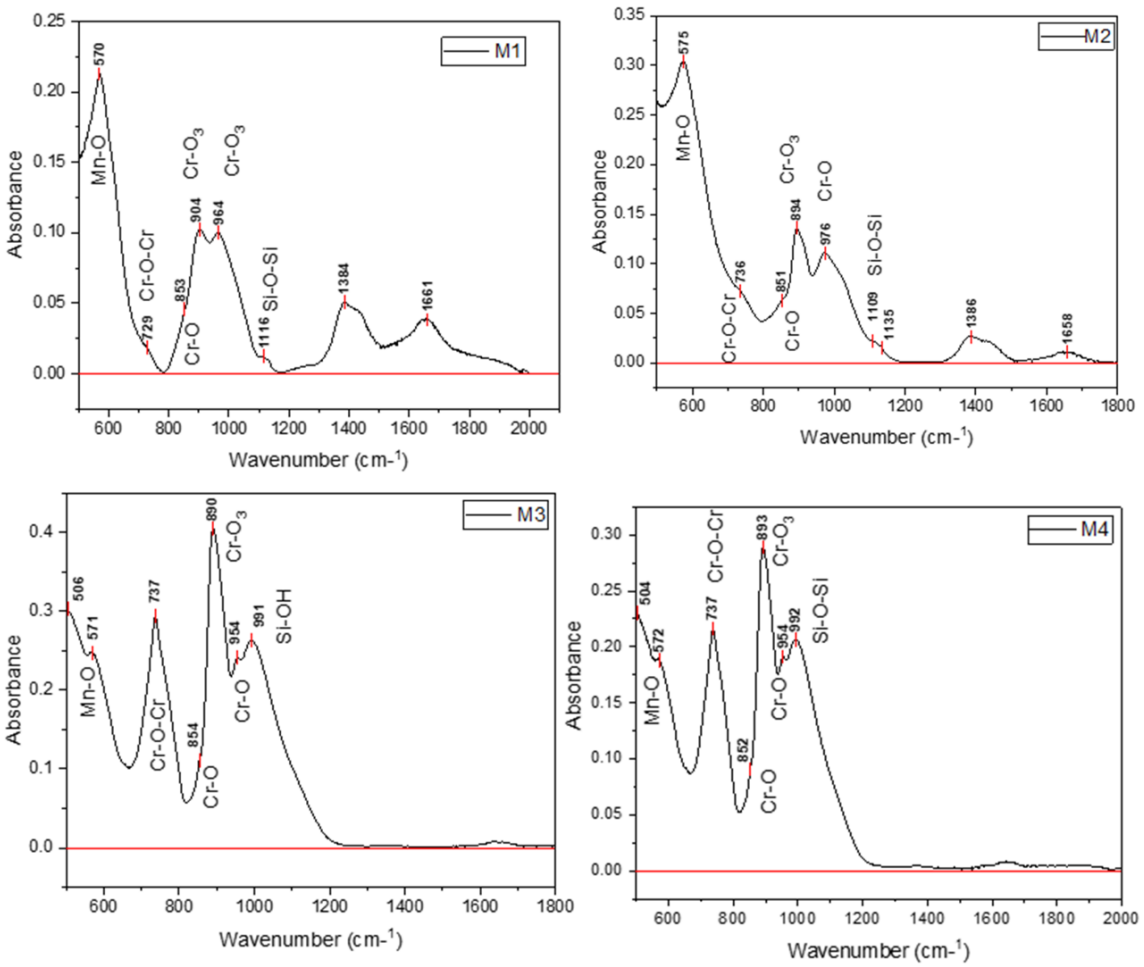

Figure 4.1: FTIR data of welding fumes from MMA welding

FTIR spectra using the ATR - Figure 4.1 shows the FTIR analysis of welding fumes generated and collected during the MMA welding process, which at first glance shows higher intensities of Cr(VI) absorption, for the rutile sample compared to the basic – this corroborates the general trend obtained by IC (Table 4.2). Further analysis of all the absorbance peaks shows the various vibrational modes due to the chemical bonding in the compounds. All welding samples show vibrations for Mn-O-Mn, Cr-O-Cr, Cr-O, O-H and Si-O.

The peak at wavenumber 570 cm^1 is due to stretching vibration of Mn-O and can be assigned to Mn_2O_3 and has been reported in many research articles [96-100]. The presence of Mn_2O_3 in welding fumes has also been confirmed in research articles, and it exists likely, as a $Fe_{3-x}Mn_xO_4$ spinel in welding fumes [101]. Mn can also exist as MnO in welding fumes [101], but those characteristic vibrations are not seen in these samples; MnO has a characteristic peak at wavenumbers 630 cm^{-1} and 525 cm^{-1} which is due to the Mn-O bond [102]. Mn-O vibrations at 630 cm^{-1} are not observed because, Mn in welding fumes exists in multiple forms, as MnO,

Mn_2O_3, MnO_2 , or Mn_3O_4. Mn is extensively soluble in Fe_3O_4, due to which it mainly exists as $Fe_{3-x}Mn_xO_4$ $(0 < \times < 1.65)$.

Most importantly, FTIR provides considerable information of the various vibrational frequencies associated with Cr-O bonding characteristic of a range of Cr compounds. FTIR peaks at 729, 735, 895, 903 cm^{-1} is usually seen in dichromates and the peak at 853 cm^{-1} observed in chromates [103-106]. Peak at 729 and 735 cm^{-1} are due to Cr-O-Cr anti-symmetric stretching vibrations. Peaks at 895 and 903 cm^{-1} are due to the symmetric stretching vibration of $Cr-O_3$ group that form a part of the CrO_4 tetrahedra [104] . Dichromate ions are known to have the bridged structure $O_3Cr-O-CrO_3$ due to which they show vibrations for Cr-O-Cr and internal vibrations for the tetrahedral CrO_4 groups [107]. MMA welding electrodes contain sodium and potassium compounds (shown in fumes from ICP-MS data, in Table 2), which are usually present in the flux materials. The Na^+ and K^+ ions present in welding electrodes are known for forming Cr(VI) compounds during welding.

Hence, formation of chromates and dichromates in our welding fume samples from MMA welding fumes due to the alkali metals is a strong possibility. Absorption intensities of chromates and dichromates are lower for basic electrodes than from rutile electrodes, and this is also reflected in the IC data, i.e. Cr(VI) formation in M1 and M2 is less compared to Cr(VI) formation in M3 and M4. It is not very clear what the role played by titania is, due of lack of compositional data of the commercial electrodes. Earlier study by Rajeshwari et al. [30] actually showed the reduction in Cr(VI) percentage in welding fumes by adding TiO_2 nanoparticles to the welding electrodes [108]. They also suggest that adding TiO_2 nanoparticles resulted in the increased mass transfer efficiency, hence promoting better deposition/ alloying of the major elements such as Fe, Cr, Ni and Mn in the weld metal rather than oxidizing/ vaporizing to fumes [108]. However, none of these studies explain the differences in Cr(VI) levels between the rutile and the basic electrodes. The only rationale for this extraordinarily high Cr(VI) levels in the rutile electrodes as seen in FTIR and in IC, is the presence of very high levels of Potassium (from the flux material), which probably leads to the dichromate formation.

While FTIR and IC data are consistent with each other, the former is able to identify signature peaks due to dichromates and a marginal presence of chromate, as well. These compounds are

not crystalline as they form via rapid condensation from vapor phase and are thus not visible from powder XRD.

An additional FTIR peak at 964 cm^{-1} occurs likely due to Cr=O vibrations, which is indication of formation of the metastable CrO_3 [109, 110]. There is an ongoing debate regarding formation of CrO_3 in welding fumes since they are formed at high temperature and CrO_3 is not a stable compound after 197^o C as it decomposes into Cr_2O_3 and O_2.

$$\mathbf{2CrO_3 \rightarrow Cr_2O_3 + 3/2\ O_2} \qquad \mathbf{(4.7)}$$

Literature shows that this happens in the stages and is mentioned in the equation below[111, 112].

$$\mathbf{CrO_3 \rightarrow Cr_8O_{21} \rightarrow Cr_6O_{15}\ (Cr_2O_5) \rightarrow (Cr_5O_{12}) \rightarrow Cr_2O_3} \qquad \mathbf{(4.8)}$$

Below equation shows the oxidation stages of Cr in this dissociation reaction.

$$\mathbf{Cr(VI)O_3 \rightarrow Cr(III)_2Cr(VI)_6O_{21} \rightarrow Cr(III)_2Cr(VI)_4O_{15} \rightarrow Cr(III)_2Cr(VI)_3O_{12} \rightarrow Cr(III)_2O_3} \qquad \mathbf{(4.9)}$$

The IR absorption peaks normally visible for Cr_2O_3, or any other Cr(III) compounds are not observed in the welding fume samples, as their relative amount is very low (between 0.1 to 0.4 wt. %).

For comparison, FTIR analysis of chemical grade Cr_2O_3 and CrO_3 was carried out and result is shown in Figure 4.2 and Figure 4.3 respectively. These result for chemical grade Cr_2O_3 shows the vibration peak for Cr–O bond stretching vibration at wavenumbers 608 and 504 cm^{-1} and chemical grade CrO_3 shows the vibrations peaks at 880, 957 and 976 cm^{-1} wavenumbers. Vibration peak at 880 cm^{-1} is also seen in dichromates as they are assumed to have the bridged structure O_3Cr-O-CrO_3 due to which they show vibrations for Cr-O-Cr and internal vibrations for the tetrahedral CrO_4 groups. In pure CrO_3 the peak at wavenumber 880 cm^{-1} appears as well, and this is entirely due the Cr=O vibration. The structure of the planar CrO_3 has three oxygen molecules therefore we also observe three vibrations for Cr=O at 880, 957 and 976 cm^{-1}, i.e., symmetric stretching, anti-symmetric stretching, and a bending vibration[104].

Vibrational modes of chromates show two vibrational frequencies around 850 and 870 cm^{-1}. The CrO_4^{2-} ion, although nearly tetrahedral, is distorted in such a way that there are two long(L)

Cr-O bonds and two short(S) ones. The anion can be written $CrO(S)_2O(L)_2$ and has molecular symmetry. It has generally been observed that force constants vary inversely with bond length, and thus the vibrations involving the Cr-O (L) bonds are likely to occur at lower frequencies than those involving the Cr-O (S) bonds. Using this model, the stretching region of 800 - 950 cm^{-1} should contain 4 bands, a symmetric and an anti-symmetric stretch each for the Cr-O(S) and Cr-O(L) pairs [107].

Chromium Trioxide, CrO_3 is different from the structure of dichromates, as it is planar. This is therefore reflected in differences in the vibrational frequencies in the data.

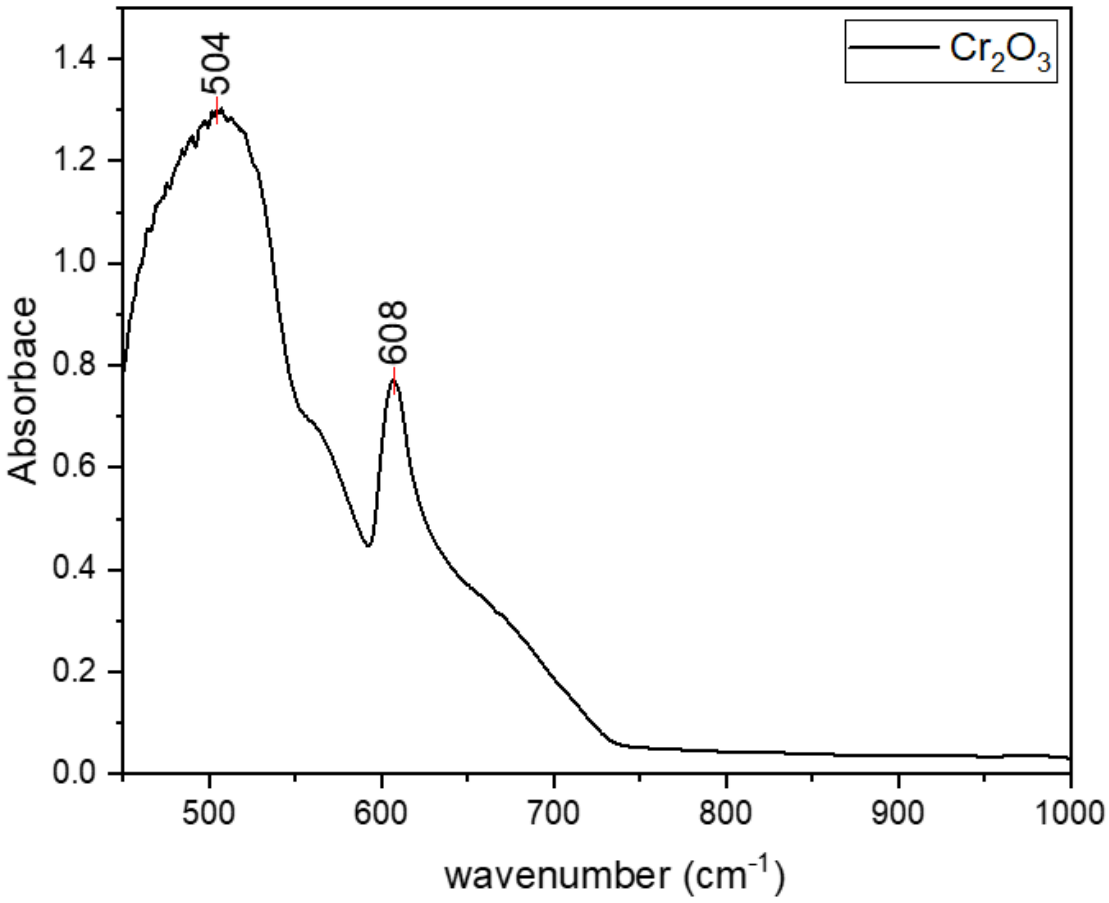

Figure 4.2: FTIR data of Cr_2O_3

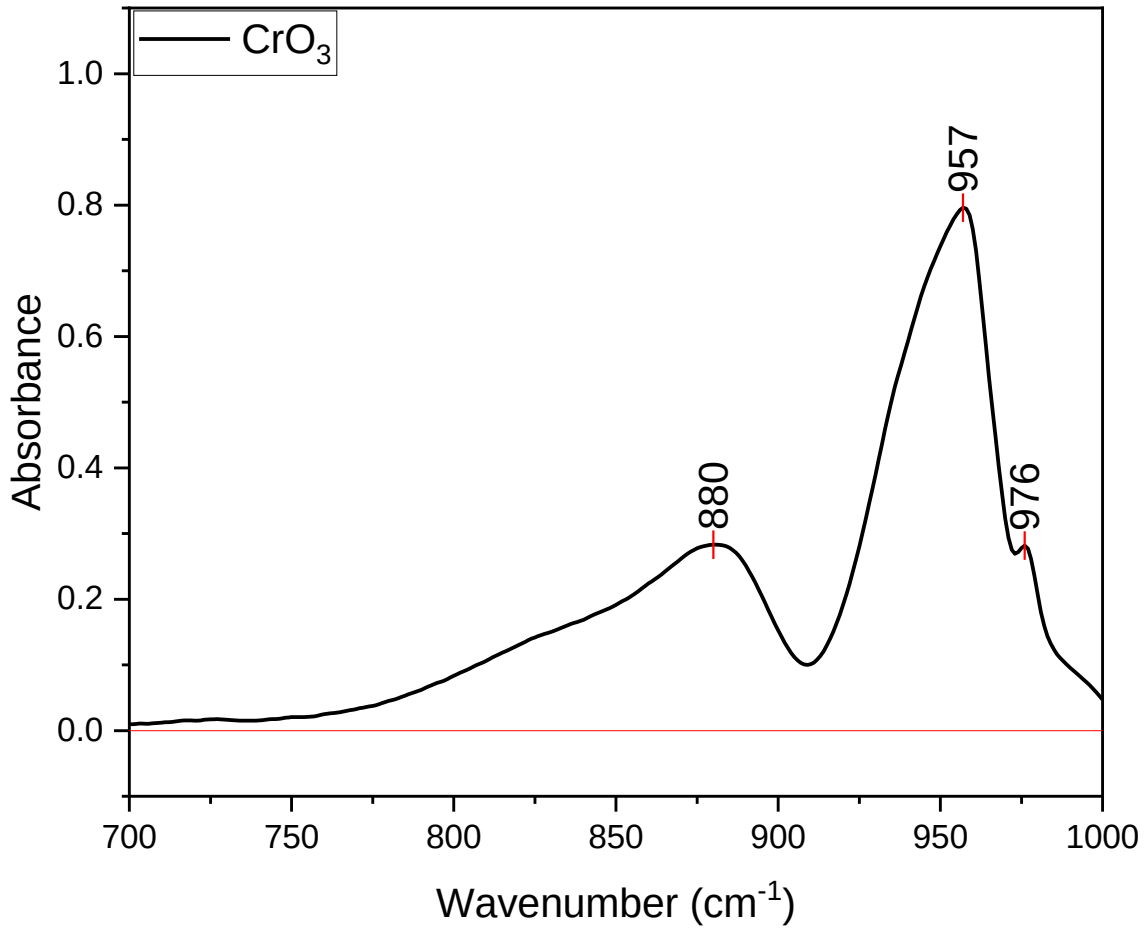

Figure 4.3: FTIR data of CrO_3

To further confirm the presence of CrO_3 at high temperature, nanoparticles which resemble the welding fumes particles were prepared in lab conditions using combustion synthesis[113]. research grade $Cr(NO_3)_3$ was used as the oxidant which has Cr in oxidation state +3 and Urea as fuel. The stoichiometric ratio of both compounds is mixed with each other using 5 ml of deionised water and then then they were kept in furnace for 20 minutes at a pre-set temperature of 600°C. After the combustion synthesis the nanoparticles were taken out from the furnace and then sent for ICP and ion chromatography analysis. FTIR of the sample was also taken and is shown in Figure 4.4. The peak at 976 cm^{-1} shows the presence of CrO_3 and other peaks at 826, 890 and 942 cm^{-1} show the presence of Cr(VI) with the bond vibration of Cr-O-Cr. The peak characteristic of Cr(III) which occurs around 600 cm^{-1} was not recorded in this experiment due to constraints in the equipment, but the ICP and Ion chromatography data confirms the results obtained from FTIR. Moreover, the goal of this experiment was to primarily measure the Cr(VI) from laboratory synthesized samples, and there is no interference from Cr(III) in this measurement.

ICP results show that total chromium content of the model sample was 11.4 wt. % while IC data shows that there is presence of 0.87 wt.% of Cr(VI). Hence majority of the Cr present the sample prepared by combustion synthesis is Cr(III), but they only have a small percentage of Cr(VI) present in the form of CrO_3. Hence, Cr(VI) as CrO_3 may exist under fume formation conditions and is not inconsistent with the thermodynamically favoured Cr(III) oxide formation.

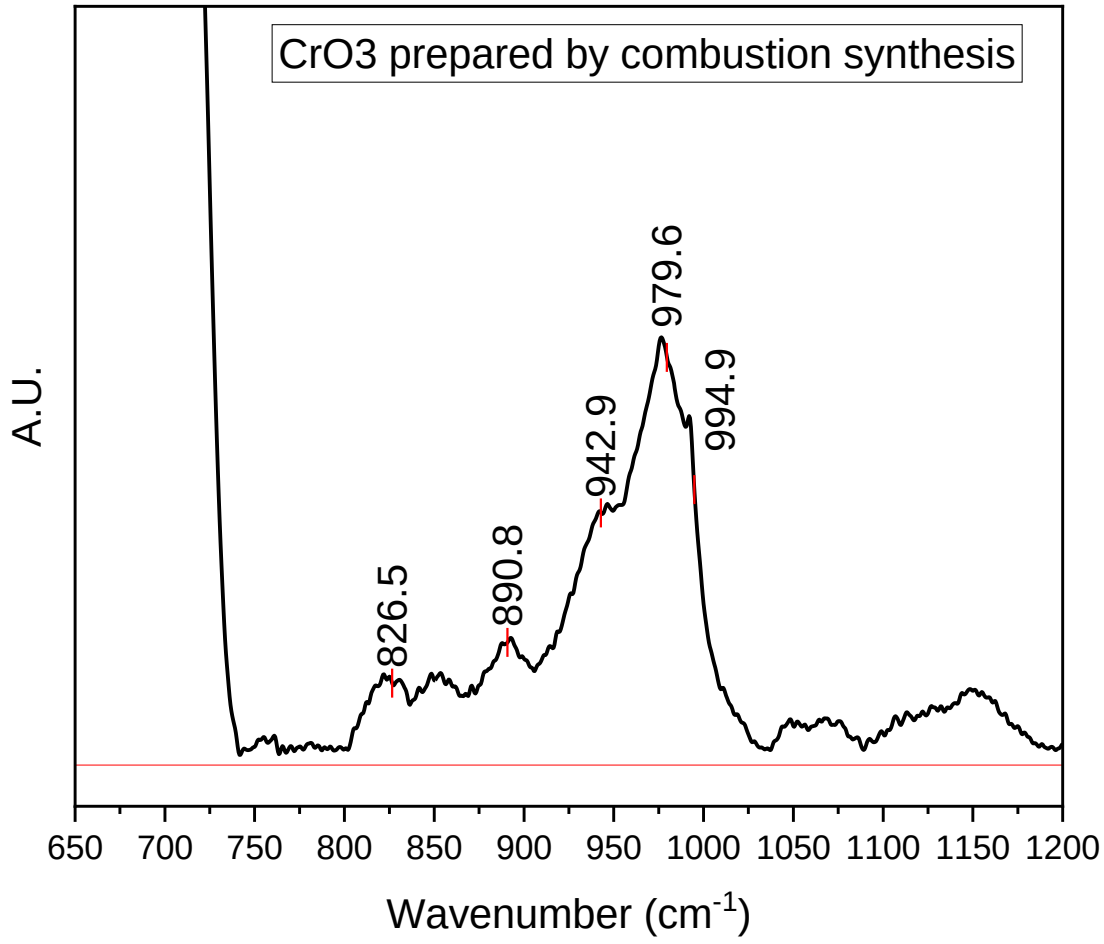

Figure 4.4 : FTIR data of CrO_3 prepared by combustion synthesis.

4.3.1.1.1 Observation of Si peaks in welding electrodes

In rutile electrodes (M3 and M4), also observed, is an absorption band at 990 cm^{-1} which is attributed to Si-O-Si [114]. SiO_2 shows its major peak between 1000-1100 [114-116] which is due to Si-O-Si stretching. In welding fume samples from basic electrodes (M1 and M2), the Si-O-Si peak is observed at 1116 cm^{-1}, which is characteristic peak observed for SiO_2 [116].

The shift in the Si–O–Si bands to lower wave numbers is well explained by Lin et al. [65] in their research article which indicates that when there is increase of silica content in the compound then we see the shift for Si-O-Si to lower wavenumber. This is also observed in the ICP data which indicated the Si content in M1 and M2 to be in the range of 2.4-2.8 %m/m and for M3 and M4 to be in range of 8.5 - 9.1% m/m [65].

Analytical grade Mn_2O_3, SiO_2, $K_2Cr_2O_7$ and K_2CrO_4 and Fe_2O_3 were analysed in lab using FTIR to match the existing peaks of welding fumes from them, and they are shown in Figure 4.5. with their characteristic peaks with the vibrations are shown in Table 4.3. The characteristic peaks in the figure 4.5 were also observed in the welding fume samples.

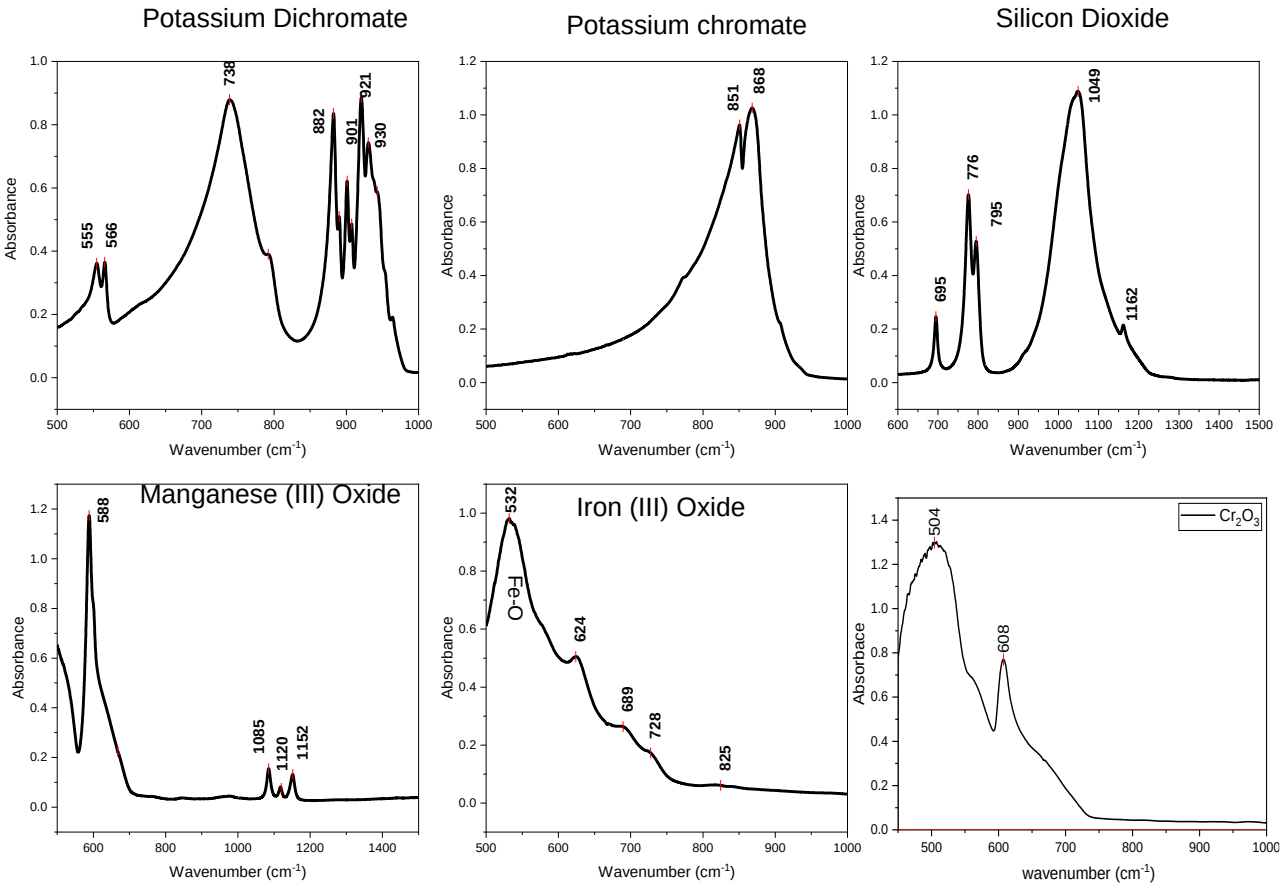

Figure 4.5 : FTIR data of analytical grade compounds founds in welding fumes.

Compounds	IR Absorption frequency (cm^{-1})	Functional groups	References
Potassium Dichromate	555	Cr-O-Cr anti symmetric	[103, 104, 106, 107, 117]
	566	Cr-O-Cr anti symmetric	[104, 107]
	738	Cr-O-Cr symmetric stretching	[104, 107]
	882	$Cr-O_4$ symmetric	[104, 105, 107]
	901	$Cr-O_4$ symmetric	[104, 105, 107]
	921	$Cr-O_4$ anti symmetric	[104, 107]
	930	$Cr-O_4$ anti symmetric	[104, 107]
Potassium Chromate	851	Cr-O-Cr	[104]
	868	Cr-O-Cr	[104]
Silicon Dioxide	695	Si-O-Si bending	[114, 118]
	776	Si-O-Si Symmetric	[114, 118]
	795	Si-O bending	[114, 118]
	1049	Si-O-Si symmetric stretching	[114, 118]
	1162	Si-O-Si anti symmetric stretching	[114, 118]
Manganese (II) Oxide	588	Mn-O stretching vibration	[119]
	1085	O-H bending vibrations joined with Mn	[119]
	1120	O-H bending vibrations joined with Mn	[119]
	1152	O-H bending vibrations joined with Mn	[119]
Iron (III) Oxide	532	Fe-O bending	[120-122]
	624	Fe-O symmetric stretching	[120-122]
	689	Fe-O antisymmetric stretching	[120-122]
Chromium (III) Oxide	504	Cr-O stretching	[123, 124]
	608	Cr-O stretching	[123, 124]

Table 4.3 : Vibration peaks of analytical grade compounds found in welding fumes and their vibration mode.

In summary, FTIR data for the two types of MMA electrodes, was scrutinized in detail, to provide clarity on the spectra. Based on FTIR data for as-procured Chromate (Cr(VI)), Dichromate (Cr(VI)), Chromium Trioxide (Cr(VI), CrO_3), Chromic Oxide (Cr(III), Cr_2O_3) Mn-compounds, Silica, and Iron Oxide, all the major compounds were identified. In future studies, this knowledge will be essential in phase equilibria modelling for fume formation, and in the quantification of specific non-crystalline phases which is also discussed in later chapters.

4.3.1.2 Flux Cored Arc welding (FCAW) fumes

The consumables used for this experiment were stainless steel wires with the core filled with a 'flux'. Samples were designated as FC1, FC2, FC3, FC4 – these samples were generated from 4 different experiments, under similar conditions, with the same flux – therefore, any variations in data obtained between FC1 through FC4, may be purely a statistical variation. A mixture of O_2 and CO_2 was used as shielding gas for all these experiments. Welding was carried out to collect fumes in accordance ISO 15011. All electrodes have a diameter of 1.2 mm and welding was carried out at 90% max current. Fumes during these experiments were collected on cellulose filters and then brushed off and stored in glass vials and then ICP-MS was carried out to detect the elemental composition of these fumes along with ion chromatography for Cr(VI) percentage in welding fume composition. Table 4.4 shows the elemental composition of welding fumes from these results.

Elements	FC1 (%m/m)	FC2 (%m/m)	FC3 (%m/m)	FC4 (%m/m)
Al	1.0	1.1	1	0.9
Bi	5	5.3	3.8	3.8
Ca	<0.1	<0.1	<0.1	<0.1
Cr	4.7	5	5.5	5.4
Cr(VI), Ion Chromatography	2.42	1.65	1.10	1.12
Fe	7.3	8.5	9.4	9.2
K	13.6	12.2	10.3	10.8
Mn	8.9	8.3	8.3	8.3
Na	8.6	7.3	6.3	6.4
Ni	0.6	0.9	1.1	1.1
Si	4.4	3.7	4.2	4.0
Ti	6.4	3.5	4.2	4.0

Table 4.4 : Elemental composition of welding fumes from FCAW electrodes

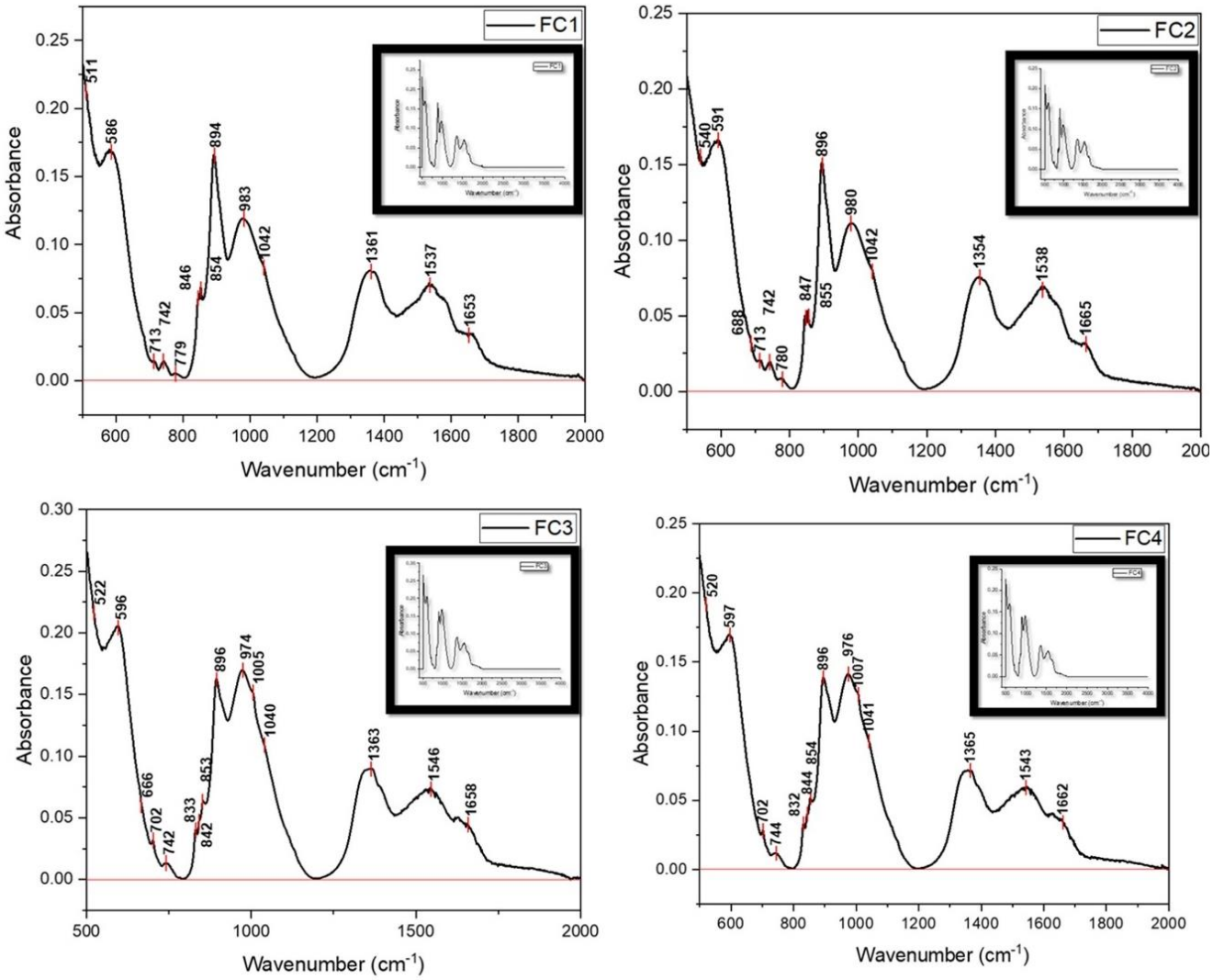

Figure 4.6 : FTIR data of the welding fumes from FCAW (Inset shows the data up to 4000 wavenumber).

Figure 4.6 shows the FTIR data of welding fumes generated by flux cored wires. Major peaks in welding fumes sample FC1 are at wavenumbers 586, 894, 983, 1042, 1361, 1537, 1653 cm^{-1}. The peak at wavenumber 894 cm^{-1} is due to the O-Cr-O_3 tetrahedra indicating formation of dichromates in welding fumes. The peak at 983 cm^{-1} is due to presence of CrO_3 in welding fumes, 1042 cm^{-1} is due to SiO_2, the peaks at 1361 and 1653 cm^{-1} are due to O-H molecular vibrations and can be assigned to in welding fumes. Since the shielding gas used was CO_2, there is possibility of formation of carbon organic compounds in welding fumes and this is what is likely visible in the region of 1535-1540 cm^{-1}. The peak at 586 cm^{-1} is due to stretching vibration of Mn-O and it indicates the presence of Mn_2O_3.

There are smaller peaks in these samples at wavenumber 511, 713, 742, 779, 846 and 854 cm^{-1}. The peak at 742 cm^{-1} is due to vibrations by Cr-O-Cr anti symmetric stretching and consistent with dichromate formation. The peaks at 846 and 854 cm^{-1} are due to formation of chromate compounds as discussed earlier. The peak at 511 cm^{-1} is due to Cr(III) compounds which appears significantly in FCAW fumes. Only a small percentage of Cr(III) generated during welding converts to Cr(VI) compounds. The peak at 713 cm^{-1} is due Fe-O vibration and is due to Fe_2O_3 compounds in welding fumes.

All the welding samples from FCAW has a similar chemical structure as the MMA welds, as they have all the major peaks for vibrations due to iron oxide, chromates, dichromates, chromium trioxide, silicon dioxide and manganese oxide. Small differences lie in the peak around 520 cm^{-1} which appears at 511 cm^{-1} in FC1 and disappears in FC2 but there is an additional peak at 540 cm^{-1} in FC2; this may be due to the interference of Fe_2O_3 with Cr(III) compounds.

Absorbance Intensities of Cr(VI) vibrations in FCAW samples are generally less than that of MMA welding fume samples. Lower absorbance Intensities in FCAW indicates lesser relative amounts of Cr(VI) compounds with respect to MMA (rutile) – this has also been detected in the prior work that flux cored wires produce less amount of Cr(VI) than MMA wires (using IC/ICP) [125, 126]. Partly, this could be explained due to the usage of shielding gases, which were not used in MMA. FTIR once again, shows the presence of Chromates and Dichromates, that come from the alkali metals, which are also visible, in the ICP-MS data, Table 4.4.

4.3.1.3 Solid Wire welding fumes (MIG/MAG)

The consumables used for this experiment were solid stainless-steel wires (SW1-SW3) and solid carbon steel wires (SW4-SW6). Fume samples from these wires were collected and designated as SW1, SW2, SW3, SW4, SW5, SW6.

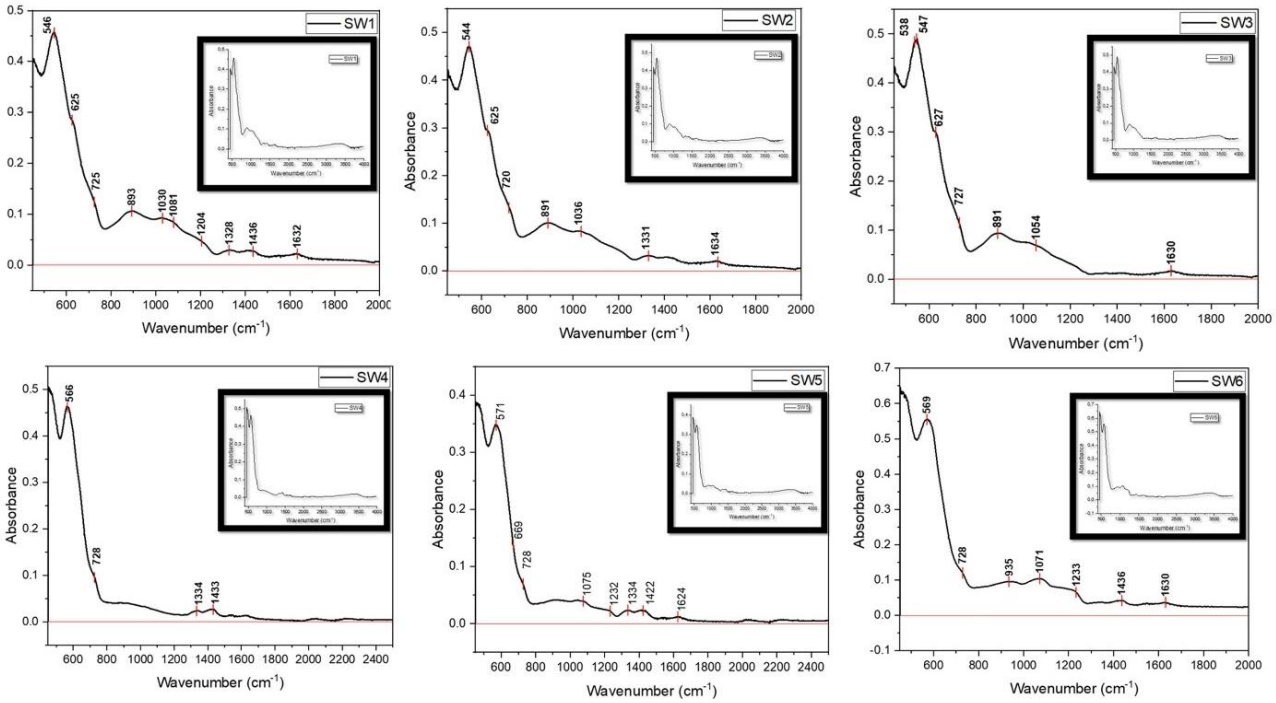

Figure 4.7 : FTIR data of welding fumes from solid wire arc welding (Inset shows the data up to 4000 wavenumber).

Figure 4.7 shows the FTIR data of welding fumes from solid wire arc welding. Compared to FCAW welding fumes and MMA, these welding fumes have lower amounts of Cr(VI) in them (IC data), and this is also borne out in FTIR results, as the absorption intensity of Cr-species at wavenumbers 900-1000 cm^{-1} is much lesser, in comparison to the absorption intensities of MMA fumes and FCAW fumes. Through all the samples analysed from the MIG/ MAG (Solid Wire data), the region for Cr(VI) is only seen as a broad bump between wavenumber 900 to 1000 cm^{-1} – this appears most likely include peaks for Cr(VI) and Si-OH peaks, and since the amount of these compounds formed was very low, they had very low intensity and could not be clearly identified.

Other peaks at 725, 625 and 540 cm^{-1} are due to formation of Fe_2O_3 and can be seen in SW2 and SW1 too. Since these welding fumes contain a majority of Fe in them it is expected they have the highest absorption intensities for these peaks. Due to the presence of large amounts of Fe_2O_3 and Mn_2O_3, peaks which are usually observed in other welding fumes at 575 cm^{-1}, which were not seen in the solid wire fume samples since there is interference by large Fe_2O_3 peaks which are very close to each other. The peak around 1035 cm^{-1} is due to formation of

SiO_2 and are seen in all SW1, SW2, SW3. The peaks at 1328 and 1632 cm^{-1-} are due to OH groups in welding fumes. The peak at 1436 and 1204 cm^{-1} is due to the C-O-C bond, which is likely, due to organic vibrations, due to CO_2 presence in the shielding gas.

The FTIR spectra of SW2 and SW3 welding fumes show major peaks at wave numbers 544, 625, 720, 891, 1036, 1331 and 1634 cm^{-1} which are also seen in SW1 fumes samples. However, there is an absence of C-O-C's vibrational peak, and this is likely, due to the shielding gas used. In SW1 the shielding gas was a mixture of 5% CO_2 and 4% O_2 with Ar whereas it was 8%CO_2 with Ar for SW2 and SW3 fume sample.

In SW3, peaks at 538, 627 and 727 cm^{-1} are due to oxides of iron. However, there is a peak at wavenumber 891 cm^{-1} which is indicative of certain other dichromates (since there is no source of alkali metals.). The peak at wavenumber 1054 cm^{-1} is due to SiO_2 and 1630 cm^{-1} is -OH.
The SW4 samples are from the carbon steel solid electrode and the shielding gas used was 18% He and 1% CO_2 and due to this there was no contact with the atmospheric oxygen and the major compound vibrations which are seen in FTIR results is Fe_2O_3 and moisture at 1334 and 1433 cm^{-1} wavenumber.

Samples SW5 and SW6 show the FTIR peaks at wavenumber 571 and 569 cm^{-1} due to spinel compounds of Mn-O-Mn's vibration. The peak at 738 cm^{-1} wavenumbers is due to Fe_2O_3. There is a small peak of CrO_3 in sample SW5 between wavenumbers of 900-1000 cm^{-1} and at 935 cm^{-1} in SW6 fume sample. The peaks at 1624 and 1334 cm^{-1} are due to moisture and the peak at wavenumber 1075 is due to SiO_2. The FTIR data of welding fumes from welding carbon steel electrodes do not show the sharp peaks for Cr(VI) seen in the other welding fume samples. Ergo from the FTIR spectra, there is very less Cr(VI) in these fumes. Stainless steel wires have 20% Cr in them whereas mild carbon steel wires have 0.15% (Composition given by wire manufacturer). ICP/IC data for MIG/MAG welding was not available due to the small sample size since the fumes generated during MIG/MAG welding were not sufficient for ICP/IC analysis; hence EDX was used for an approximate elemental composition of the fume samples.

4.3.2 Scanning Electron Microscopy (SEM) and EDX

Scanning Electron Microscopy (SEM) images reveal the welding fume particles size distribution (Figure 4.8). Welding fume particles range from nano particles (particle diameters up to 50~300 nm) to micron sized aggregates and are spherical in shape. The majority of the particles are agglomerates, and this has also been reported in literature findings [12, 30, 89, 105, 127-129] . This occurs due to the solidification and oxidation after the metal vaporisation[30]. Particle size may vary, depending upon welding conditions, such as welding voltage[12], shielding gases used for welding[75] and type of weld transfer (such as globular or spray transfer). Welding fume particles from MIG/ MAG welding were notably smaller than the welding fume particles from MMA and FCAW.

Nanoparticles from MMA and FCAW welding were rich in Na, K and Fe due to the likely composition of the flux in the welding wires and this is also demonstrated in the EDX data of these nanoparticles (Table 4.5), which expectedly corroborates with the ICP-MS data for the MMA and the FCAW. The EDX data for the MIG/MAG (Single Wire) shows a high proportion of Fe, and Mn, which is clearly visible in the FTIR data.

Solid wire stainless steel Composition (Normalised wt.%)	**Solid wire carbon steel Composition (Normalised wt.%)**	**MMA rutile Composition (Normalised wt.%)**	**MMA basic Composition (Normalised wt.%)**	**FCAW Composition (Normalised wt.%)**
Si (2.20)	Si (4.3-5.3)	Si (6.5-6.9)	Si (8.9-11.4)	Si (4.1-5.6)
Ni (3.4-4.0)	Ni (0.6-1)	Ni (0.8-1)	Ni (0.7-1)	Ni (0.8-1)
Mn (9.2-11.3)	Mn (11.9-12.5)	Mn (10.9-11.4)	Mn (4.2-6.9)	Mn (10.9-11.4)
Fe (34.9-28.2)	Fe (87.4-98.3)	Fe (10.9-42.2)	Fe (28.3-49.7)	Fe (7.6-11.4)
		Na (7.5-7.9)	Na (7.3-8)	Na (7.5-7.9)
		Al (0.8-0.9)	Al (0.2-0.5)	Al (0.8-0.9)
		K (12.8-14.3)	K (20.3-28.9)	K (14.2-21.2)
			Ti (1.8-2.0)	Ti (1.8-4.2)

Table 4.5: EDX of welding fume particles

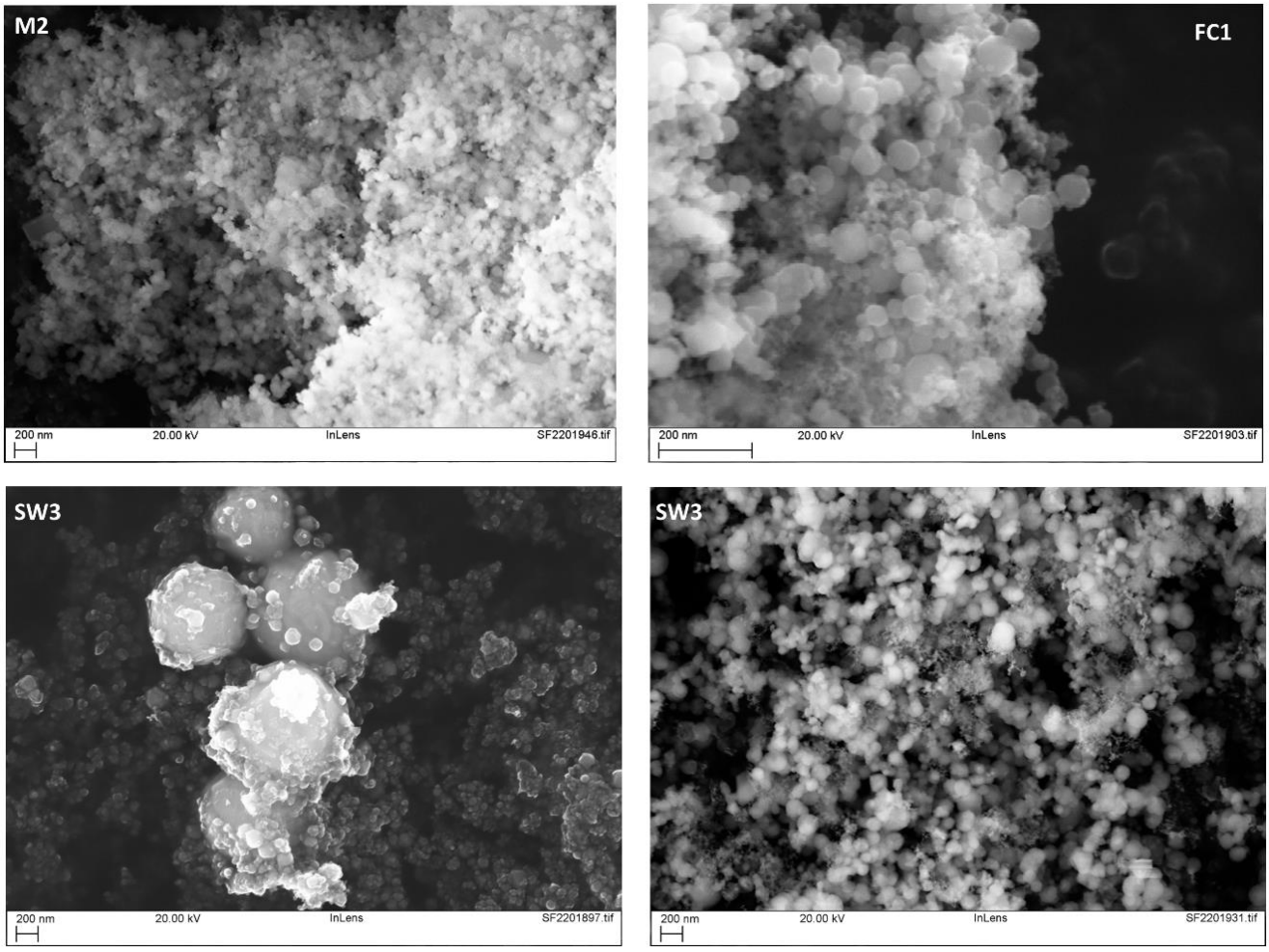

Figure 4.8 : SEM images of welding fume particles (MMA - 54 nm, FCAW- 93 nm, and SW3 32.6 nm, Courtesy: ImageJ software)

4.3.4 XRD

Since the purpose of this work is to understand the speciation of the welding fumes, XRD is also expected to complement the FTIR data, as a way of confirming the various species seen in the fumes.

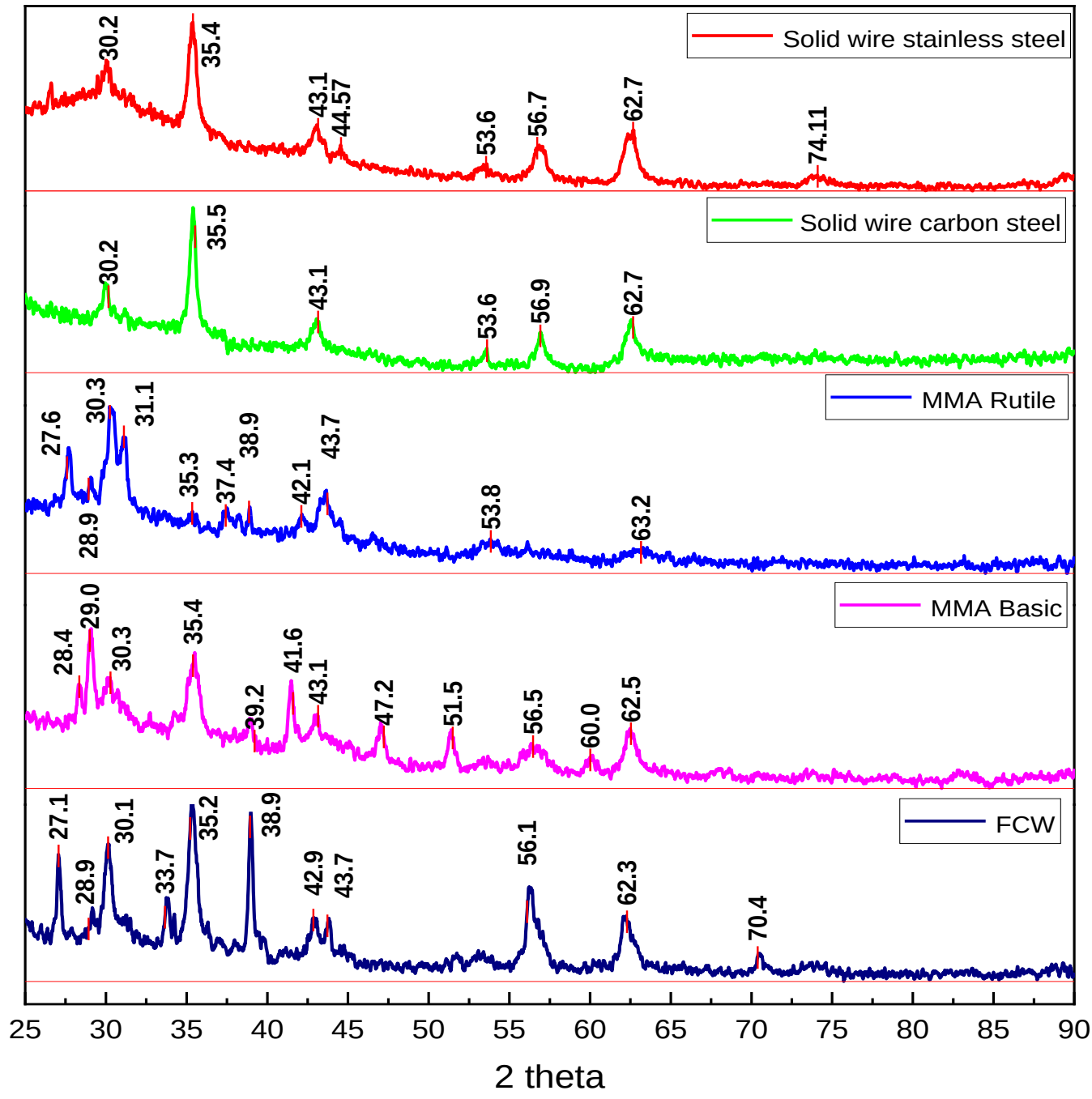

Figure 4.9 : XRD data of welding fumes.

Figure 4.9 shows the XRD data for different types of fumes. In agreement with previous studies, from XRD data it is clear that the solid wire welding fume particles are rich in magnetite (X_3O_4 with X = Fe, with a mixture of Mn and/ or Cr and/or Mn and/or Ni), which is a spinel of iron with manganese oxide[30]. XRD spectra of fumes from FCAW and MMA electrodes shows the alkali-alkaline earth fluoride phases, alongside other phases of mixed spinel iron oxides and Manganese oxides [30, 105]. As discussed by Floros et al. [26], it is likely that Cr^{3+} is stabilized as spinel phases (Cr, Fe, Ni-spinels), while Cr^{6+} finds its way into alkali chromate/ dichromate formations (which is strongly observed in FTIR spectra). Key reflections in the XRD (Figure 10) spectra, at 2θ values of 30.5, 35, 43.1, 56.5, 62.7^o are most likely $MnFe_2O_4$ spinels [53], AB_2O_4 , where the A site is Fe, and B could be a combination of Mn, Cr and/or Ni. However, due to the very small particle sizes (very broad peaks), the A and B sites could also include dopants such as Mn, Cr, and/or Ni in different proportions. The peak at 37.4^o in MMA rutile electrode welding fume particles is identified as titanium oxide, ascertained simply by comparison with standard rutile TiO_2 compounds[130].

4.4 Conclusions

FTIR has been shown to be an alternative method for direct measurement of Cr(VI) in welding fumes, compared to traditional wet chemistry approaches such as Ion Chromatography and Spectrophotometry (with DPC complexation). It is also complementary to elemental analysis like ICP-MS, and analysis of crystalline phases by powder XRD. Welding fumes collected from Arc Welding processes such as Manual Metal Arc (MMA) welding, using basic and rutile electrodes show significant differences in Cr(VI) speciation and intensity, in the FTIR spectra. The primary peaks observed for MMA are at wavenumbers of 729, 735, 895 and 903 cm^{-1} (verified to be from Dichromates), and at 853 cm^{-1} due to chromates. There is considerable clarity in distinguishing the characteristic Cr-O-Cr anti-symmetric vibrations from the symmetric stretching vibrations associated with the CrO_4 tetrahedra, both of which are found only in the dichromates). The intensities of the absorption due to various Cr(VI) vibrations, are much lower for the basic electrodes compared to rutile electrodes (corroborated by IC data), which is can only be rationalized by the presence of Potassium that is known to stabilize the Cr(VI) as dichromates.

Similarly, fumes from Flux Cored Arc Welding (FCAW) were also analysed by FTIR and showed the characteristic absorption wavenumbers for Cr(VI), viz., 742 cm^{-1} (Cr-O-Cr anti-

symmetric stretching), 894 cm^{-1} (symmetric stretching of the CrO_4 tetrahedra), distinctive of Dichromates. A prominent absorption peak, at around 846, 854 cm^{-1} is attributed to Chromate compounds. Comparison of the relative levels of Cr(VI) (from IC) with total Cr (ICP) shows that the Cr(III) does not convert strongly to Cr(VI), under these conditions, compared to MMA. This is most likely due to the 'flux cored' architecture of the electrode and due to the usage of a shielding gas that limits oxygen supply.

For the Solid Wire Welding fumes (MIG/ MAG welding) where no flux material was used in the electrode, shielding gases were used, instead (5% CO_2 and 4% CO_2/Ar; 8% CO_2/Ar; 18% He, 1% CO_2). In all these cases, contact with atmospheric oxygen was minimal, and the overall levels of Cr(VI) seen from both FTIR and from IC, were considerably lesser than MMA and FCAW. The primary peaks reflecting absorption intensities were those on Fe-oxides, and likely, some iron-based spinels. Powder XRD data show crystalline phases in the welding fumes, which are primarily spinel oxides (Fe, Mn, Cr spinels). SEM study reveals the welding fume particles range in size, from about 50-300 nm, and are therefore represent a huge airborne hazard, despite being agglomerated during the collection stage.

In summary, while XRD, ICP, and IC, are useful in terms of identifying spinel phases, elemental analysis, and an overall Cr(VI) content respectively, FTIR can go one step further and identify characteristic vibrational frequencies of the various Cr(VI) bonds, and there with, the individual compounds themselves. Further work on quantification of the absorbances is part of a next chapter.

Chapter V: Quantification of Cr (VI) using FTIR and Electrochemical analysis.

5.1 Quantification using FTIR.

5.1.1 Introduction:

In Chapter IV of this thesis, I have discussed the topic of using Fourier Transform Infrared Spectroscopy (FTIR) for qualitative analysis of welding fumes. From that, it was determined that the majority of particles found in welding fumes are spinal oxides. Additionally, it was noted that there is a wide variety of phases and elements present within these particles. Given the complexity of the composition of welding fumes, quantifying the concentration of Chromium (VI) within these particles is a challenging task.

To address this issue, in this chapter I have tried to explore a method called the "Intensity Ratio Method" which utilizes FTIR to quantify the concentration of Chromium (VI) in welding fumes. This method is explained in detail in this chapter. The Intensity Ratio Method is a way to use the Infrared spectra of the compound of interest and a reference compound to determine the concentration of the compound of interest in a sample. This is done by comparing the intensity of the absorption bands of the compound of interest to the reference compound.

5.1.2 Methodology

The method proposed for quantifying Chromium (VI) in welding fumes is based on Beer's Law, **A = a.b.c**, which states that the absorbance of a substance (A) is proportional to its concentration (c) and the molar absorptivity of the substance (a), as well as the optical path length (b) of the instrument used. In order to use this approach, the molar absorptivity of Chromium (VI) must be known. To determine this value, we use the ratio method.

To determine the molar absorptivity of Chromium (VI) we used the ratio method, where a known amount of Cr (VI) is mixed with a known amount of silica. Silica is used as a reference compound as it is present in all welding fume samples. The absorbance intensity ratio of Cr (VI) to silica is plotted against the weight percentage ratio of Cr (VI) to silica. The slope of the

line generated by this plot gives the λ value, which is the concentration constant. This constant is then used to quantify the concentration of Chromium (VI) in welding fumes. Essentially, by mixing a known amount of Cr (VI) with a known amount of silica and measuring the absorbance of the mixture, they can plot the absorbance ratio against the weight ratio of Cr (VI) and silica, which gives a linear relationship. The slope of this line is the molar absorptivity of Cr(VI) and that is used to determine the concentration of Cr(VI) in the welding fumes.

5.1.3 Calibration samples preparation

As welding fumes contains Cr (VI) in the form of chromates and dichromates we tried to find $\lambda_{chromate}$ and $\lambda_{dichromate}$. To find the λ we made calibration mixtures of potassium chromate and potassium dichromate with known quantities, and we added known quantities of silica and 10ml of distilled water to the mixture. The mixture was sonicated and stirred until a clear mixture was formed and then the mixture was dried in furnace for 10hrs at 110°C. The composition of these sample calibration compounds is shown in table 5.1.After drying the mixture was ground to fine power and FTIR analysis was performed on the samples to see if there are any impurities.

Compound name	Composition
F1	200mg $K_2Cr_2O_7$ + 800mg SiO_2
F2	400mg $K_2Cr_2O_7$ + 600mg SiO_2
F3	600mg $K_2Cr_2O_7$ + 400mg SiO_2
F4	800mg $K_2Cr_2O_7$ + 200mg SiO_2
E1	200mg K_2CrO_4 + 800mg SiO_2
E2	400mg K_2CrO_4 + 600mg SiO_2
E3	600mg K_2CrO_4 + 400mg SiO_2
E4	800mg K_2CrO_4 + 200mg SiO_2

Table 5.1 : calibration samples for quantification

5.1.4 Results and discussions:

FTIR analysis of the calibration samples were done using the same equipment and following the same procedure as explained in previous chapter. The FTIR spectra of these calibration samples is shown in Figures 5.1 and 5.2. These results demonstrate that there were no vibration peaks of any other compounds present in the samples apart from silicon oxide, chromates and dichromates, which confirms that there were no chemical reactions occurring between these compounds during preparation and that these compounds were simply homogeneous mixtures of chromates and dichromates with silica. This proves that the calibration samples are pure and can be used to accurately determine the concentration of Chromium (VI) in the welding fumes.

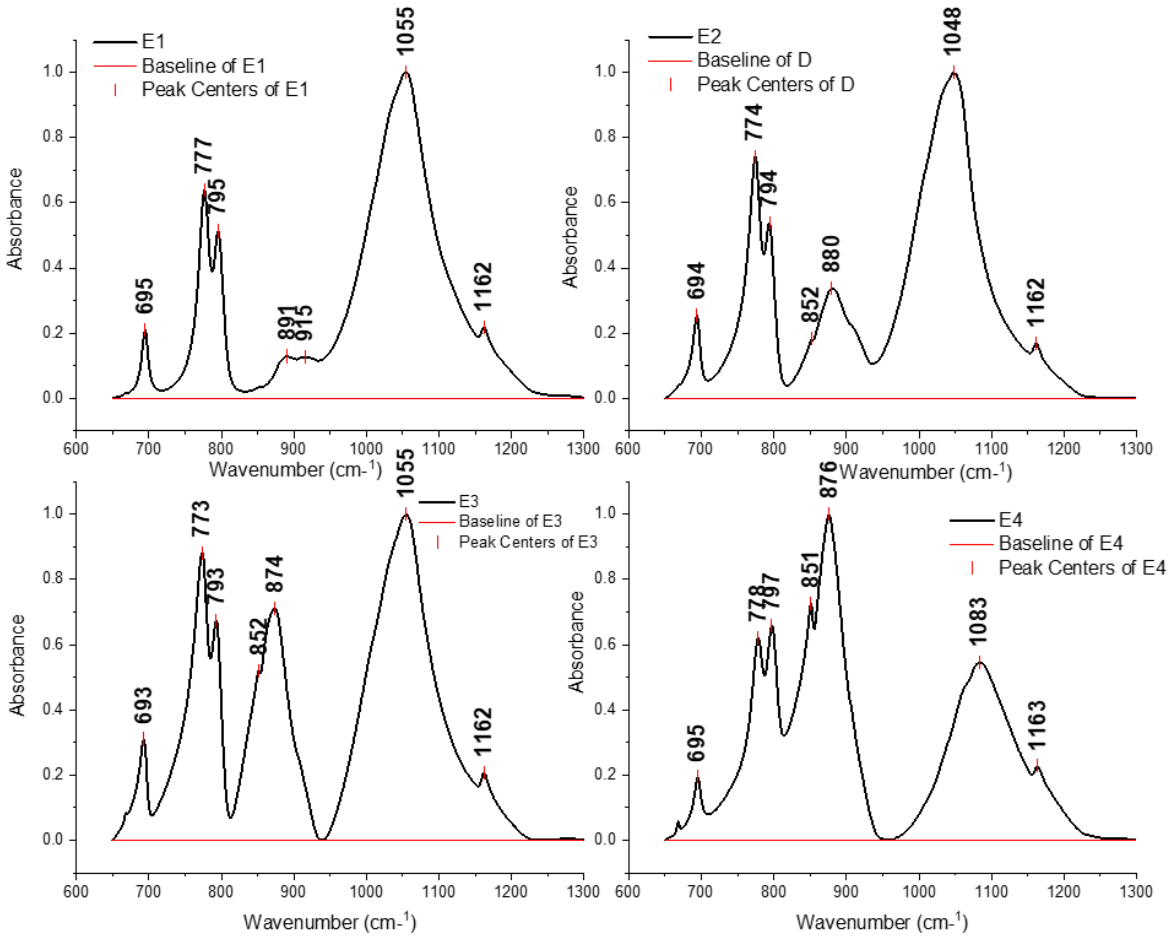

Figure 5. 1 : FTIR data of calibrated samples containing potassium dichromate.

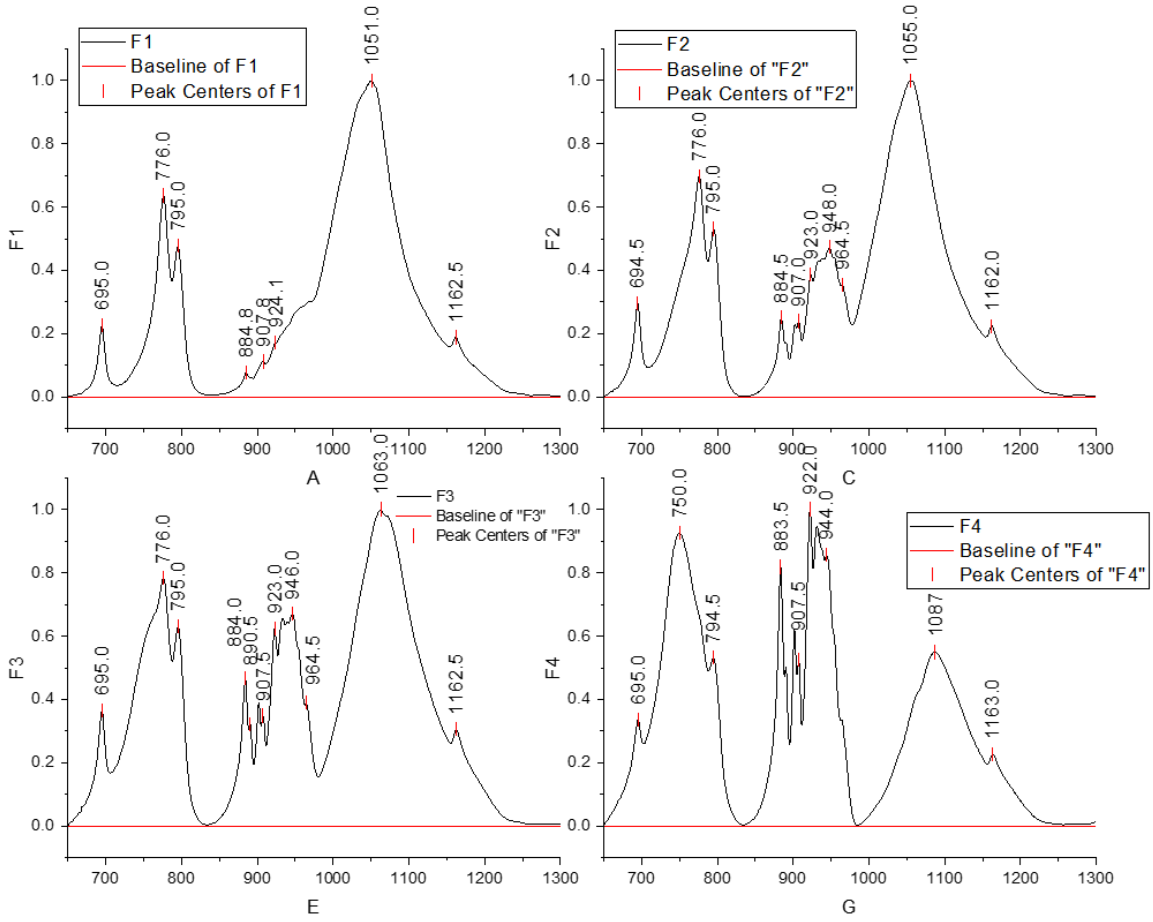

Figure 5.2 : FTIR data calibrated samples containing potassium chromates.

After assuring that there were no new compounds formed beers law was used to calculate $\lambda_{chromate}$ and $\lambda_{dichromate}$.

We assumed A_{Cr} to be the absorbance intensity of Cr (VI) and A_{Si} to be the absorbance intensity of silica.

Hence, using Beer's law, it can be stated:

$$\frac{A_{Cr}}{A_{Si}} = \frac{a_{Cr} b_{Cr} C_{Cr}}{a_{si} b_{si} C_{si}} \qquad \textbf{(5.1)}$$

The instrument is same for all the experiments, hence $\mathbf{b_{cr} = b_{si}}$ and as a result equation (5.1) can be written as

$$\frac{A_{Cr}}{A_{Si}} = \frac{a_{Cr} C_{Cr}}{a_{si} C_{si}} \qquad \textbf{(5.2)}$$

Equation (ii) can again be written as:

$$\frac{\frac{A_{Cr}}{A_{Si}}}{\frac{C_{Cr}}{C_{Si}}} = \frac{a_{Cr}}{a_{Si}} = \lambda = Slope \qquad (5.3)$$

To calculate λ, graphs were produced by plotting ratios of calibration samples F, absorbance intensities of Cr(VI) and absorbance intensities of Si were plotted on y-axis (from FTIR) and weight percentage of potassium chromate/potassium dichromate with weight percentage of silica in the sample were plotted on the x-axis. Plots of these intensities are shown in fig 5.3 and 5.4.

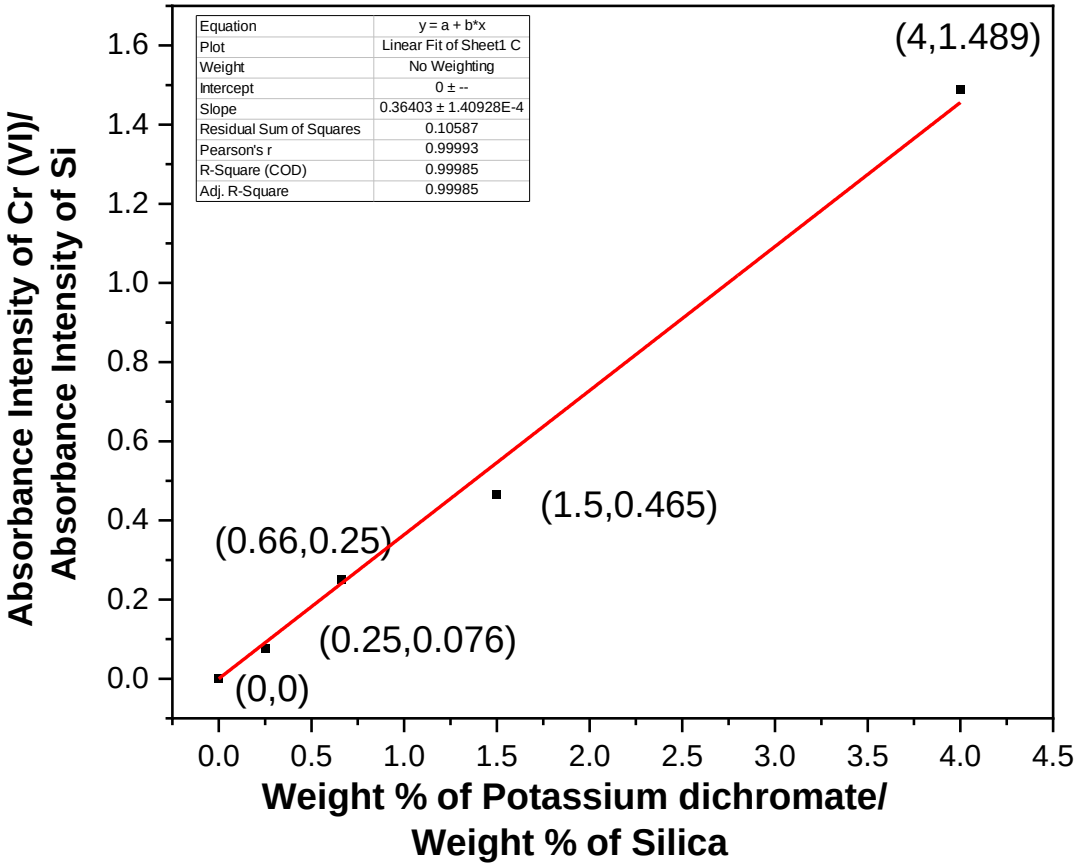

Figure 5.3 : Graph for λ dichromates

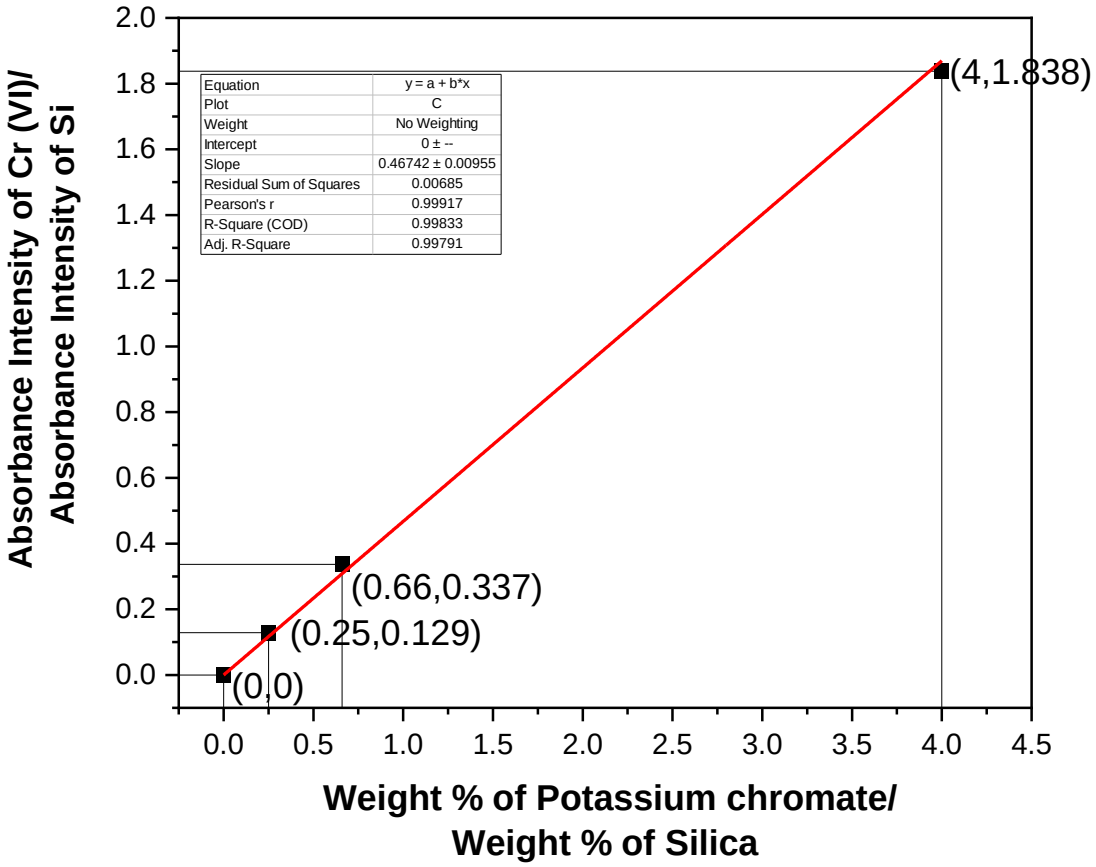

Figure 5.4 : Graph for λ chromates

After getting the values of λ for chromates and dichromates from these plots, the concentration ratio of Cr (VI)/Si in welding fumes were calculated. Equation 5.4 was used to calculated total Cr (VI) concentration in welding fumes. The amount of Si present in welding fumes was known via ICP data.

$$Total\ Cr(VI) = \sum_{i=1}^{N} \lambda_{Cr(VI),i} I_{Cr(VI),i} \quad \textbf{(5.4)}$$

Since there were multiple peaks for chromates and dichromates present in the welding fumes samples we needed to add all the concentrations from all the peaks.

Thus, FTIR can be used to calculate the Cr (VI) concentration in welding fumes which is shown in table 5.2. The ICP data and the welding fumes samples are same which were discussed in chapter IV.

Sample	Cr (VI)/ Si FT-IR	$Cr(VI)_{IC}$/ Si_{ICP}
M1	4.9	0.16
M3	3.28	0.31
M4	0.74	0.56
M5	0.55	0.51
F3	0.84	0.26
F4	0.77	0.28

Table 5.2 : Results of Cr (VI)/Si via intensity ratio method and ICP/Icon chromatography method.

The results of the study indicate that the ratio method is not highly precise when applied to welding fumes. This is because the selection of peaks is crucial for this method, and there were multiple peaks for Cr(VI) vibrations present in the welding fumes, making it challenging to calibrate all the vibrational peaks accurately. Additionally, the ratio method has limitations as it requires the calibration samples to be prepared with great care. In this specific case, the method did not yield the desired results as the Si peak used in the calibration samples was distinct from the Si peak found in the welding fume samples. Hence additional samples were prepared using different form of SiO_2. to understand their calibration curve and analyze if they can be used to detect the Cr(VI) percentage in welding fumes.

The samples prepared are listed in the table below along with their compositions:

Sample Name	Sample composition	Silica used
Si1(a)	800mg $K_2Cr_2O_7$ + 200mg SiO_2	Amorphous Silica anhydride
Si1(b)	600mg $K_2Cr_2O_7$ + 400mg SiO_2	Amorphous Silica anhydride
Si1(c)	400mg $K_2Cr_2O_7$ + 600mg SiO_2	Amorphous Silica anhydride
Si1(d)	200mg $K_2Cr_2O_7$ + 800mg SiO_2	Amorphous Silica anhydride
Si2(a)	800mg $K_2Cr_2O_7$ + 200mg SiO_2	Silica sand/White Quartz
Si2(b)	600mg $K_2Cr_2O_7$ + 400mg SiO_2	Silica sand/White Quartz
Si2(c)	400mg $K_2Cr_2O_7$ + 600mg SiO_2	Silica sand/White Quartz
Si2(d)	200mg $K_2Cr_2O_7$ + 800mg SiO_2	Silica sand/White Quartz

Si3(a)	800mg $K_2Cr_2O_7$ + 200mg SiO_2	Silicon dioxide nanoparticles 10-20nm
Si3(b)	600mg $K_2Cr_2O_7$ + 400mg SiO_2	Silicon dioxide nanoparticles 10-20nm
Si3(c)	400mg $K_2Cr_2O_7$ + 600mg SiO_2	Silicon dioxide nanoparticles 10-20nm
Si3(d)	200mg $K_2Cr_2O_7$ + 800mg SiO_2	Silicon dioxide nanoparticles 10-20nm
Si4(a)	800mg $K_2Cr_2O_7$ + 200mg SiO_2	Silica fumed
Si4(b)	600mg $K_2Cr_2O_7$ + 400mg SiO_2	Silica fumed
Si4(c)	400mg $K_2Cr_2O_7$ + 600mg SiO_2	Silica fumed
Si4(d)	200mg $K_2Cr_2O_7$ + 800mg SiO_2	Silica fumed

Table 5.3 : Additional Calibration samples for quantification

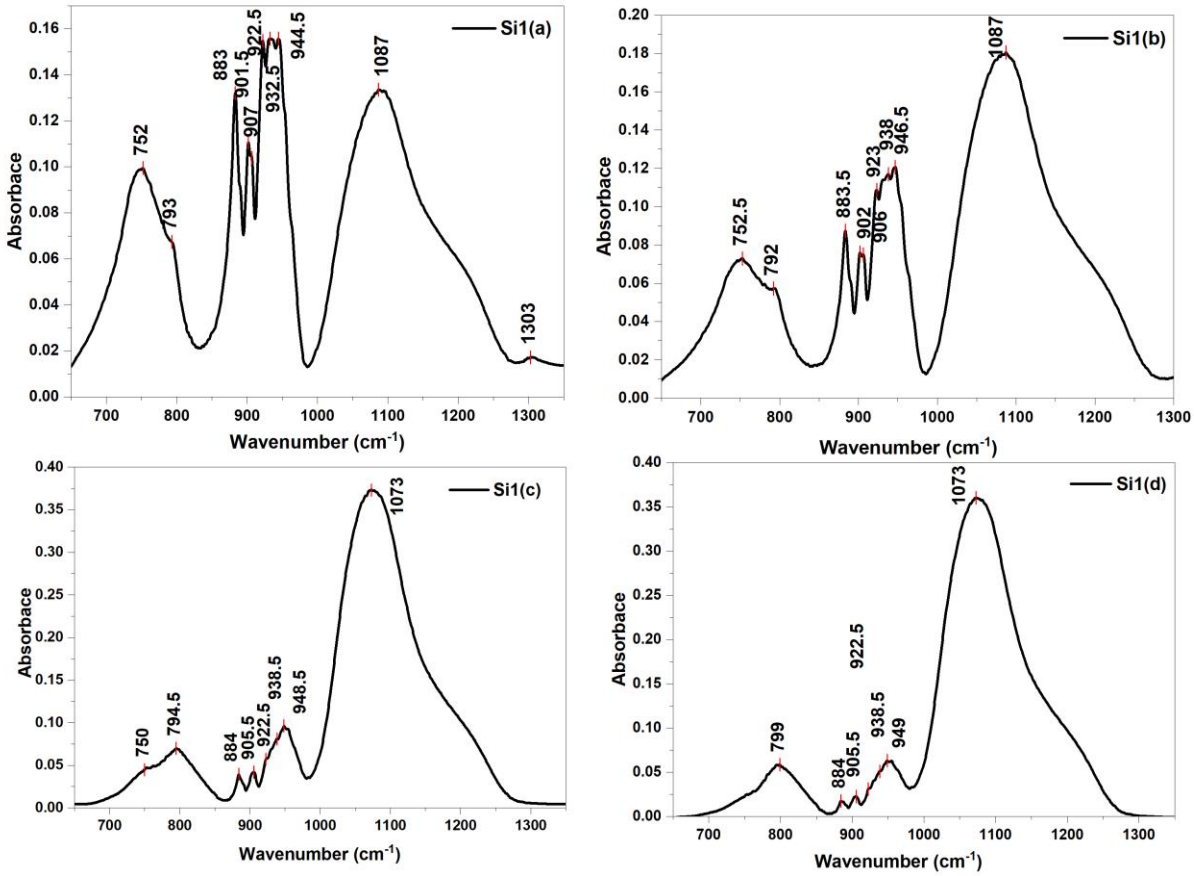

Figure 5.5 : FTIR data calibrated samples containing Amorphous Silica anhydride.

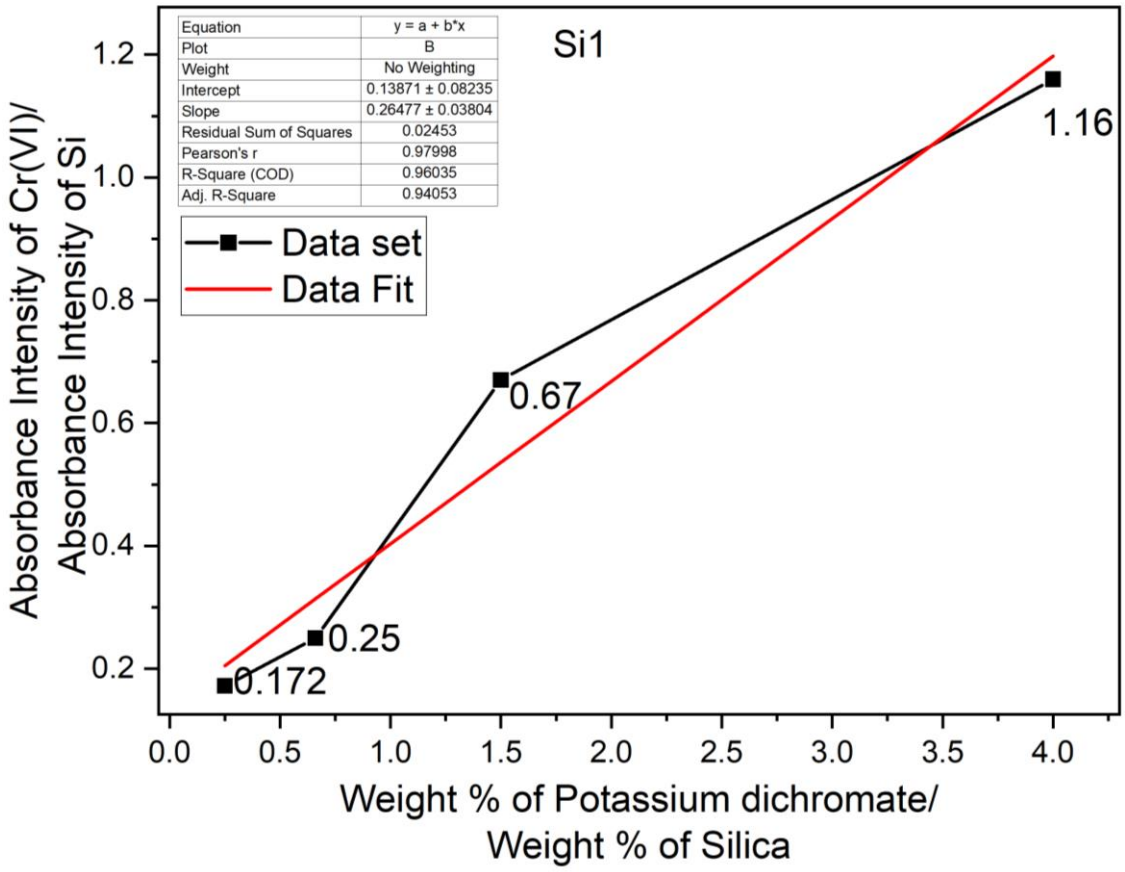

Figure 5.6 : Graph for λ Amorphous Silica anhydride

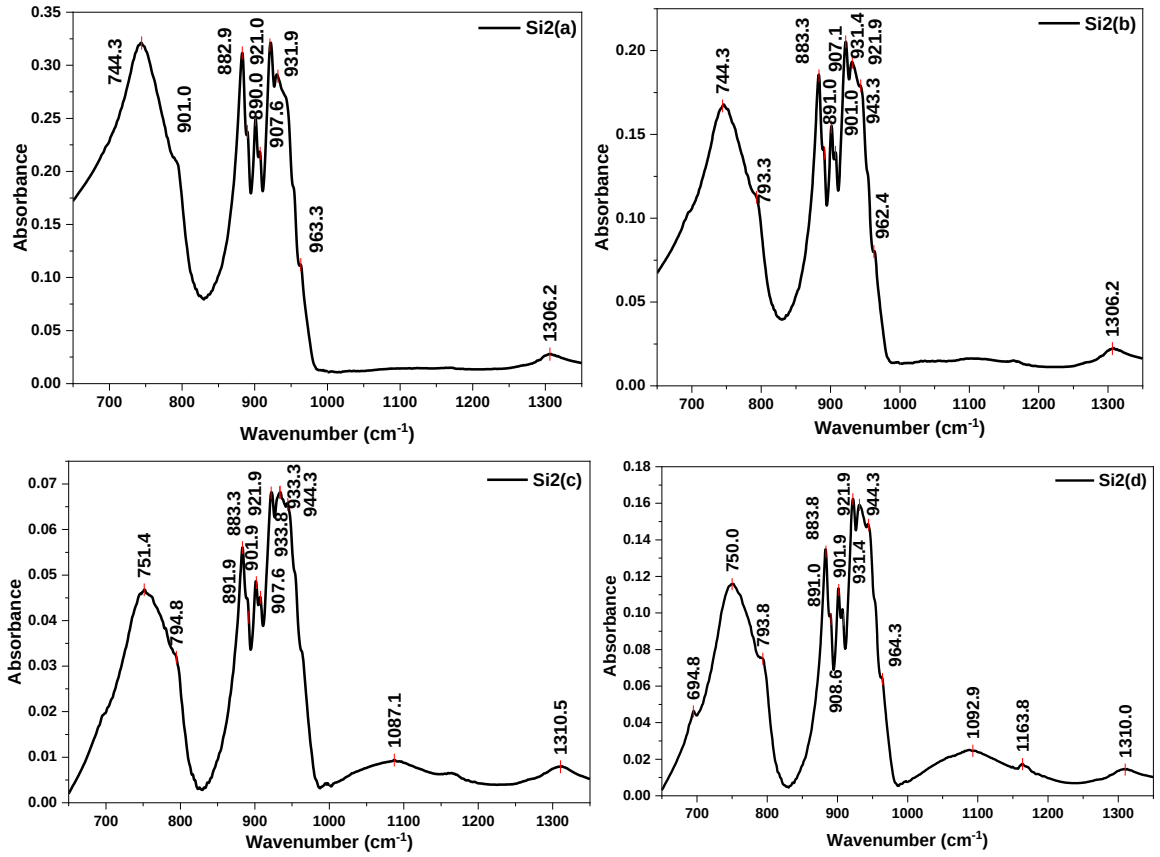

Figure 5.7 : FTIR data calibrated samples containing Silica sand/White Quartz.

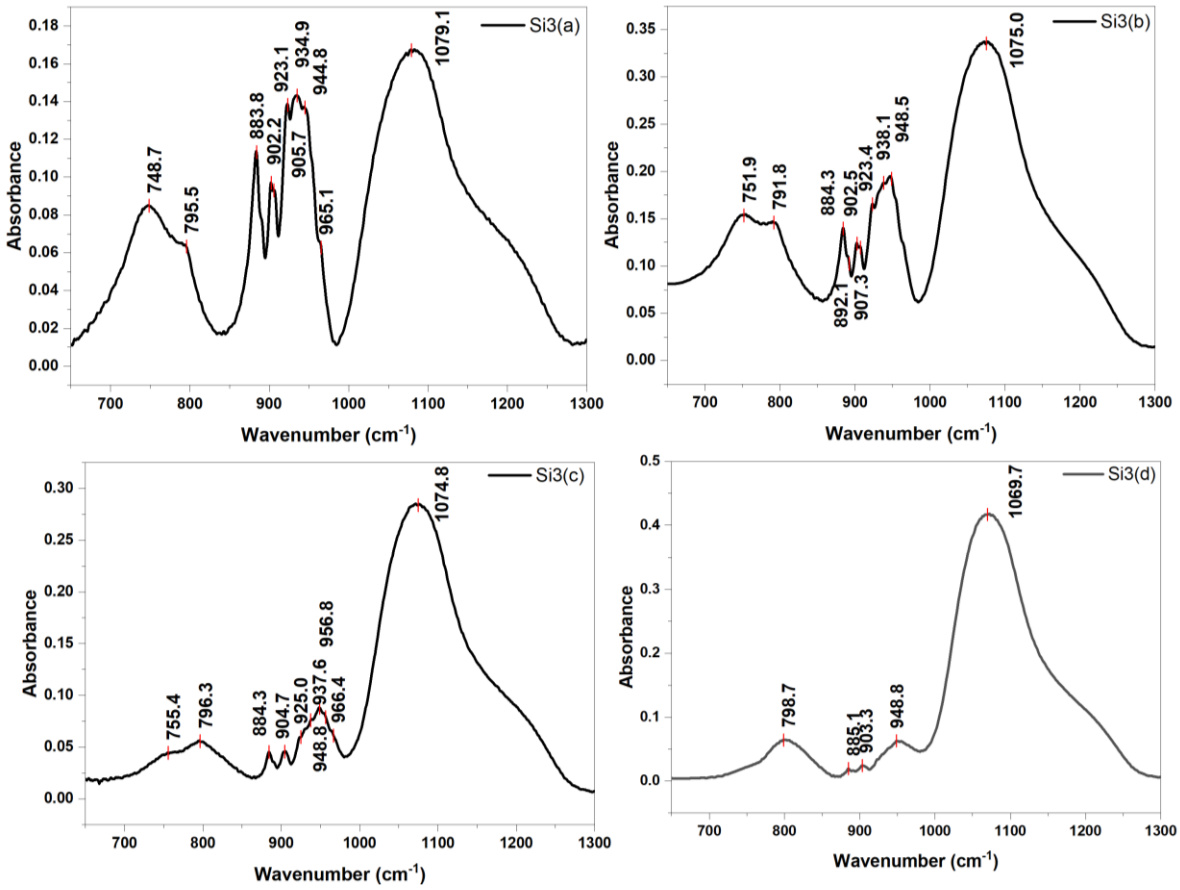

Figure 5.8 : FTIR data calibrated samples containing Silicon dioxide nanoparticles 10-20nm.

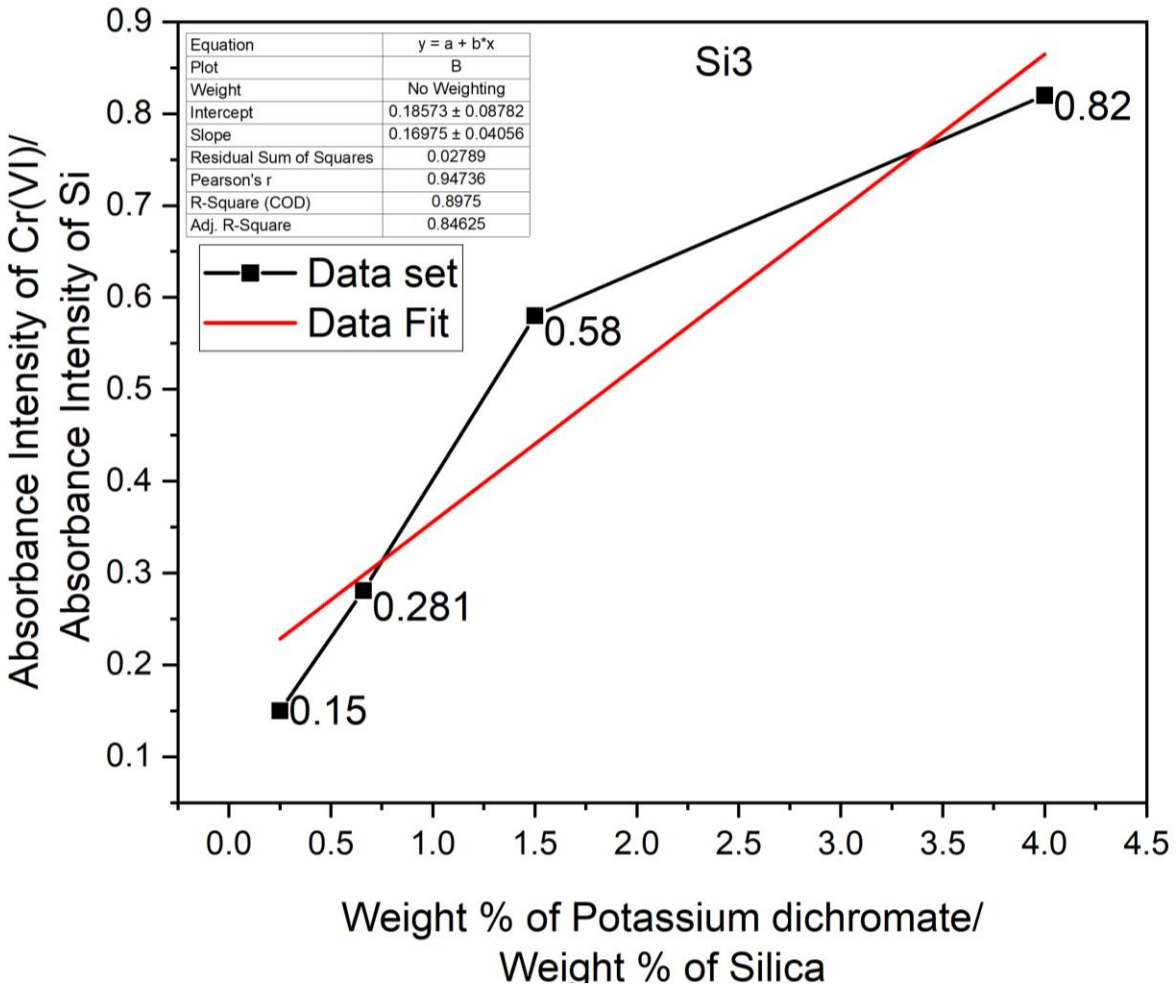

Figure 5.9 : Graph for λ Silicon dioxide nanoparticles 10-20nm

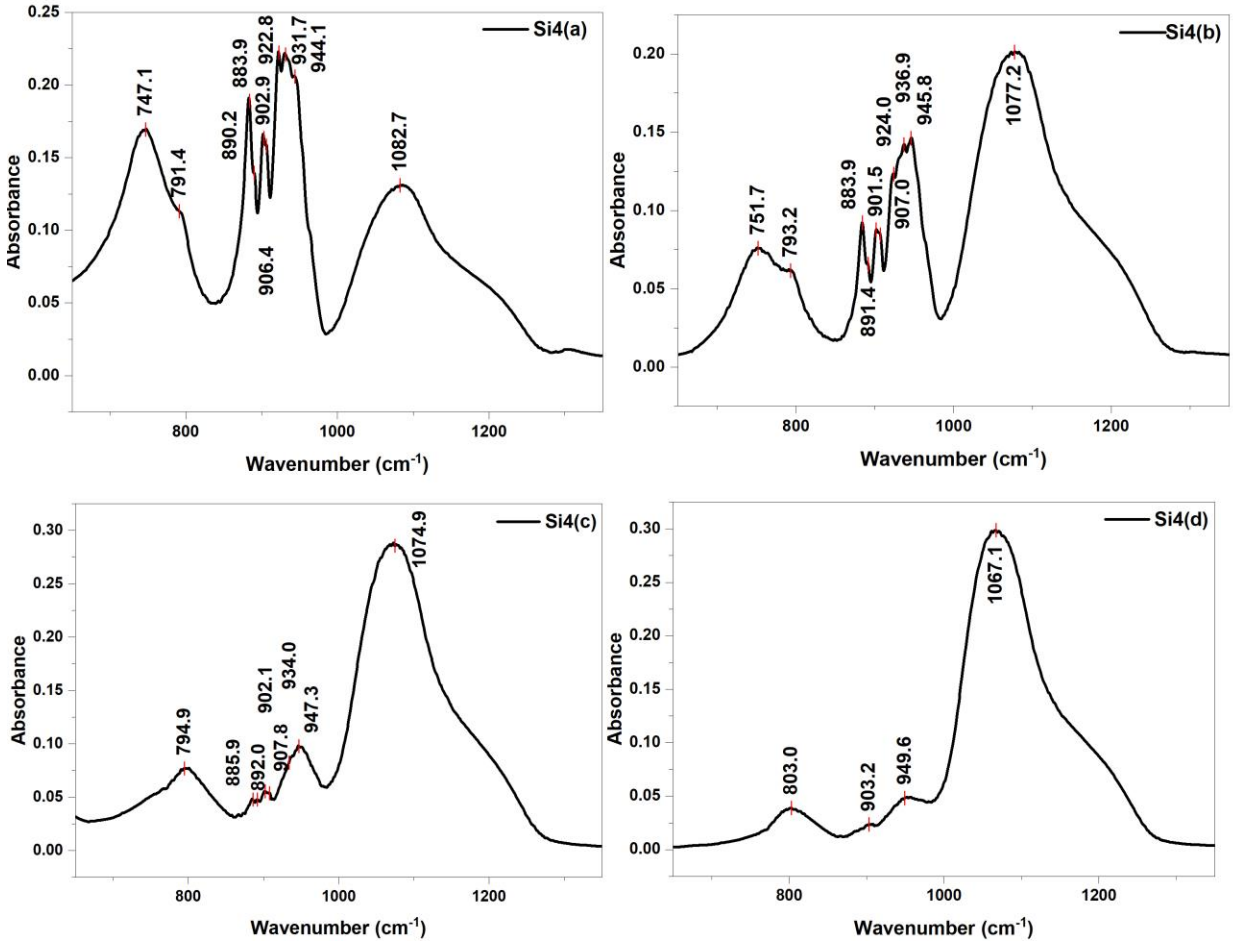

Figure 5.10 : FTIR data calibrated samples containing Silica Fumed.

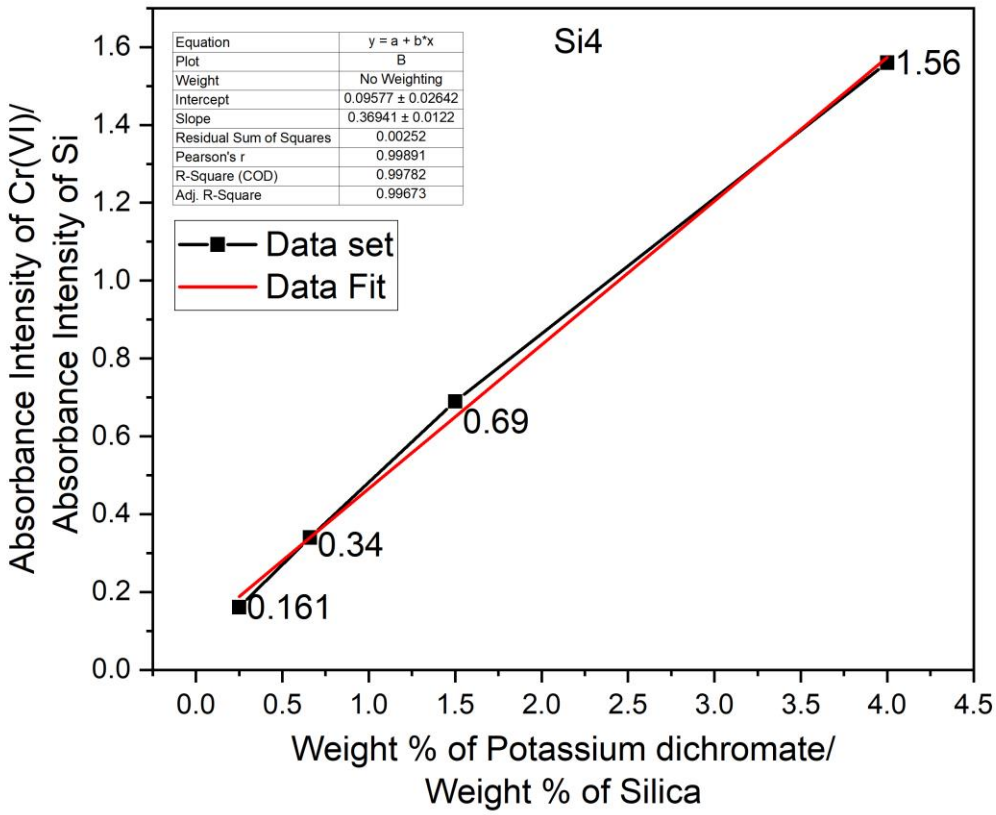

Figure 5.11 : Graph for λ Silica Fumed.

Figures 5.5, 5.7, 5.8, and 5.10 exhibit the FTIR spectra of various calibration samples, each comprising different types of silica. However, Figure 5.7 lacks any discernible silica peak, which is typically observed in welding fumes and other silicates. This absence of a peak suggests the possible absence of crystalline silica in welding fumes. Consequently, samples Si2(a)-Si2(d) were excluded from the parameter (λ) determination. The calculated values of λ obtained from samples Si1, Si2, and Si4 were 0.263, 0.169, and 0.369, respectively. These λ values were later employed to ascertain the Cr(VI) ratio in welding fumes. The results revealed inconsistencies between the Cr(VI) values determined using the intensity ratio method and the ICP method. Several factors could be contributing to this discrepancy:

Complex Formation: Silica in welding fumes might form complexes with other elements, hindering accurate identification using FTIR. The Si-O vibrations from these minute complex compounds are not easily detectable by FTIR, leading to potential underestimation or misidentification of certain species.

Formation of Other Compounds: Besides Silica, Chromium (Cr) could form various compounds in welding fumes. These compounds might be challenging to identify using FTIR, resulting in incomplete analysis and potentially excluding important species from the results.

Limitations of FTIR: Despite its potency, FTIR has limitations. It may not capture certain chemical species or accurately detect trace amounts, which could impact the overall determination of Cr(VI) in the samples.

Overlapping Peaks: In complex samples, multiple analytes may have overlapping peaks in the infrared spectrum, making it difficult to precisely quantify individual components. Deconvolution techniques and multivariate analysis could be used to address this limitation, but it remains a significant challenge.

Sensitivity: FTIR might lack the sensitivity of other analytical techniques like chromatography or mass spectrometry. It may not detect analytes present at low concentrations, particularly in complex matrices.

Despite these limitations, with further research to address these shortcomings, the intensity ratio method can be enhanced.

5.2 Electrochemical analysis

5.2.1 Introduction

In this part, I have explored the possibility of using electrochemistry for detection of Cr(VI) in welding fumes, which can be possibly used in developing electrochemical sensors. These sensors can directly be used in industries for constant monitoring of the Cr(VI) exposure to the welders.

Electrochemical sensors are basically the devices that use electrochemical processes to measure various physical and chemical parameters. Presently these sensors are being used widely in many applications such as medical diagnostics, environmental monitoring, and industrial process control. These sensors are very advantageous as they have high sensitivity, and they can be selective too. These sensors are very accurate and can detect very low concentrations of analytes and can also differentiate between similar compounds[131]. Additionally, many electrochemical sensors are relatively inexpensive and easy to use.
These sensors are mainly divided into two types:

- Amperometry sensors
- Potentiometric sensors

Amperometry sensors uses current, while potentiometric sensors use a voltage. In medical fields amperometry sensors are widely used to detect the amount of lactose, glucose and other biomolecules in blood and other body fluids. Most of glucose meters works on these sensors for measuring blood sugar levels in diabetic patients.

Potentiometric sensors are used mainly in the environmental monitoring such as to measure the pH, ion concentration in water and soil samples. Potentiometric analysis is also used commonly in industries to measure the concentration of dissolved oxygen, chlorine, and other chemicals in water and other liquids. Electrochemical analysis has proved very powerful for metal analysis because of the rapid response and easy operation[131-133].

In order to facilitate the development of these sensors, a comprehensive comprehension of the electrochemical behaviour of Cr(III) and Cr(VI) is imperative. The optimal approach to attain

a profound understanding of their electrochemical behaviour lies in the application of cyclic voltammetry. Cyclic voltammetry (CV) represents a potent and widely utilized electrochemical technique, employed primarily for investigating the reduction and oxidation processes of molecular species[134-136]. Furthermore, this method proves invaluable in the examination of chemical reactions initiated by electron transfer events[136]. Cyclic voltammetry consists of several distinct stages: (1) the initial potential is set, (2) the potential is swept in either a forward or reverse direction, (3) the potential is scanned back to its original value, and (4) the scan is reversed to complete a cycle. This process can be repeated multiple times to obtain steady-state voltammograms and average out experimental noise. The CV technique can be performed under different experimental conditions, including variations in the scan rate, potential range, and electrolyte composition. These variables enable researchers to study the kinetics of electrochemical reactions, adsorption phenomena, and diffusion processes, among others.
The occurrence of oxidation or reduction at the electrode surface is intrinsically associated with the electrode potential. The potential applied to the electrode induces ions in the solution to either gain or lose electrons. A more negative potential signifies a strongly reducing electrode, while a more positive potential indicates a highly oxidizing electrode. As a result, by controlling the electrode potential within an electrochemical cell, the redox reaction taking place at the electrode-electrolyte interface can be manipulated and regulated[134, 136].

Thus, it becomes essential to investigate the electrochemical reactions transpiring at the electrode-electrolyte interface. Cyclic voltammetry emerges as a potent tool for comprehensively studying the electrochemical behaviour of a system through systematic analysis of current-voltage measurements obtained from the electrochemical cell under investigation.

5.2.2 Materials and method

5.2.2.1 Selection of electrolyte

The reduction of dichromate to chromic ions using various cathodes, such as carbon, lead, stainless steel, titanium, and copper, have been studied in acid solutions containing Cr(VI) from the electroplating industry and their rinsing waters[137]. However, hydrogen evolution can occur as a secondary reaction, leading to low current efficiency and passivation of the electrode surface shown in equation (5.6).

$$HCrO4^{-} + 7H^{+} + 3e^{-} \leftrightarrow Cr^{3+} + 4H_2O \quad (5.5)$$

$$H_3O+ + 2e^{-} \rightarrow H_2 + OH^{-} \quad (5.6)$$

Owlad et al. have reported the precipitation of chromium compounds when carbon cathodes are used without pH control[138]. Some research also showed the low current efficiency for reduction reaction of dichromats ions and passivation of electrode surface in acid electrolyte[139]. At low pH and concentrations of Cr(VI) in water, the main species present is $HCrO_4^-$. As the pH becomes more neutral to basic, the predominant species shifts to CrO_4^{2-} equation (5.7).

$$H_2CrO_4 + H_2O \leftrightarrow HCrO^{-}_4 + H_3O^{+} \quad (5.7)$$

Polarographic studies of Cr(VI) reduction by Lingane et al. using Hg electrodes shows that when NaOH is used as an electrolyte shows that in highly basic conditions, the peak for reduction of Cr(VI) is observed at 0.85 V vs. SCE(standard calomel electrode) [140]. This peak was observed to be independent of concentration (in the 0.47 to 2.1 mM range) and it also attributed to the reduction of CrO_4 to Cr(III) in the form of CrO_2 . In unbuffered solutions with KCl as the electrolyte, the more complex behaviour of Cr(VI) is observed, four distinct peaks were observed. One of these peaks was due to the formation of a film on the electrode (chromic hydroxide or basic chromic chromate). The highly acidic and reactive nature of H_2CrO_4 and formation of film on the bare electrodes renders measurement challenging. There is also possibility of formation of many complexes by chromates and dichromates at low PH. Thus, for our experiments we have used NaOH solution.

5.2.2.2 Sample preparation

0.5M NaOH and 0.5M NH_4OH solution was used as an electrolyte for all our experiments. For fume sampling the sample was mixed and then heated at 80°C for 40 minutes to dissolve the insoluble Cr(VI) compounds.

5.2.2.3 Electrode selection

Three electrode system was used for the analysis, where working electrode was glassy carbon, the reaction of Cr(VI) reduction happens at the working electrode. Platinum wire was used as counter electrode and Ag/AgCl electrode was used as reference electrode.

5.2.3 Results and Discussions

The main objective of these electrochemical experiments was to explore the possibility of analysing and quantifying Cr(VI) in welding fumes. Hence first approach was to identify Cr(VI) and find the most suitable scan rate for our electrochemical reaction. For this, cyclic voltammetry experiment was conducted using potassium dichromate and NH_4OH solution as electrolyte at varying scans rate which is shown in Fig 5.5. In cyclic voltammetry different voltage is applied to the electrode and the current is recorded for the applied voltage. Cyclic voltammetry is an important experiment to find the voltage at which the reduction of Cr(VI) happens which in our experiment occurs at 0.6V.

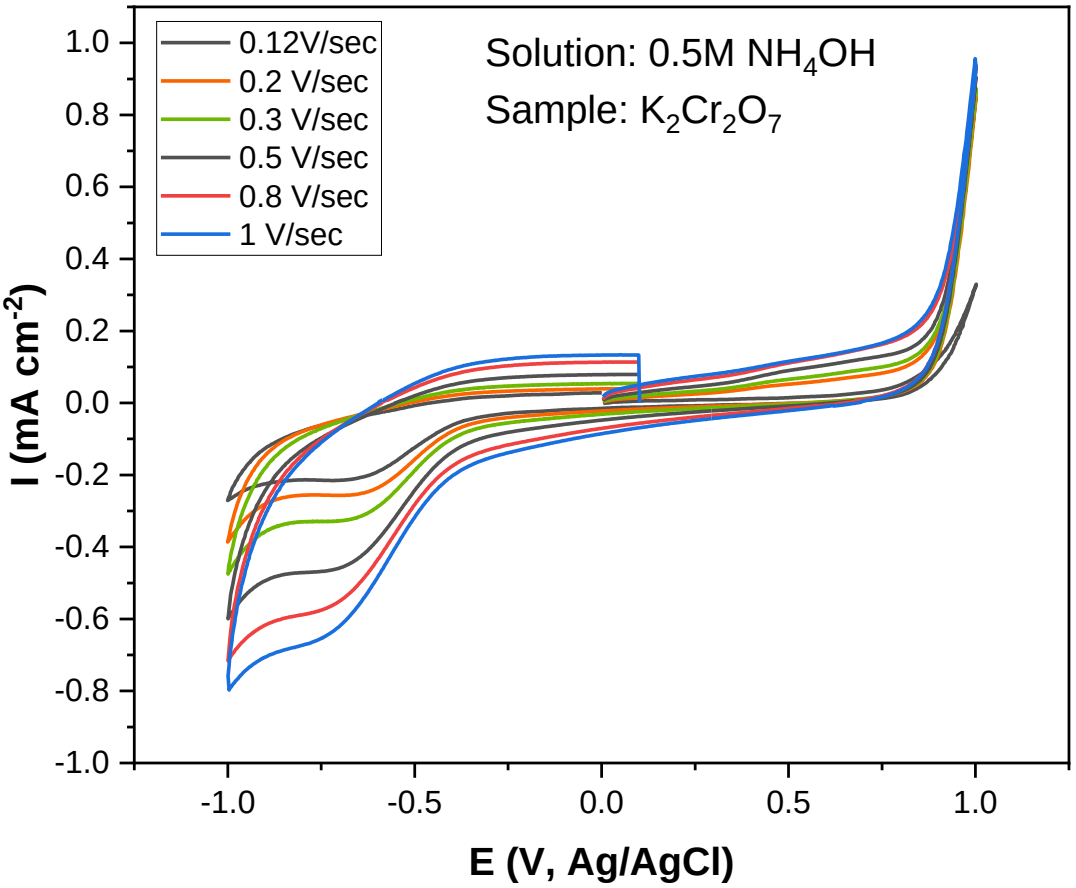

Figure 5.12 : Cyclic voltammetry of potassium dichromate at various scan rates

The results of the experiment indicate that the peak for the reduction of Cr(VI) occurs at 0.6V, and this peak is independent of the scan rate used. However, the clearest peak for Cr(VI) was observed at a scan rate of 0.2V/sec. As a result, all subsequent experiments were conducted at this scan rate.

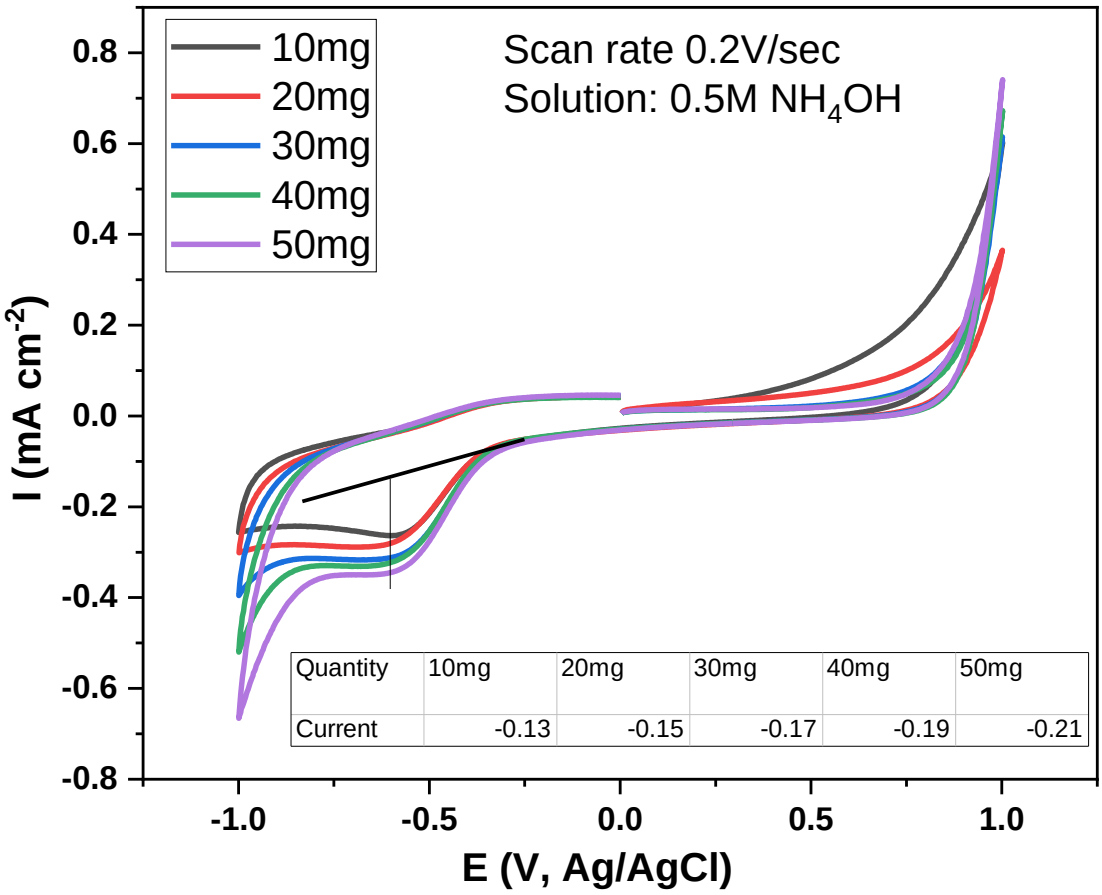

Figure 5.13: Cyclic voltammetry of different concentration of potassium dichromate at 0.2V/sec scan rate

The study's second approach involved exploring the potential to quantify Cr(VI) using cyclic voltammetry (CV). To achieve this, I prepared several solutions by mixing varying concentrations of potassium dichromate in a 0.5M NH_4OH solution. Then CV was carried out on these samples, as depicted in Figure 5.6. The outcomes of these experiments provided clear evidence that, as the concentration of potassium dichromate increased, the current intensity for Cr(VI) reduction also increased. For instance, the sample with a 10mg concentration displayed the lowest current of 0.13mA, while the sample with a 50mg concentration exhibited the highest current of 0.21mA. These results strongly suggest that an increase in the amount of Cr(VI) in the solution leads to a corresponding increase in the current, thereby providing a basis for quantifying Cr(VI) in welding fumes through the creation of calibration curves.

A graph plotting concentrations against current based on these results was drawn, as shown in Figure 5.7. This graph clearly indicates a linear relationship, reinforcing the correlation

between the concentration of Cr(VI) and the observed current intensity. This linear relationship serves as a foundation for developing calibration curves, which can be employed later to accurately quantify the amount of Cr(VI) present in welding fumes.

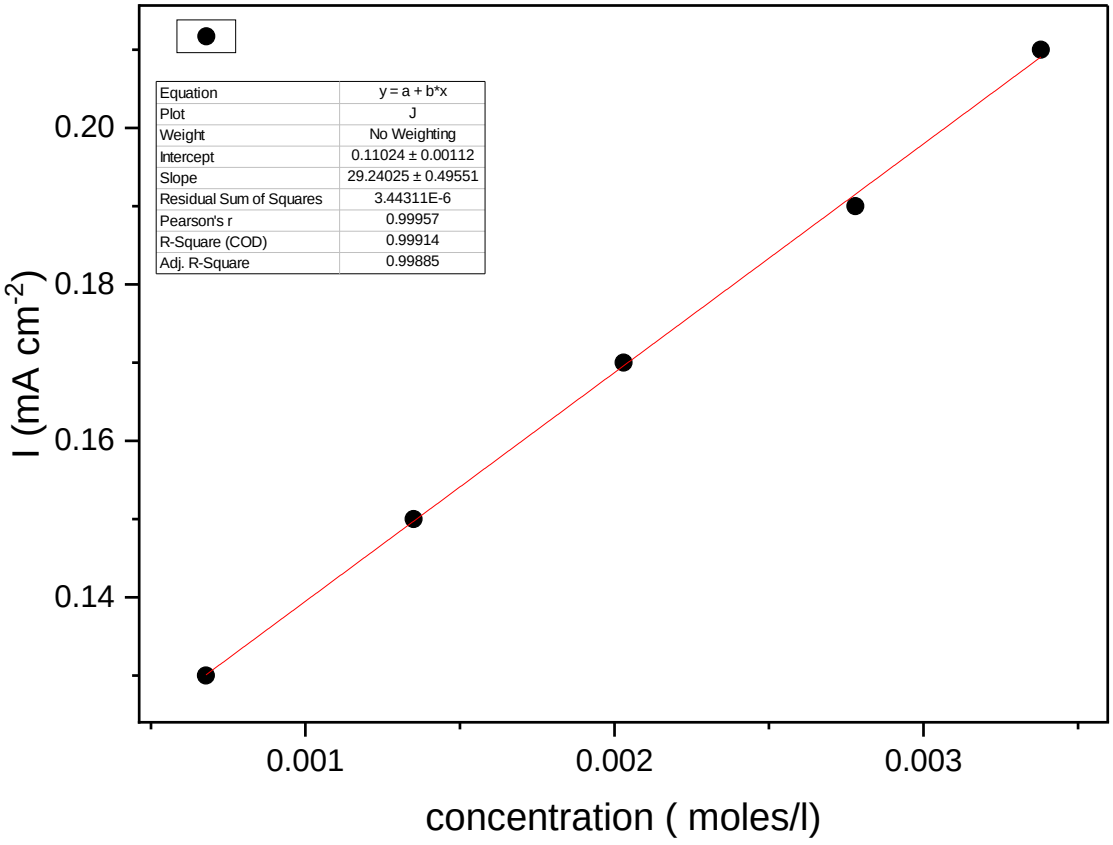

Figure 5.14 : Current vs concentration of potassium dichromats.

In subsequent experiments, the same approach was used to quantify Cr(VI) in welding fumes by dissolving them in a 0.5M NH_4OH solution, as shown in Fig 5.8. However, this approach was not successful for welding fumes because the welding fumes showed a single peak for the combined reduction of Cr(VI), FeO, and MnO at 0.6V, making it challenging to isolate and focus solely on the reduction of Cr(VI).

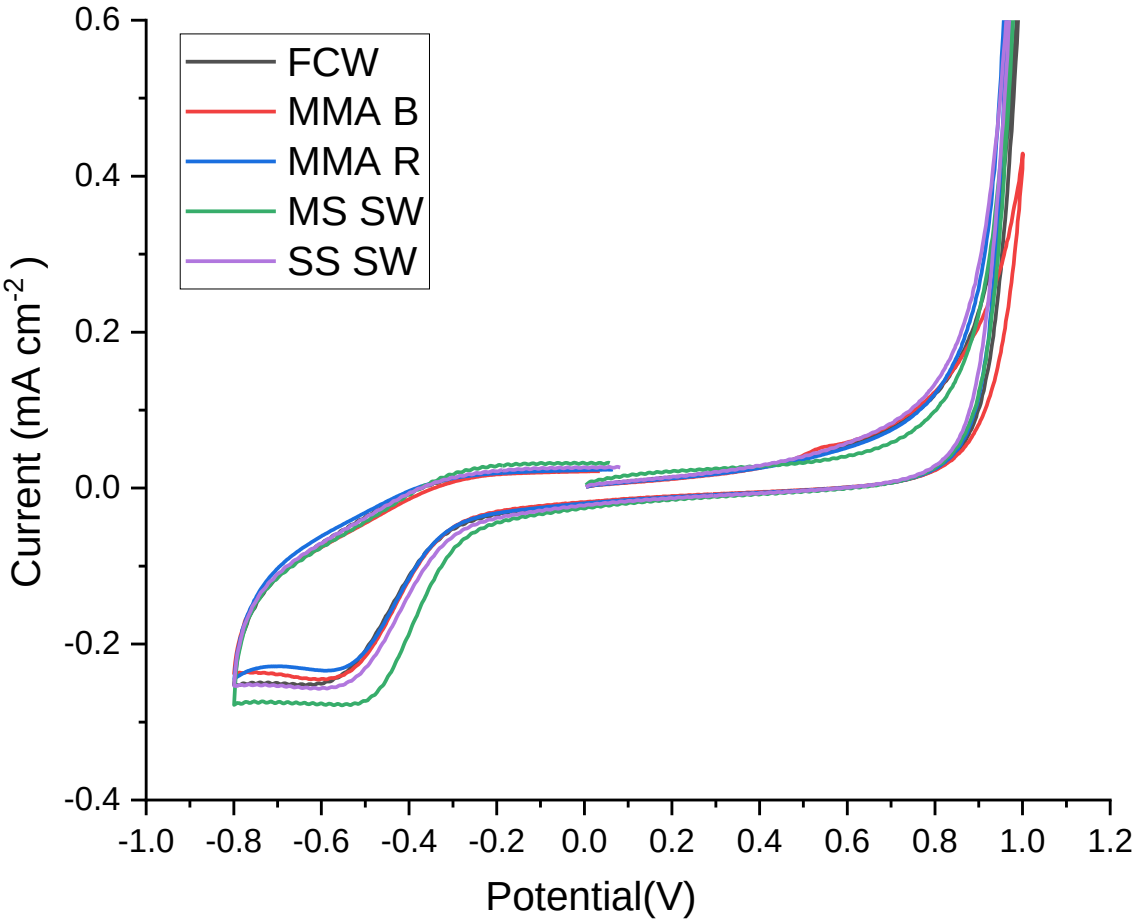

Figure 5.15 : CV of welding fumes in 0.5M NH_4OH solution at 0.2V/sec scan rate

5.2.4 Conclusions

In this study, the aim was to find the most sensitive solution and suitable pH for detecting Cr(VI) reduction to Cr(III) in welding fumes without interference from other elements. The experiments were conducted using an Ammonium hydroxide buffer solution with ammonium chloride. Different types of welding fumes were analysed using this solution, and the reduction peak of Cr(VI) was observed at 0.6V. To quantify the amount of Cr(VI), different concentrations of potassium dichromate were dissolved in a 0.5M ammonium hydroxide solution, and the peak was fitted, and the current was measured. However, one limitation of this method is that all chromates, dichromates, and CrO3 along with FeO and MnO show a peak together at 0.6V, making it difficult to identify the peak due to any specific compound and quantify the peak.

Chapter VI : Effect of shielding gas oxidation potential on Cr (VI) generation during MIG/MAG and Flux Cored arc Welding processes

6.1 Introduction

When the consumables melt at high temperatures, they form molten droplets which are exposed to the environment before they cool down. These droplets are at high temperature and have high potential to oxidise that may affect the structural integrity of the weld. To protect the weld and the molten metal from contamination, different shielding gases are used which cover the weld during welding and provide protection from atmospheric gases. Although the shielding gases are used to protect the weld from getting oxidised, in literature it has been found that the oxygen content of the shielding gas, especially the proportion of CO_2 and O_2 directly affects the FFR (fume formation rate) this is due to the oxidising nature of O_2 and CO_2 gases[68, 71, 126].

From past work it is known that FFR increases with a rise in shielding gas oxidising potential[68]. Hence oxygen is an important element with respect to welding fume formation. Due to the oxidising nature of oxygen, there is a chance that it oxidises Cr (III) to Cr (VI) during welding processes. Hence, it is important to study the effects of oxygen on Cr (VI) formation during welding.

Shielding gases are not just added to protect the metal droplet during welding but also for many other important reasons, such as to stabilise the arc to ensure smooth transmission of material, providing cooling for welding torch and weld pool[141]. CO_2 is also one of the shielding gases which is mixed with argon during welding of stainless steel for improving arc stability and decreasing the spatter formation[142]. At lower CO_2 levels it has been reported that there is more fume formation due to more spattering which eventually decreases with the percentage increase of CO_2 in argon but after 5% addition of CO_2 it has been seen that there is more fume formation due to the oxidising nature of CO_2 [68].

Shielding gases also have effects on the thermal conductivity and temperature of arc. Pure argon and oxygen both have low thermal conductivity which means that the temperature of the arc will be higher than in the case of carbon dioxide[143]. Hence, we may see the maximum amount of oxidation of Cr (III) to Cr (VI) in the Ar and O_2 gas mixture. But in the case of CO_2, when mixed with argon, it's more complicated to predict Cr(III) oxidation as CO_2 is known for increasing the thermal conductivity of the arc, but at the same time CO_2 dissociates to carbon monoxide and oxygen, and this dissociation creates the difference in the temperatures as this dissociation is endothermic near the arc and exothermic further from the arc which makes it hard to predict the change in the temperature of the arc by changing the composition of CO_2. Therefore, making predictions about the oxidation of Cr (III) during the welding is very complicated.

The other important factor which needs to be kept in mind during these experiments is the effect of droplet size as in the case of increased droplet size an increase in droplet surface area would be seen, which would also influence the rate of oxidation of Cr (III).

It would be interesting to investigate the shielding gases mixtures from the perspective of Cr (VI) formation as the results cannot be predicted. With the different gas mixtures, we might see the effects on Cr (VI) formation and be able to study which factor has a greater impact on the results.

6.2 Materials and methods

6.2.1 Collection of welding fumes

The welding trials were carried out with an inverter MIG/MAG power source operating in the open arc transfer mode(globular transfer mode with nonpulse current).Welding conditions were set manually on the power source and recorded, welding conditions (average voltage and current) during these welding runs are mentioned in table 6.2.Wire feed rate for the welding was set to 10.2m/min. CTWD (Contact Tip to Work Distance**)** was set to 20mm. A standard swan neck welding torch was connected to the power source and clamped by the handle above a moving traverse. The torch nozzle was angled at 90 degrees to the vertical and welding progressed in the 'push' direction. A fume hood as specified in EN ISO 15011-1 [82] was suspended above the welding torch to collect the welding fume.

Welding was carried out on 304SS plates (500 X 50 X 10 mm), clamped in a fixture on the traverse and the weld progressed by moving the plate under a stationary welding torch. The travel speed of traverse was set up to 300mm/min. The welding fumes were sucked through the fume hood and collected by the cellulose filter paper inserted on the top of hood. Cellulose filter paper was used , as it is an inert medium, and would not contaminate the fume sample. Samples can also be easily brushed off from these filter paper easily. The fumes were brushed off from the filter paper after the welding and further analysis on the fumes was carried out. The filler material used for welding was 1.2mm diameter flux cored wires (EN ISO 17633-A-T 19 9 L P C/M 1) and solid stainless steel 1mm diameter (EN ISO 14343-A: G 19 9 L Si) wires. Typical composition of the materials as provided by the supplier is listed in table 6.1.

	C (%W/W)	**Mn (%W/W)**	**Si (%W/W)**	**Cr (%W/W)**	**Ni (%W/W)**
Base Plate	0.08	2.0	0.75	18.0-20.0	8.0-10.5
Solid stainless steel wire consumable	0.02	1.7	0.90	20	10
Flux cored wire consumable	0.06	1.3	0.50	19.3	9.5

Table 6.1 : Composition of consumables

6.2.2 Welding fume Samples

When investigating the effect of shielding gases on welding fumes, oxygen index is the key parameter for investigation. Oxygen index is defined by IIW (International Institute of Welding) by an empirical formula, (%O + 0.5%CO_2), and this is used in our experiments to estimate the oxidising effect of the shielding gases. In welding literature, the oxidising effect is also referred as the oxygen potential. Solid molten metal interacts with shielding gases and then the fume condensation happens so the shielding gases makes one of the important factors for Cr (VI) conversion from Cr (III). The different welding fumes samples generated by varying shielding gases) are as listed in table 6.2. Not all these shielding gases mixtures are

recommended for welding stainless steels, but they were used to provide a wide range of oxygen index.

Sample name	Consumable	Shielding gases	O_2 index	Welding Current (Amps)	Welding Voltage (Volts)
SS1	Solid Stainless-Steel Wire	100% Ar	0%	185	29.1
SS2	Solid Stainless-Steel Wire	98% Ar+ 2% O_2	2%	180	28.3
SS3	Solid Stainless-Steel Wire	98% Ar+ 2% CO_2	1%	190	27.1
SS4	Solid Stainless-Steel Wire	92% Ar+ 8% CO_2	4%	200	30.2
SS5	Solid Stainless-Steel Wire	93%Ar+2% O_2+5%CO_2	5.5%	200	30.3
FCW1	Flux Cored Wire	100% Ar	0%	260	33.0
FCW2	Flux Cored Wire	80% Ar+ 20% CO_2	10%	230	32.5
FCW3	Flux Cored Wire	83% Ar + 15% CO_2 + 2% O_2	9.5%	225	32.7
FCW4	Flux Cored Wire	78% Ar +20% CO_2 +2% O_2	12%	225	32.8

Table 6.2: Welding fume samples and welding conditions

These welding fume samples were collected on cellulose filters and then brushed off and stored in glass vials. ICP-MS was carried out to detect the elemental composition of these fumes. Simultaneously using another batch of the sample, ion chromatography (IC) was carried out with the purpose of measurement of Cr (VI) in welding fume composition. Particle size and elemental composition of the welding fumes was investigated using Scanning Electron

Microscopy (SEM) and Energy Dispersive X-ray spectroscopy (EDX). SEM images were taken by Zeiss ∑igma FEGSEM attached with EDX spectroscopy. EDX was performed on the particles by Oxford Instruments X-Max^2 silicon drift detector. The phase analysis and crystal structure of the welding fume particles were analysed by XRD using a Siemens D501 Diffractometer.

FTIR was performed using a Thermo Fisher iS5 attached with a ID7 ATR accessory. The FTIR spectra were obtained after 128 scans with 2cm^{-1} resolution in absorbance mode. The background was measured for each sample and subtracted from the final spectra.

6.3 Results and Discussions

6.3.1 XRD

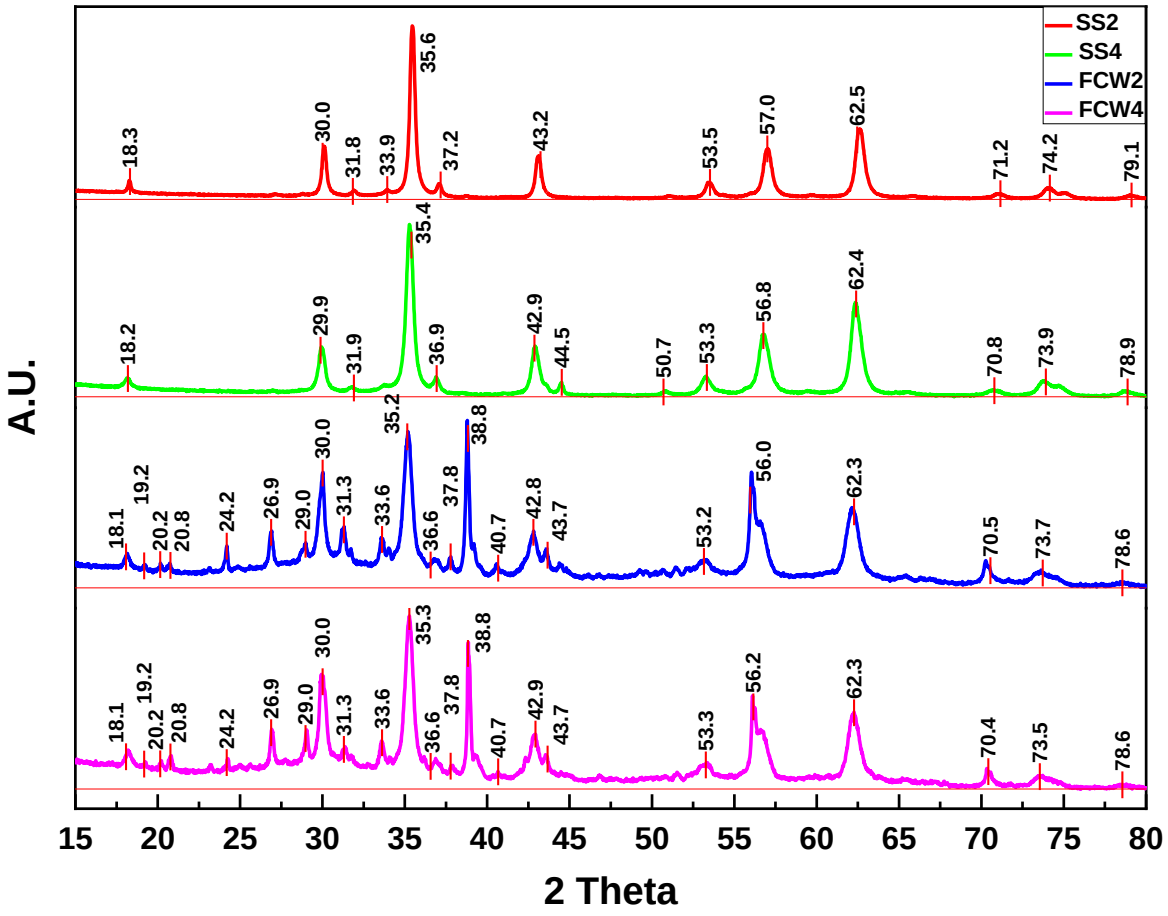

Figure 6.1 : XRD of welding fume samples

XRD analysis of the (bulk) fume was carried out and is shown in fig 6.1 These result shows no evidence that shielding gas composition affects the composition of welding fumes. Solid wires (SS1 an SS2) show similar peaks, as do flux cored wires (FCW1 and FCW2) despite having different shielding gases. The majority of the peaks observed in solid wires indicate the presence of the spinel oxides of iron (X_3O_4 with X = Fe, Cr, Mn, and/or Ni), with some manganese oxide impurities[30, 101, 105]. The peaks observed for flux cored wire fume samples (FCW1 and FCW2) are due the formation of both alkali-alkali earth fluoride phases and the spinel oxides which were also observed in solid wire welding fume samples. All welding fume samples were a mixture of amorphous and crystalline particles, and this was observed during XRD as there were some broad peaks with mixed sharp peaks. These amorphous particles are the particles which are smaller than 50nm and are essentially on the surface of the crystalline particles and cannot form standard crystal lattices. It is hard to allocate the peaks to individual phases in welding fumes as each fume particle contains more than one phase and cannot be justified in marking the peaks of individual phase[30, 128]. There are a few small peaks which were observed in SS2 and were not observed in SS1 and vice a versa, these peaks do not represent any new phase as they are minor peaks of the spinel phases and were not detected due the variation in particle sizes of fumes. The peaks which are around 2-θ values of 30, 35, 43, 56.2, 62.3º are the spinel's, AB_2O_4, with A, and B = Fe, Cr, Mn, and/or Ni[105],where the A site is Fe, and B could be a combination of Mn, Cr and/or Ni. However, due to the very small particle sizes (very broad peaks), the A and B sites could also include dopants such as Mn, Cr, and/or Ni in different proportions.

6.3.2 SEM and EDX

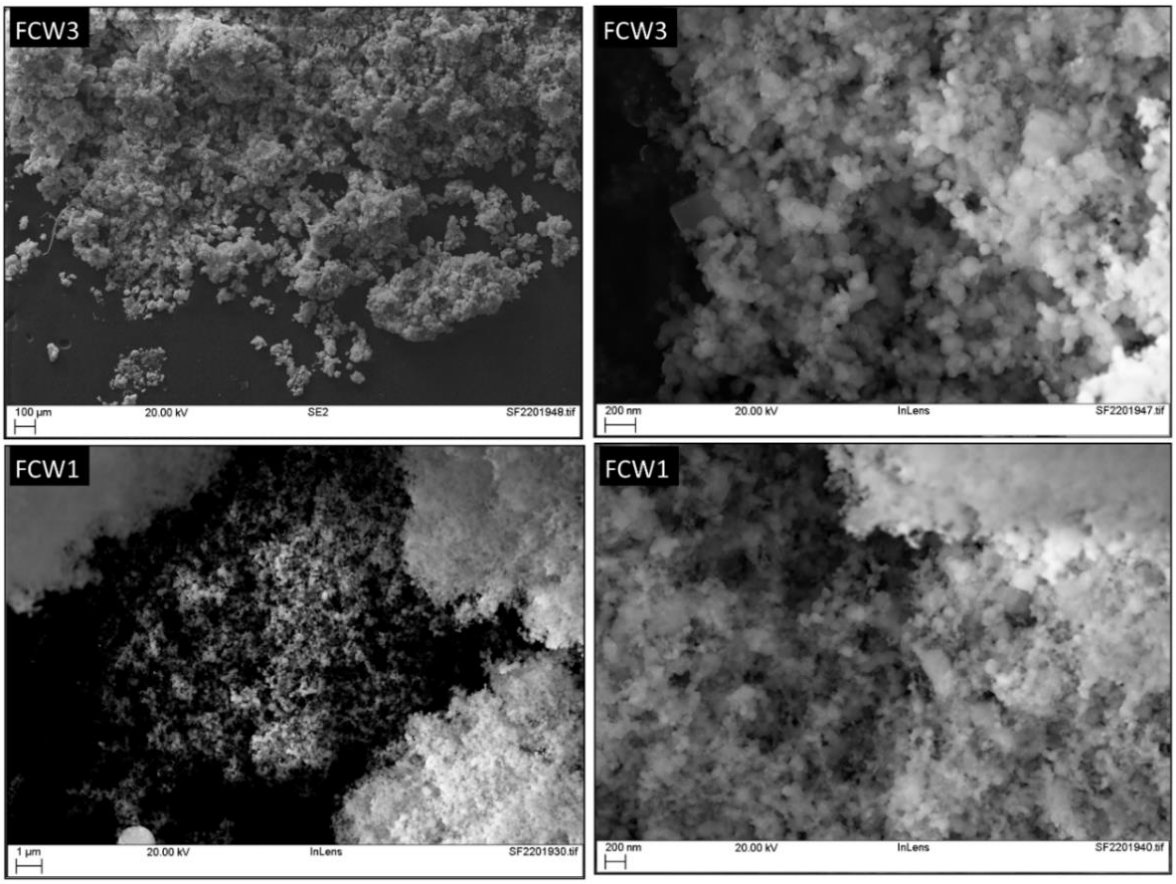

Figure 6.2 : SEM images of flux cored wire welding fume samples

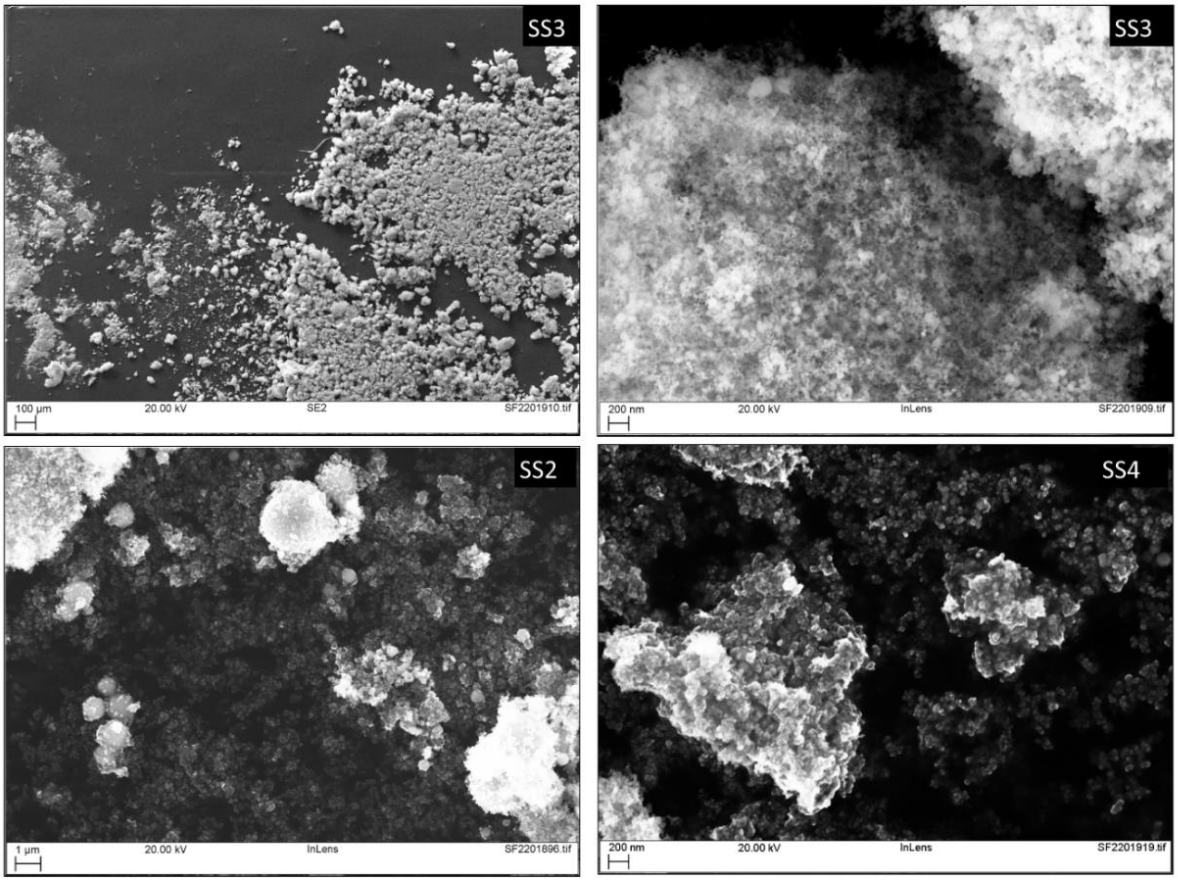

Figure 6.3 : SEM images of solid stainless steel wire welding fume samples

Figure 6.2 and figure 6.3 shows the SEM data of FCW and solid wire welding fume samples. SEM images are used to analyse the particle size distribution and morphology of the welding fumes. These images reveal that fumes from both the flux cored wires and solid wires have welding fume particles which vary from nanoparticles to micro sized particles. The particles are formed due to solidification and oxidation, forming agglomerates as reported in literature[12, 30, 89, 90, 105, 127]. These images shows that the welding fume particles are spherical in shape and nanosized and hence can be inhaled by welders thus are very hazardous to lungs. Literature shows that ability of particles to penetrate deeper into the respiratory system increases significantly with proportional to their particle size, smaller the particles, more is their penetration and more hazardous they are [144, 145]. SEM images show that the fumes from solid wires are comparatively smaller in size than the fumes particles from FCW electrodes.

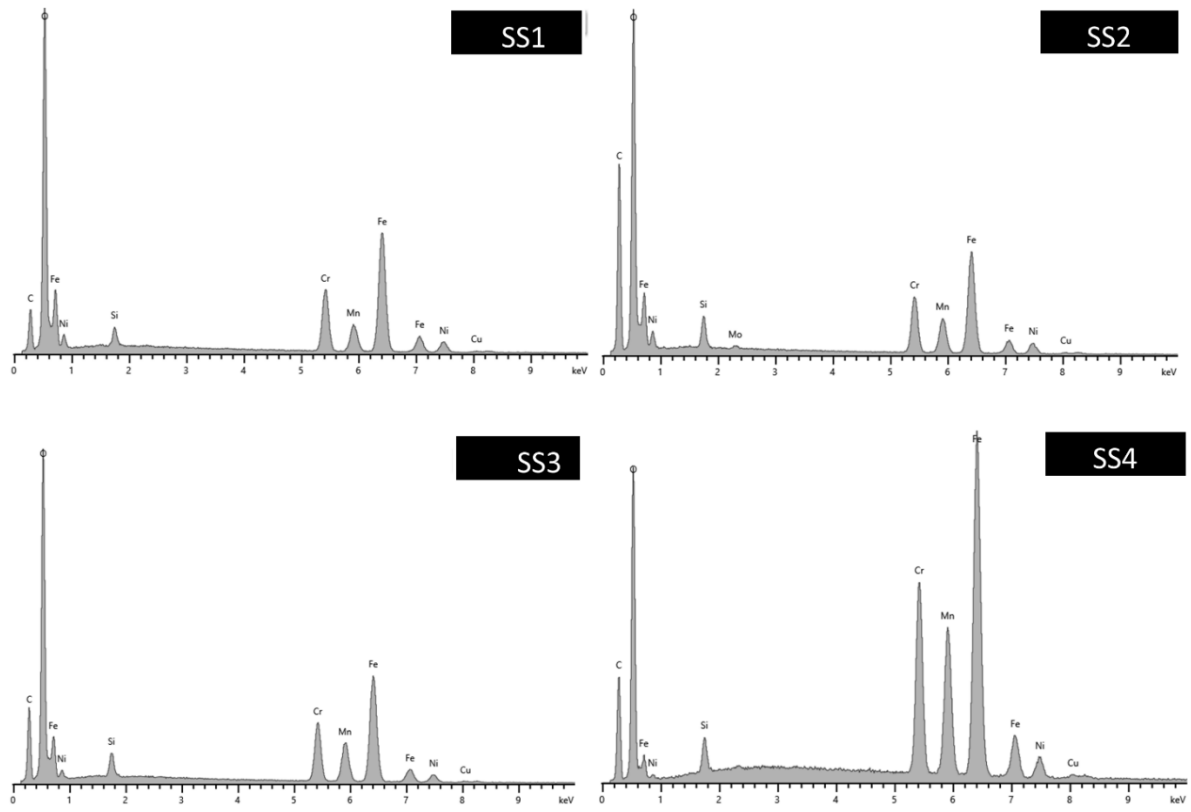

Figure 6.4 : EDX data of solid stainless steel wire welding fume samples

Figure 6.4 shows the EDX data for the welding fumes particles from solid wire electrodes. Irrespective of the shielding gases, all fume samples show the presence of C, O, Fe, Ni, Si, Mn, Cr and Cu. This data compliments the ICP data of welding fumes. All samples have the same chemical structure since the shielding gases used do not affect the chemical structure of the fumes. Fig 6.5 shows the EDX data for welding fume particles from FCW electrodes and this also shows that the shielding gases have no effects on the chemical structure of fumes. EDX data of welding using FCW electrodes shows the presence of C, O, Fe, F, Ni, Al, Na, Bi, K, Ti, Cr, and Mn elements in them.

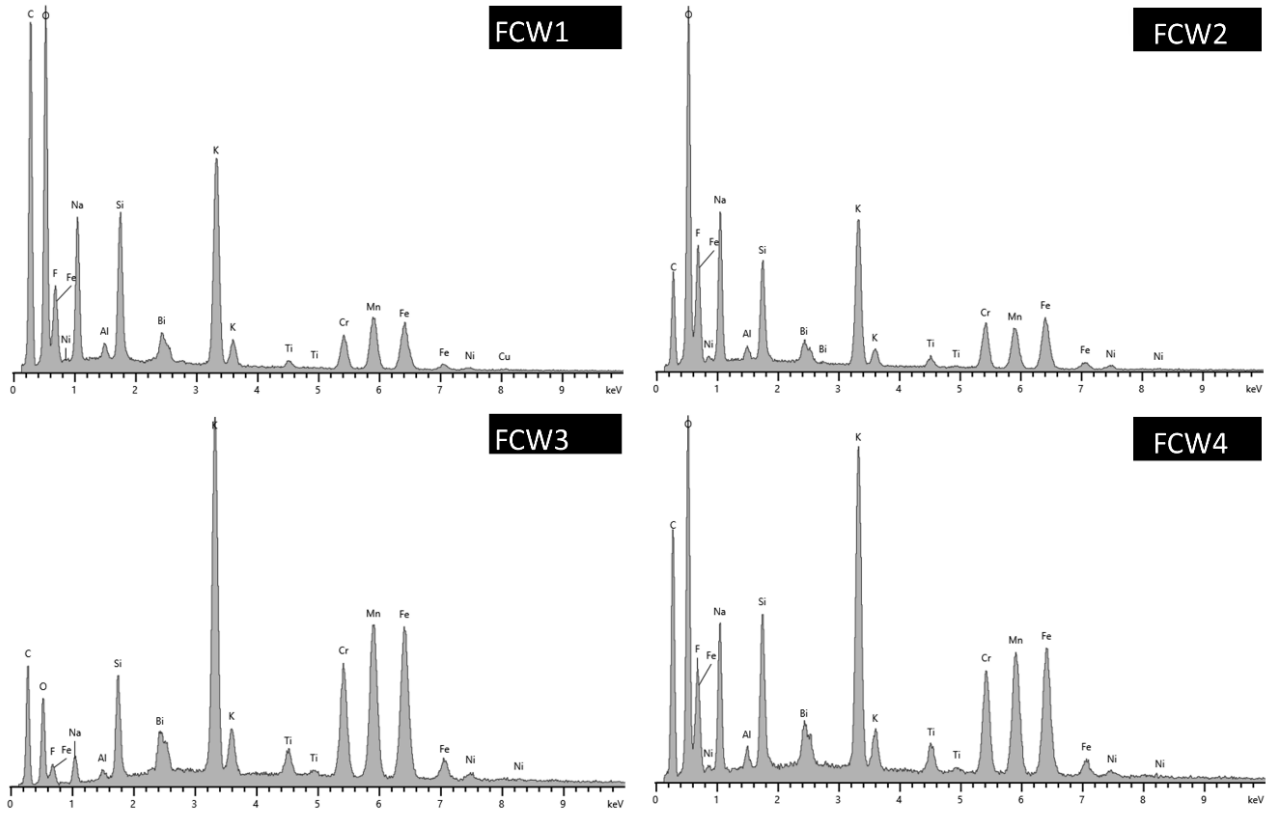

Figure 6.5 : EDX data of flux cored wire welding fume samples

6.3.3 FTIR

Figure 6.6 shows the FTIR data for welding fumes generated by MIG/MAG welding using solid stainless-steel wire. Welding fumes from solid wires are rich in iron oxide compounds and as a result, all the samples show the broad peak before 700cm^{-1} wavenumber which is due the large amount of iron spinels the peak around 690 cm^{-1} wavenumbers is caused due to the Fe-O antisymmetric stretching. To see the minor peaks the FTIR graphs were plotted in the narrow range. All these fume samples also show the peak around wavenumber 725 cm^{-1} which is due to Fe-O-H vibration. Peaks in the range of 930-950 cm^{-1} in different samples are due to the vibration of Cr=O and this vibration is seen in CrO_3, which could be the Cr (VI) compound which we observe in solid stainless steel wire welding fumes. Vibration peaks in the range of 1020-1035 cm^{-1} is due the vibration of the Si-O-Si symmetric stretching mode indicating the presence of SiO_2 in welding fumes. The peaks after 1100cm^{-1} are hard to assign as welding fumes particles can form large numbers of possible organic and inorganic compounds as the peaks in those wavenumber regions are due to the organic compounds of carbon. However,

peaks around 1630cm^{-1} can be assigned to the absorbed H_2O molecules on fume samples as this occurs to due to the O-H bending vibrations.

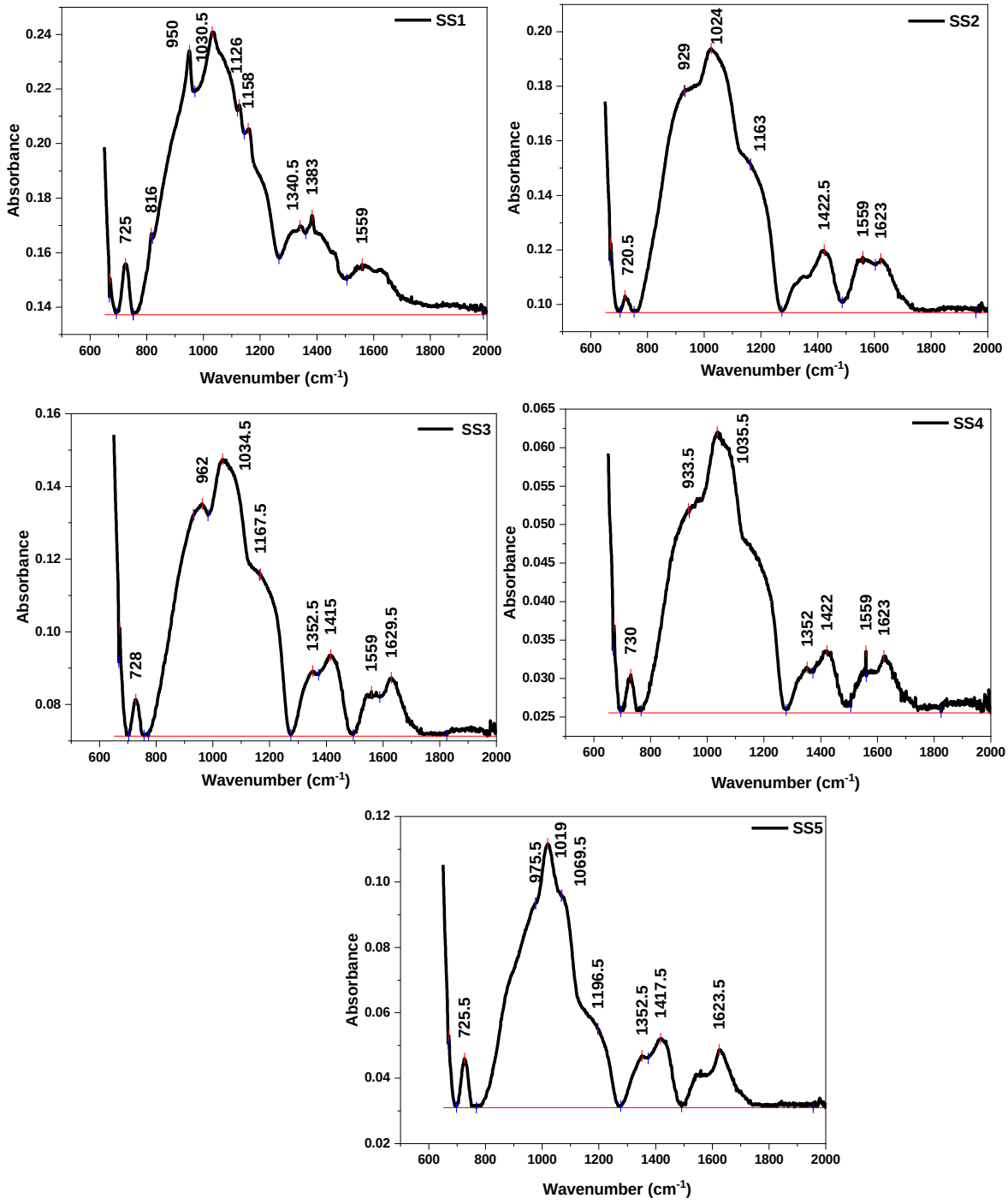

Figure 6.6 : FTIR data of stainless-steel wire welding fume samples

Figure 6.7 demonstrates the FTIR data for flux cored arc welding fumes. Flux cored wires have alkaline earth metals in them and as a result they form large number of chromates and dichromates and this is clearly seen in our data, the FTIR peaks at 725, 832, 853, 884, 890,

886, and 971 cm^{-1} are representing either chromates or dichromates formed in samples. The vibrational peak shift is seen in all samples from their characteristic peaks because the compounds formed are not in their pure phases. Welding fumes contain different mixed oxide phases and spinel phases of the metal oxides. FTIR peaks at wavenumber 832cm^{-1} and 853cm^{-1} are due to the formation of chromates, as these peaks occurs due to Cr-O-Cr vibrations. FTIR peaks at 884, 890 and 886cm^{-1} is due to formation of dichromates, as these peaks are caused due to Cr-O_3 symmetric vibrations. FTIR peaks around 730 cm^{-1} are due to the Cr-O-Cr symmetric stretching molecular vibrations of dichromates. FTIR vibrational peaks around 960 cm^{-1} are due to the Cr=O vibration indicating the presence of CrO_3 in these samples. FTIR Peaks at 1110 cm^{-1} are due to silica compounds as this indicates the Si-O-Si stretching. This peak is not observed as a sharp peak in FCW1 and FCW2 samples because of the interference by Cr (VI) peak at 975 and we see a broadening of the peak. FTIR peaks between 1200-1500 cm^{-1} are due to carbon organic compounds, and the peak at 1648.5 cm^{-1} is due to the O-H bending vibrations.

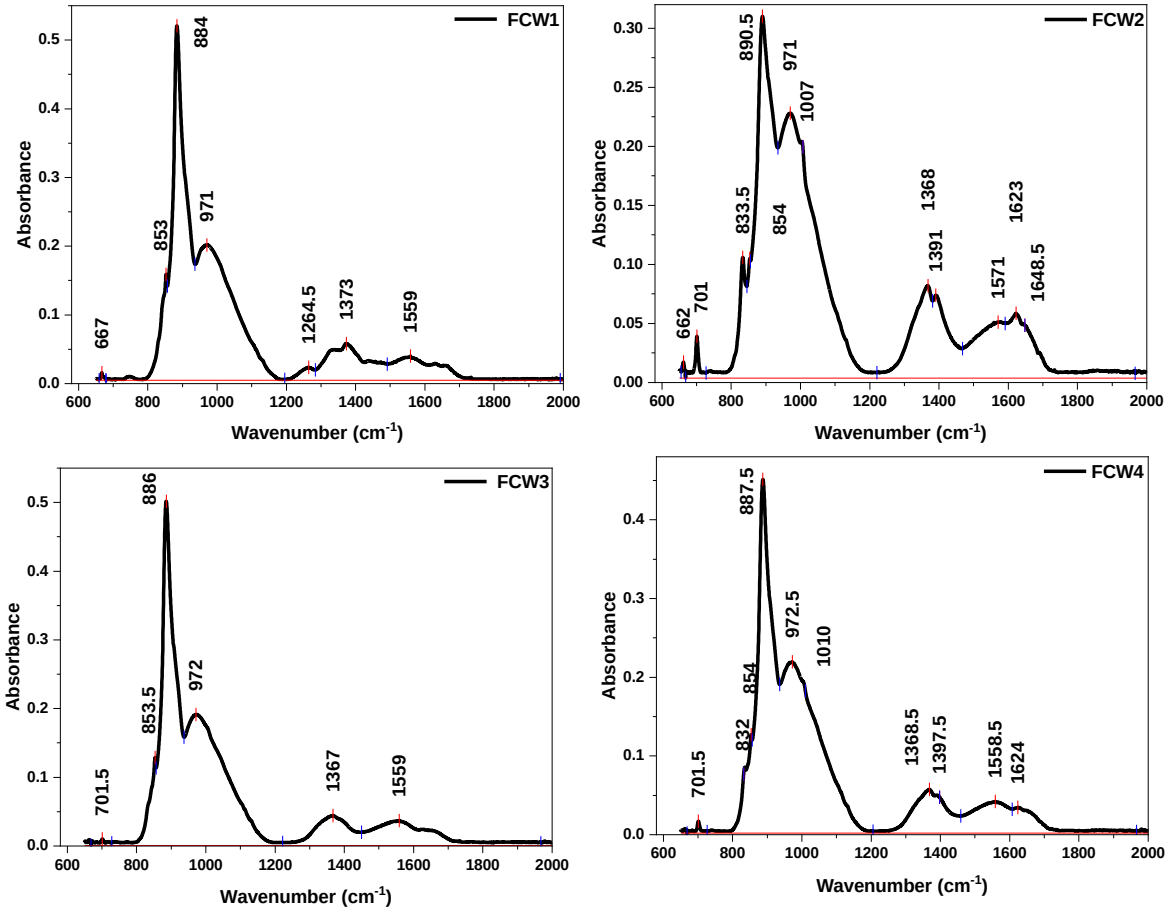

Figure 6.7 : FTIR data of Flux cored wire welding fume samples

6.3.4 ICP and Ion Chromatography:

Table 6.3 displays the ICP-MS data of welding fumes generated using different shielding gases. In welding fume samples from both types of consumables, stainless steel consumables and flux cored consumables, we observe the least amount of total Cr 12.7%m/m and 4.2%m/m respectively in 100% Ar. But this is not the case with Cr (VI), although we observe the least amount of Cr(VI) formation in solid stainless-steel consumables (0.25%m/m) with inert gas (100% argon), but we do not observe this in flux cored consumables, in flux cored consumables we observed the highest amount of Cr (VI) present compared to other welding fumes with the oxidising shielding gases. This observation is very critical in understanding the role played by shielding gases. The fume formation during welding happens by two mechanisms, firstly, as the vaporisation of the metal or compounds near the arc and subsequent condensation of the species and oxidation may follow during condensation [74].

The second method is enhanced vaporisation by formation of more volatile oxides on the surface of the weld droplet, followed by condensation and further oxidation [74]. The first mechanism is happening almost every time and is inevitable, but the second can be minimised or enhanced by the shielding gases [74]. If the oxidation potential of the shielding is lowered the second type of mechanism can be lowered too. Argon has the lowest oxidation potential amongst the all the shielding gases we have used, hence there is very low possibility of the second type of fume formation and due to which we observe the least amount of total chromium from both types of consumables. With respect to Cr(VI) we know that during welding Cr(VI) stabilises itself by forming chromates and dichromates of alkaline earth metals. Since the solid stainless-steel consumables do not have any basic earth metals present in them the generation of Cr(VI) depends highly on oxidation and there is less possibility of second type of fume formation mechanism (in which oxidation happens due to formation of volatile oxides) during welding with argon as the shielding gas, whereas in flux cored wires the Cr(VI) formation depends on multiple factors along with oxidation. In flux cored consumables the presence of alkaline earth metals such as sodium and potassium have a significant role in Cr(VI) formation. Hence the oxidation of these alkaline earth metals also plays a role in Cr(VI) formation.

Using argon as the shielding gas for flux cored wire consumables we observed the least amount of Fe, Mn, Ni and Ti compared to oxidising gases. But this is not the case with solid stainless consumables. Fumes from solid stainless-steel consumables show the highest amount of iron

and nickel in them when welding using argon. Hence just looking at oxidation indexes and making conclusions will not justify this study. To understand the role of shielding gases in details, we have used correlation coefficients.

	FCW 1 (%m/m)	FCW 2 (%m/m)	FCW 3 (%m/m)	FCW 4 (%m/m)	SS1 (%m/m)	SS2 (%m/m)	SS3 (%m/m)	SS4 (%m/m)	SS4 (%m/m)
Al	0.8	0.9	0.9	0.9	0.1	0.1	0.1	0.1	0.1
Bi	3.6	4.5	5.3	4.7	-	-	-	-	-
Ca	0.1	0.1	0.1	0.1	-	-	-	-	-
Cr	4.2	5.9	6.2	6.5	12.7	13.8	14.3	12.8	13.1
Cr (VI) (IC)	4	3.61	1.48	2.55	0.25	0.62	0.4	0.30	0.29
Fe	8.1	11.1	9.3	15.3	44.7	40.8	36.4	35.9	37.1
K	15.6	13	12.6	11.9	-	-	-	-	-
Mn	8.5	9.5	9.3	9.1	4.8	5.9	8.8	10.4	11
Na	8.2	7.3	7.2	6.8	-	-	-	-	-
Ni	0.3	0.7	0.7	0.8	6.2	5.7	4.3	3.9	3.6
Si	4.1	2.2	2.3	1.8	1.1	1.8	1.6	1.8	1.8
Ti	0.7	1.3	2.3	1.5	-	-	-	-	-
% of Cr (VI) in total Cr	95.23	61.18	23.87	39.23	1.96	4.49	2.79	2.34	2.21

Table 6.3: Elemental composition of welding fumes

In our study we have used Pearson's correlation coefficients to understand the relation of different elements and the oxidation index of shielding gases in relation with the hexavalent chromium generation in welding fumes. In simple terms, Pearson's correlation coefficients are used to measure the strength of relationships between two variables. It is a statistical test and therefore it only measures the statistical relationships between two variables. Pearson's correlation coefficients are represented by 'r', and they are derived using the following formula.

$$r = \frac{\sum(x_i - \bar{x})(y_i - \bar{y})}{\sqrt{\sum(x_i - \bar{x})^2 \sum(y_i - \bar{y})^2}}$$

Where,

$$r = \text{correlation coefficient}$$
$$x_i = \text{values of the } x \text{ variable in a sample}$$
$$\bar{x} = \text{mean of the values of the } x \text{ variable}$$
$$y_i = \text{values of the } y \text{ variable in a sample}$$
$$\bar{y} = \text{mean of the values of the } y \text{ variable}$$

Pearson's correlation coefficients value ranges from -1 to 1 and they represent the degree of association. If the value is ±1, then it signifies a perfect correlation. Perfect correlation means, if one variable increase then the other variable will also increase if the value is +1 and if its -1 then the other variable value will decrease. If the value lies between ±0.50 and ±1, then it is considered as a strong correlation. If the values are between ±0.30 and ±0.49, then it is said to be medium correlation and if the values lie below ±0.29 then it is considered as a small correlation. If the correlation value is zero, then there is no correlation between the variables. Different values of correlations alongside their data point representation are demonstrated in the figure 6.8.

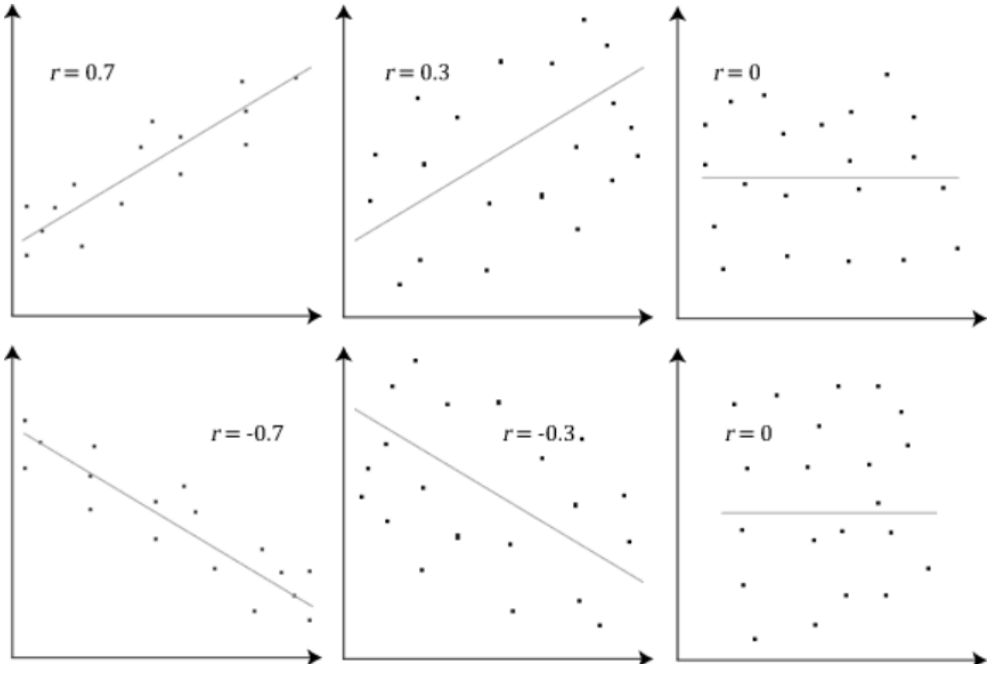

Figure 6.8 : Data sets represented by different corelations coefficients.

6.4 Effects of shielding gases on Cr(VI) formation in welding fumes generated by solid stainless-steel consumables.

Table 6.4 demonstrates the Pearson's correlation coefficients of solid stainless-steel consumable welding fumes elements and their oxygen index. The correlation coefficient doesn't prove to be very helpful in the case of solid stainless-steel consumables because of the limitation of shielding gases. Recommended gases for these electrodes don't provide large differences in their oxidation indexes and as a result we do not see much difference in the composition of the elements by ICP data. But we can compare the oxidation effect of oxidising gases to non-oxidising gases, CO_2, O_2 and mixture of $CO_2 + O_2$. It is well known fact that the thermodynamics of chemical reactions are responsible for the formation of different types of oxides, but the oxidation kinetics are responsible for nucleation and growth of oxides [14, 76]. In welding fume formation, the thermodynamics and kinetics of the formation of oxides are determined by the temperature of arc, temperature of the weld pool, exposure periods (speed of weld), oxidation index of the shielding gas and chemical composition (type of consumable). The correlation coefficients show that as we increase the oxidation index of the shielding gases, we experience a decrease in the content of iron and nickel in welding fumes and an increase in manganese content. It may appear that the iron and nickel doesn't oxidise in the presence of more oxygen, but this is not the case, we have to keep in mind that welding is a metal deposition process and fumes are the by-products, the better the welding conditions and the stable the arc, the better the metal deposition and less by-product i.e., welding fumes.

In welding fumes, Cr (VI) is generated by the chemical reactions happening in arc and during solidification and nucleation of fume particles, whereas Fe is present in large amounts in consumables hence the presence of iron depends mainly on the quality of welding, for example if the arc is not stable, we experience more spattering, and this would increase the Fe content in the welding fumes. Shielding gases such as O_2 and CO_2 provide better arc stability then Ar. Hence, we see the maximum amount of Fe in fumes from Ar shielding gas. CO_2 and O_2 have different properties such as CO_2 has high ionisation energy because of its dissociation into carbon and oxygen which is not provided by oxygen alone as a result it gives deep penetration and high voltage and better arc stability which is seen during the generation of SS3 and SS4 fume samples and a result of this we observe less Cr(VI) and Fe in our samples compared to

SS1 which was Ar mixed with O_2. Although oxygen also stabilises the arc when mixed with Ar, it has low thermal conductivity and as a result its oxidising effect is greater, compared to CO_2 , and we observe more Cr(VI) and Fe in 2% oxygen and Argon mixture compared to 8% carbon dioxide and Argon mixture which has higher oxygen index. The best results are observed in the mixture of CO_2 and O_2 as we observe the least amount of Cr(VI) in these samples among all oxidising shielding gases mixtures. From these results we can conclude that oxygen index does play a role in Cr(VI) generation as we observe the least amount of Cr(VI) in non-oxidising gases i.e. Ar but if using oxidising shielding gases which are more practical in terms of welding, a mixture of both oxygen and CO_2 provides the best results for minimising Cr(VI) generation by improving the arc stability and welding conditions.

	Cr	**Cr(VI)**	**O_2**
Cr	1	0.68	-0.16
Cr(VI)	0.68	1	-0.31
Mn	-0.02	-0.32	0.98
Fe	-0.31	0.03	-0.84
Ni	-0.06	0.29	-0.95

Table 6.4 : Pearson's correlation coefficients of stainless-steel consumable welding fumes elements and oxygen index

6.5 Effects of shielding gases on Cr(VI) formation in welding fumes generated by flux cored consumables.

Table 6.5 shows the Pearson's coefficients for fluxed cored consumable welding fumes and their oxygen index. These results reveals that the oxygen index has an impact on all the elements present in the welding fumes from flux cored wires. With the change in oxygen index, we observe changes in the composition of welding fume. Oxygen, which is present in the oxidising gases, oxidises elements present in the fumes and thus increase their quantities, and this is shown for Cr, Mn, Fe, Ni and Ti and this was expected as the welding fumes are generated by the oxidation of the elements present in the consumables. The new finding by observing Pearson's coefficient is that with the increase of oxygen index we observe the

reduction of Cr(VI) which was unexpected. We observe the maximum amount of Cr (VI) in the FCW1 sample which was generated with 100% Ar gas which is inert in nature. Although we observe mostly Cr(VI) in fluxed cored consumables in the form of chromates and dichromates our FTIR results show small amounts are also present as CrO_3. To understand this, we have collected slag of these welding trials and then used ICP/IC to analyse its elemental composition, which is shown in the table 6.6. Sample FCW1 shows the highest amount of Cr(VI), K and Na in fumes whereas in the slag samples it shows the least amount of Na and K which might be due the fact that Na and K reacts with Cr in welding electrodes and generate Na and K chromates and dichromates, as a result of which the amount of Na and K is least in the slag. This observation is not true for the FCW2, FCW3 and FCW4 since these do not have the inert gas environment and as well as with Na and K, oxygen index plays the role too. It is a well-known fact that Na and K are highly reactive to oxygen, and this might be the reason we observe more Cr(VI) in FCW1 samples because of absence of oxygen most of Na and K from the electrodes reacts with chromium instead of oxygen. In the fume samples FCW2, FCW3 and FCW3 we observe less Cr(VI) because some of the available Na and K may react with oxygen and form alkali oxides or peroxides. Welding fluxes contains sodium and potassium in the form of silicates as a binder. Sodium and potassium silicates are mixtures of silica with sodium and potassium carbonates. During welding (because of high temperature) in presence of oxygen, these potassium and sodium carbonates dissociates into sodium oxide and carbon dioxide via following reaction.

$$\mathbf{Na_2CO_3 \rightarrow Na_2O + CO_2} \qquad \mathbf{(6.1)}$$

Sodium oxide forms the slag to protect the weld from oxidation and carbon dioxide is released as a gas, but during limited supply of oxygen (in FCW1) sodium carbonates dissociates into CO_2 and Na ion and this sodium ion reacts with chromium (III) to form chromium (VI) chromates and dichromates. Sample FCW2(oxygen index 10) does not have oxygen as the shielding gas and therefore regardless of having a lower oxygen index than FCW3(oxygen index 12) it has more Cr(VI). Hence, we can say the oxygen when mixed with CO_2 as shielding gas helps to reduce Cr(VI) emission during welding.

	Cr	Cr (VI)	Mn	Fe	Ni	K	Na	O2
Cr	1	-0.71	0.81	0.71	0.91	-0.99	-0.99	0.99
Cr (VI)	-0.71	1	-0.45	-0.21	-0.52	0.69	0.65	-0.66
Mn	0.81	-0.45	1	0.35	0.57	-0.78	-0.73	0.83
Fe	0.71	-0.21	0.35	1	0.93	-0.76	-0.82	0.73
Ni	0.91	-0.52	0.57	0.93	1	-0.94	-0.97	0.91
K	-0.99	0.69	-0.78	-0.76	-0.94	1	0.99	-0.99
Na	-0.99	0.65	-0.73	-0.82	-0.97	0.99	1	-0.99
Ti	0.76	-0.96	0.65	0.15	0.49	-0.73	-0.67	0.72

Table 6.5 : Pearson's correlation coefficients of flux cored consumable welding fumes elements and oxygen index.

	Slag from FCW1	Slag fromFCW2	Slag from FCW3	Slag from FCW4
Al	3.5	4.3	4.4	4
Cr	8.4	10.1	10.4	10.1
Cr(VI)	0.01	0.02	0.02	0.02
Fe	1	1.9	1.9	2.0
K	0.6	0.9	0.8	0.8
Mn	6.8	6.8	7.0	6.8
Na	0.5	0.7	0.7	0.6
Si	2.2	2.7	2.8	2.9
Ti	36.1	33.7	33.4	33.2
Oxygen index	0	10	9.5	12

Table 6.6: Elemental composition of slag

6.6 Conclusions

Results from XRD, SEM, EDX suggests that there is no effect of shielding gases on the structure of the welding fume particles. Fume particles generated during welding using different shielding gases have similar spinel structure. XRD of all fume samples have both amorphous and crystalline morphology. EDX and SEM shows that welding fume have similar elemental composition(qualitative) irrespective of the shielding gases used. FTIR data indicates that welding fumes from flux cored wires have Cr(VI) in the form of chromates, dichromates and chromium trioxide. Whereas solid stainless-steel consumables do not show any chromates and dichromates peaks.

ICP data indicates that the shielding gases plays an important role in the elemental composition (quantitative) of the welding fumes. Composition of the Cr(VI) in welding fumes depends on the type of shielding gas used. When performing welding using solid stainless-steel wires as the consumable, the oxidation index of shielding gases plays an important role as we observe the least amount of Cr(VI) with argon as a shielding gas compared to other oxidising shielding gases. Along with the oxidation index of shielding gases the other important variables are the arc stability and ionisation potential of the shielding gases. Since mixture of CO_2 and O_2 provide the most stable arc we observe the least amount of Cr(VI) among the other oxidising shielding gas mixture, irrespective of having the highest oxygen index.

ICP data of welding fumes from flux cored wires shows the strong negative correlation between the oxygen index of shielding gases and Cr(VI) formation. We observe the highest amount of Cr(VI) in the sample which was generated using Ar as the shielding gas. This is due to the fact that flux cored wires contain Na and K in them which are the main reason for oxidation of Cr(III) to Cr(VI) in welding fumes and in the absence of oxygen they mostly react with Cr and form chromates and dichromates as a result we observe the highest amount of Cr(VI) in FCW1 sample compared to other samples. In the samples where oxidising shielding gases are used, we observe the decrease in the Cr(VI) because Na and K reacts with the oxygen and forms their oxides as a result there is less Na and K is present to form chromates and dichromates and we observe the reduction in the Cr(VI) formation.

Chapter VII: Mathematical modelling approach for understanding mechanism of Cr(VI) formation in welding fumes.

7.1 Introduction

Understanding the mechanism of Cr(VI) formation is important for finding solutions for Cr(VI) mitigation in welding fumes. In this chapter, I have tried to understand the physics and chemistry behind the Cr(VI) formation mechanism. Mathematical modelling of fume formation during arc welding can be a complex process, as it involves multiple variables such as the type of welding process, the composition of the materials being welded, the welding parameters (e.g., current, voltage, and travel speed)This aim can be achieved by developing a mathematical model which is bases on the basics of arc physics and thermodynamics of the vaporisation. During welding fumes are generated from the three main sources.

- Molten droplet from the consumable
- The weld pools
- Spatter

In this study, mathematical model is based on the fumes formed from the molten metal droplet from the consumable. Since the previous studies shows that majority of the fumes comes from the vaporisation of the consumable electrode, more than 90%[67, 69]. The procedure used in this model is divided into following stages.

- Determining the size of the droplet
- Determining the droplet falling time.
- Determining the temperature of the droplet.
- Mass and energy balances on formed droplet.

7.2 Model setup

7.2.1 Size of the droplet

Previous studies shows that the shape of droplet changes as it travels down the arc[16]. Simpson et al. has developed a one dimensional droplet model which predicts the droplet shape as the function of time[63]. To keep this model simple, I have derived equations for the size and volume of the droplet assuming the droplet to be spherical in shape since the droplet shape is very similar to the sphere. Size and volume of the droplet depends on the wire feed rate. which means the volume of wire fed per unit time or mass of wire fed per unit time.

The volume of the droplet is the volume of wire fed divided by the number of the droplets formed per unit time. The mass of droplet is directly proportional to wire feed rate.

Hence,

$$\textbf{Volume of drop } (V_d) = \frac{V_w \times \pi \times R^2{}_w}{\dot{n}} \qquad (7.1)$$

Where, V_w is wire velocity in m/s

R_w is radius of wire in m

$\dot{n}$ is frequency (1/s)

Volume of droplet can easily be determined using Equation (7.1) since wire feed rate/wire velocity is the parameter set before welding and radius is also know. Frequency, voltage, and current is measured during welding.

Since our droplet is spherical in shape hence, using volume of sphere.

$$\textbf{Volume of sphere} = \frac{4}{3}\pi r^3 \qquad (7.2)$$

Using equations (7.1) and (7.2)

$$\textbf{Radius of droplet } R_d = \left(\frac{v_w R_w}{\dot{n}}\right)^{1/3} \qquad (7.3)$$

From these equations we can determine the size and volume of the droplet. As the droplet travels in the arc its temperature and size grow. Due to which its evaporation also increases because of the increase in surface area and temperature. These above equations don't consider the account for energy and mass loss due to evaporation. This issue is addressed later in the

chapter while calculating the fume formation rate. Once the droplet grows it detaches from the wire and travel through the arc column. It is subjected to energy and mass transfer while it is travelling in the arc. To calculate its energy losses during its time in arc column it is important to evaluate the droplet falling time.

7.2.2 Droplet falling time.

The falling time of droplets in welding arc is determined by the distance travelled, the initial velocity, and the acceleration. The acceleration is the sum of the gravitational acceleration and the drag force due to the plasma flow. The droplets also experience other forces such as electromagnetic force, surface tension force, and vapor jet forces. These forces act together to determine the shape and falling time of the droplets. The mass and volume of the droplets are also important factors in the calculations and can be determined from the velocity of the wire and the frequency of droplets forming per second. The falling time for droplet is calculated assuming the constant acceleration,

$$\mathbf{S = ut + \frac{1}{2}\, at_f^{\,2}} \quad \mathbf{(7.4)}$$

Where, s = distance travelled(m),

u= initial velocity (m/s)

t_f =falling time (s)

a= acceleration (m/s^2)

Since the initial velocity is zero and the distance travelled is arc length (L_a) equation (7.4) can be rearranged to give falling time i.e.

$$\mathbf{t_f = (2\,\frac{L_a}{a})^2} \quad \mathbf{(7.5)}$$

Unknown in the equation 7.5 is acceleration.

The droplet after detaches from electrode it is subjected to gravitational forces and to drag forces due to plasma flow from anode to cathode (in the electrode positive MIG arc welding)

7.2.2.1 Acceleration on droplet

$$\mathbf{a = g + \frac{F_d}{m_d}} \quad \mathbf{(7.6)}$$

where, a = acceleration (m/s^2)

g= gravitational acceleration (9.81 m/s^2)

F_d= Drag force due to plasma (N)

m_d = mass of droplet (Kg) = Mass of droplet = volume of droplet * density of droplet

7.2.2.2 Forces acting on the droplet.

When the droplet is forming it experiences several forces on it and they determine the shape and the falling time of the droplet into the weld pool. The forces which act together on the droplet are as follows.

- Gravitational force, F_g
- Aerodynamic (drag) force, F_d
- Electromagnetic force, F_e
- Surface tension force, F_s
- Vapor jet forces, F_v

All the forces which act upon the falling molten droplet of electrode is shown in fig 7.1.

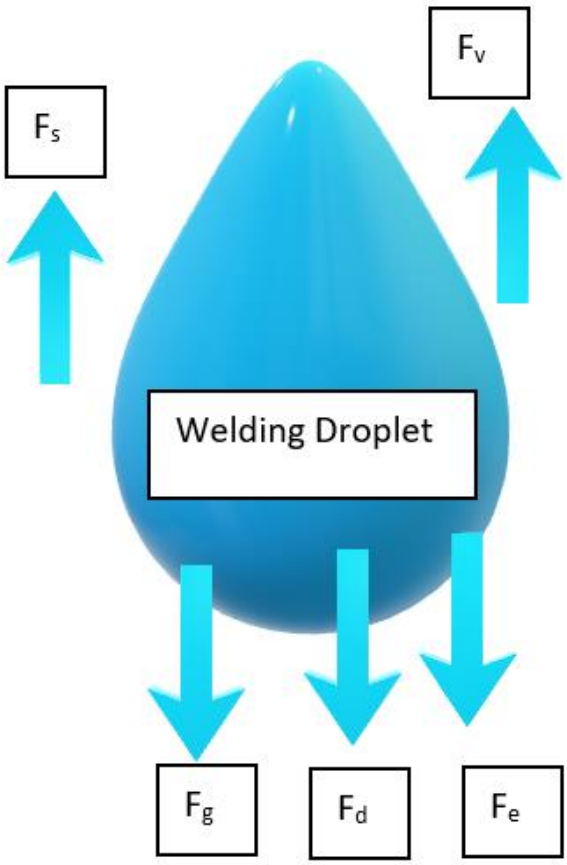

Figure 7.1 : Forces acting on droplet in welding arc.

There are three conditions and phases of the development of the welding droplet:

Growth of Droplet

$F_v + F_s > F_e + F_d + F_g$

Detachment of droplet

$F_v + F_s < F_e + F_d + F_g$

Equilibrium Condition

$F_v + F_s = F_e + F_d + F_g$

- **Gravitational force, F_g**

It is the downward force which pulls the droplet into the weld pool due to gravity.

$$\mathbf{F_g = mg} \qquad \mathbf{(7.7)}$$

Where, m is the mass of the droplet.

g is the vertical component of the acceleration due to gravity (9.81 m/sec 2 or 9.81cosϴ, where ϴ is the angle between the arc axis and the vertical).

Mass of droplet = volume of drop * density of drop

Volume of drop

Volume is calculated from equation (7.1)

$$\textbf{Volume of drop } (\mathbf{V_d}) = \frac{\mathbf{V_w \times \pi \times R^2_w}}{\dot{\mathbf{n}}} \qquad \mathbf{(7.1)}$$

Where V_w is wire velocity in m/s

R_w is radius of wire in m.

ṅ is frequency of drops forming per second?

- **Aerodynamic (Drag) Force, F_d**

The gas flow (atmosphere/ shielding gases) around and within the arc induces aerodynamic drag (Fa) on the droplet given by

$$\mathbf{F_d = 0 \cdot 5V^2 \rho (\pi r^2) C_d} \qquad \mathbf{(7.8)}$$

Where , V is the plasma velocity,

ρ is the plasma density,

r is the droplet radius

C_d is dragging coefficient.

This force is higher with higher droplet radius and gas velocity. All these properties determine the shape of droplet hence the shielding gases properties such as ionisation potential play important role in determining the fume formation rate and the composition of the welding fumes. Role of shielding gases is discussed in detail in previous chapters.
Radius can be determined by using equation 7.3.

(a) Plasma velocity

Plasma is basically an ionised gas at very high temperatures. The arc consists of plasma with a current flowing through it. This current then creates a magnetic field and when the moving charged particles(ions and electrons) in the plasma interacts with this magnetic field, it results into creating the force on to these particles. We have assumed arc as a cylindrical in shape and for the current carrying cylinder this interaction results in the force towards the centre of the axis. This force is balanced by the pressure which is maximum at the centre. If we assume the arc to be a cylindrical conductor with evenly distributed current, the pressure at the axis of the arc can be calculated by the equation 7.9.

$$\mathbf{P_{axis} = \mu_o \frac{Ij}{4\pi} + P_{ambient}} \quad \mathbf{(7.9)}$$

Where, μ_0 is permeability of free space= $4\pi 10^{-7}$

I current (A)

j current density= $I/(\pi R_{arc}^2)$

R_{arc} = arc radius assuming cylinder

P_{axis} is pressure at axis

$P_{ambient}$ is ambient pressure

(b) Plasma Density

It is the density of shielding gas assuming it as perfect gas

$$\mathbf{\rho_P = \frac{PM}{RT}} \quad \mathbf{(7.10)}$$

Where, ρ_P is plasma density

P is pressure of gas (N/m^2)

M is molecular weight (kg/mole)

R universal gas constant= 8.314 (J/mole.K)

T temperature of arc (K)

Different shielding gases has different plasma densities.

(c) Plasma viscosity

Arc plasma viscosity is a complex phenomenon that is influenced by several factors, including the temperature, density, and composition of the plasma, as well as the properties of the electrodes and the surrounding gas or vacuum. In general, the viscosity of arc plasma tends to be lower than that of other types of plasma, due to the high temperatures and high ionization levels that are present in the plasma. Plasma viscosity of the pure monoatomic gas can be calculated using equation (7.11) [146].

$$\textbf{Viscosity} = 2.6693 \times 10^{-6} \times (MT)\frac{0.5}{\sigma^2}\Omega_u \qquad (7.11)$$

Where, M is molecular weight (g/mole)

T is temperature of plasms (K)

σ is collision diameter (Angstroms)

$\Omega_u = \text{fn}(\frac{KT}{\epsilon})$ it is Lennard – Jones collision integral

K is Boltzman constant = 1.3805* 10^{-23} (J/K)

ϵ is energy of Interaction (J)

(ϵ/K) and σ can be found from tables and for argon the values are 128 K and 3.418 Angstroms respectively .

Value of Ω_u between 10 and 100 is given by $\Omega_u = 1.04966 - 0.2333\text{Log}(\frac{KT}{\epsilon})$

Hence, for Argon at 6000K $\Omega_u = 1.70 * 10^{-4}$ N/(m^2s)

- **Electromagnetic Force**

Electromagnetic force in arc plasma is the force that arises from the interaction of charged particles in the plasma with the magnetic and electric fields that are present in the plasma. It plays a significant role in the dynamics of the arc plasma, influencing the movement and

behaviour of the charged particles. It can be used to manipulate and control the behaviour of the plasma. Due to the welding current, the electromagnetic force is given by

$$\mathbf{F_e = \frac{\mu}{4\pi} I^2 \ln \left| \frac{r_a^2}{R} \right|} \quad \mathbf{(7.12)}$$

Where, μ is the magnetic permittivity of the material,

I is the welding current,

r_a is the exit radius of the current path

R is the entry radius of the current path

- **Surface Tension**

Surface tension is the force that holds the surface of a welding droplet together and makes it behave as if it were a stretched elastic membrane. It is caused by the cohesive forces between the molecules at the surface of the molten metal, which are stronger than the adhesive forces between the molecules and the surrounding air.

In droplet formation, surface tension plays a crucial role as it is responsible for the spherical shape of droplets and their stability. As a droplet of molten electrode is formed, the surface molecules at the droplet's edge are pulled inwards by the cohesive forces between the molecules, creating a surface that is curved inwards (concave), which results in the spherical shape of the droplet.

The surface tension of a liquid can also affects the size of droplets formed. For example, a liquid with a high surface tension will tend to form smaller droplets than a liquid with a low surface tension because the cohesive forces between the molecules are stronger.

The droplet's stability is also determined by the surface tension. The droplets that have a lower surface tension tend to be more unstable as the cohesive forces between the molecules are weaker, resulting in droplets that are more likely to merge or deform. Droplets with higher surface tension tend to be more stable due to the stronger cohesive forces that holds their shape. Force which determines the surface tension can be determined by equation 7.13

$$\mathbf{F_s = 2\pi r_w \sigma f \left(\frac{r_a}{c} \right)} \quad \mathbf{(7.13)}$$

Where, r_w is the radius of wire

σ is surface tension

f (r_a/c) is function of wire diameter, C is the constant of capillarity

- **Vapor jet forces, F_v**

At higher welding currents, significant vaporization at the surface of the molten droplet can occur in the arc root area. Thermal acceleration of the vapor particles into the arc plasma results in a force called the vapor jet force, which opposes the droplet transfer. This vapor jet force for a flat surface at uniform temperature and composition is given by

$$\mathbf{F_V = \frac{m_0}{d_V} Ij} \quad \mathbf{(7.14)}$$

where m_0 is the total mass vaporized per second per ampere,

I is the current,

j is the current density

d_v is the vapor density

Balancing these equations will help to find the time the droplet is exposed to arc temperatures and the time for fume formation from a single drop. Next step in developing this model is to find the way to calculate the temperature of the droplet at a given time which will eventually be used to balance the heat and mass transfer equations. From the mass and heat transfer equations the total loss in the elements from the welding wire in the form of fumes can be calculated.

7.2.3 Equations for determining the temperature of the droplet

This part describes a set of equations and methodologies used to calculate the temperature of a droplet in welding. It involves the calculation of energy input, heat content, and density, along with the parameters of the electrode wire, such as cross-sectional area, wire current density, and wire feed rate. The droplet temperature is calculated using a complex equation that considers various factors such as ambient temperature, heat content, and droplet density. The equation also contains variables such as radius of wire, welding current, wire feed rate, wire

density, droplet density, and electrode extension. This method is based on the model of resistance heating in the wire proposed by Halmoy et al[147]

Cross-sectional area of wire (A_w)

Assumption: Diameter of wire: 1mm

$$\mathbf{A_w = \pi r^2} \quad \textbf{(7.15)}$$

r=radius of wire

Wire current Density (j_w)

$$\mathbf{j_w = \frac{I}{A_w}} \qquad \textbf{(7.16)}$$

I= welding current

Volume of droplet (V_d)

$$\mathbf{V_d = \frac{u_w A_w O_w t}{O_d}} \qquad \textbf{(7.17)}$$

Where,

u_w= wire feed rate (m/s)

A_w = Wire crosssectional area (m^2)

O_w = wire density (kgm^{-3}) Assumed 304 stainless steel 8000 kgm^{-3}

O_d =droplet density (kgm^{-3})

Droplet density (O_d)

Calculated for 304 stainless steel

$$\mathbf{o_d = 75512 - 1 \cdot 1167 \times 10^{-4} T_d - 1 \cdot 5063 \times 10^{-7} T_d^{\,2}} \qquad \textbf{(7.18)}$$

Where,

T_d is droplet temperature

Heat constant (H_L)

Heat constant HL is the heat content per unit volume at the end of the electrode extension as a result of resistance heating in the wire. It is given by the following equation.

$$\mathbf{H_L = 1.67 \times 10^7 + 2.232 \times 10^{-7} \left(\frac{L j_w^2}{u_w}\right) + 5.98 \times 10^{-23} \left(\frac{L j_w^2}{u_w}\right)^2} \qquad \textbf{(7.19)}$$

Where, L is electrode extension (m)

j_w is wire current density (Am^{-2})

M_w is wire velocity (ms^{-1})

From above equations the droplet temperature equation is formed which is shown in equation 7.20

Droplet temperature (T_d)

$$\mathbf{T_d = \left\{\frac{1}{1+\left(\frac{3kI}{2eu_wA_wO_wc_P}\right)}\right\}\left\{T_a + \left(\frac{H_F}{c_p}\right) + \left(\frac{V_{wf}+V_a+(3k/2e)T_p}{u_wA_wO_wc_P}\right)I + \left(\frac{H_L}{O_wc_P}\right)\right\}}$$

(7.20)

Where,

k is Boltzmann's constant= $1.38* 10^{-23}$ ($J\ mol^{-1}\ K^{-1}$)

I is welding current

e is charge on an electron =$1.60*10^{-19}$ (C)

u_w is wire velocity (ms^{-1})

A_w is wire cross sectional area (m^2)

O_w is wire density ($kg\ m^{-3}$)

c_P specific heat capacity of droplet ($Jkg^{-1}K^{-1}$) = 753 $Jkg^{-1}K^{-1}$

T_a ambient temperature (K) = 293 K

H_F wire latent heat of fusion ($J\ kg^{-1}$) =247000 $J\ kg^{-1}$

V_{wf} droplet material work function potential (V) = 4.18

V_a anode potential (V) = 1vV

T_p plasma arc temperature (K)

H_L wire tip volumetric heat constant ($J\ m^{-3}$)

7.2.4 Equations for determine the Heat and mass loss of the droplet

In this part, I have discussed how the net energy received by a droplet is determined by the balance of heat received from the surrounding plasma through conduction and convection, and

heat lost through radiation from the droplet's surface. The heat transfer coefficient 'h' is described by the Nusselt number, which considers the thermal conductivity of the plasma and the droplet's Reynolds and Prandtl numbers. A correction factor is also provided for argon plasma, which considers the drag coefficient. Thermal conductivity of the plasma is also described. Later equations discuss the mass transfer, specifically the flux of a component between the droplet and the surrounding plasma, described by the Vapour phase mass transfer coefficient and the interfacial pressure.

7.2.4.1 Heat transfer equations

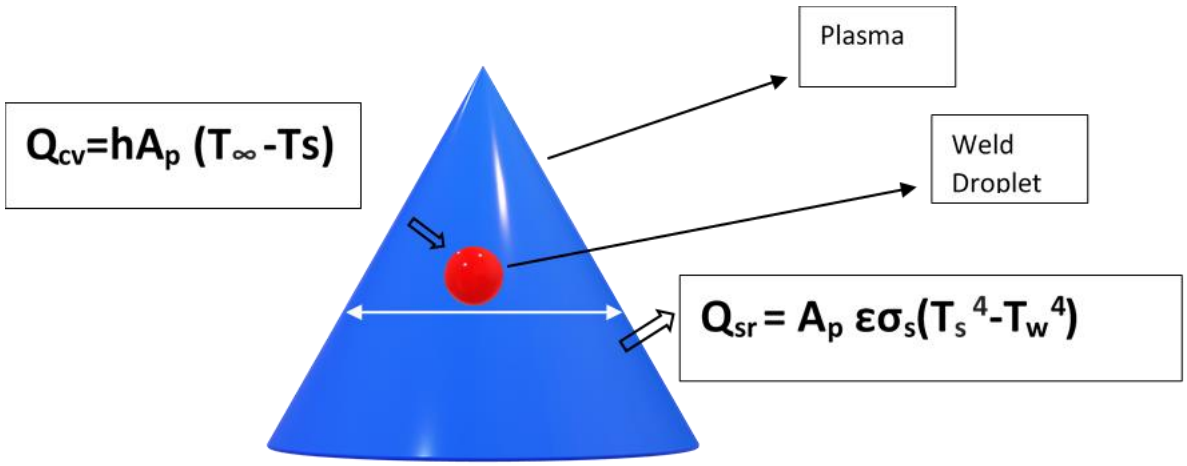

Figure 7.2: Schematic representation of the net heat exchanged between droplet and its surrounding

Net energy received by droplet Q_n is heat balance between heat received by droplet from plasma by conduction and convection and heat lost by radiation from droplet surface by radiation to the surrounding.

$$\mathbf{Q_n = Q_{cv} - Q_{sr} = hA_P(T_\infty - T_s) - A_p\varepsilon\sigma_s(T_s^4 - T_a^4)} \quad \textbf{(7.21)}$$

where

h heat transfer coefficient ($W/m^2\ K$)

Ap surface area of the droplet,

T_∞ the free-stream plasma temperature (K)

Ts the surface temperature of the droplet (K)

E particle emissivity (varies from 0 to 1.0)

σ_s Stephan-Boltzmann constant ($5.67 * 10^{-8}\ W/m^2\ K^4$)

the main factor in equation 7.21 is the heat transfer coefficient 'h' which is a measure of the heat transferred per unit area per unit temperature difference. It is used to quantify the rate of heat transfer between a solid surface and a fluid, in our case from the electrode to the molten droplet. The heat transfer coefficient depends on various factors such as the properties of the fluid and solid, the velocity of the fluid, the temperature difference between the fluid and the solid. Heat transfer coefficient is calculated using Nusselt number, Reynolds number and thermal conductivity of the electrode materials. Equations (7.22)- (7.26) is used to determine heat transfer coefficient.

$$\mathbf{N_u} = \frac{\mathbf{h\,dp}}{\mathbf{k}} \qquad \mathbf{(7.22)}$$

Where, Nu is Nusselt number

K is thermal conductivity of plasma surrounding the droplet

Nu is 2 when droplet is stationary

$$\mathbf{N_u = 2 + 0.6R_e^{0.5}P_r^{0.33}} \qquad \mathbf{(7.23)}$$

Where, Re is Reynolds number, and the Pr is Prandtl number

In our case we consider argon plasma so Nu can be further corrected

$$\mathbf{N_u = 2f_0 + 0.473R_e^{0.552}P_r^{m}} \qquad \mathbf{(7.24)}$$

where m= 0.78 $Re^{0.552}$ $Pr^{0.36}$

$$\mathbf{f_0 = \frac{\left(1-T_0^{(1+x)}\right)}{(1+x)(1-T_0)T_0^{x}}} \qquad \mathbf{(7.25)}$$

$f_0 = (1-T_o^{1+x})/[(1+x)(1-T_o)T_o^{x}]$ x= 0.8 for Ar at T < 10000K

Thermal conductivity of the electrode is calculated using equation (25)

$$\bar{\mathbf{k}} = \left(\frac{1}{T_\infty - T_p}\right)\left[\int_{T_p}^{T_\infty} \mathbf{k(t)dT}\right] = \left(\frac{1}{T_\infty - T_p}\right)\left[\mathbf{S(T_\infty) - S(T_p)}\right] \quad \mathbf{(7.26)}$$

Where, T_p is the temperature of the droplet and T_∞ is the temperature of the plasma.

7.2.4.2 Mass Transfer equations

Last step in modelling the amount of different elements generated during welding is to find the mass transfer from the molten droplets into the fumes. In this approach however it is difficult to calculate the composition of each elements accurately and precisely as we are not considering the chemical equilibriums and chemical kinetics. The model developed here is hard to be used practically for determine the elements in the fumes, but it depicts the clear picture how the different parameters in welding affect the chemistry of the fume composition.

For developing mass transfer equations, I have considered the droplet surface at equilibrium. AB is the droplet with molten electrode, BC is the equilibrium. At CD the mass transfer occurs and at DE it stabilises.

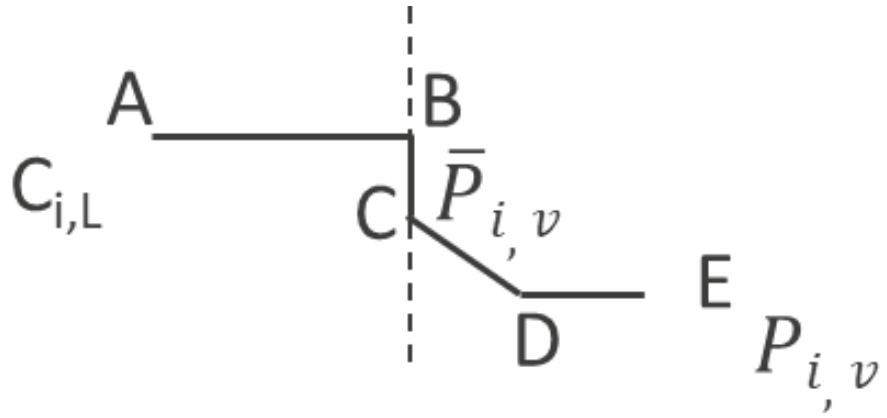

Figure 7.3 : welding droplet mass transfer surface

Flux between CD can be written as

$$\mathbf{N_i = K_V(\bar{P}_{i,v} - P_{i,v})} \qquad \mathbf{(7.27)}$$

Where,

K_V is Vapour phase mass transfer coefficient for i component.

$\bar{P}_{i,v}$ is interfacial pressure

$P_{i,v}$ is Bulk Pressure in Vapour phase

$C_{i,L}$ is Bulk Concentration in liquid phase

Henry's Law

Henry's law is a gas law that states that the concentration of vapour phase and Liquid phase at equilibrium is proportional to its partial pressure. The proportionality factor is called Henry's law constant

Hence at the film we can apply Henry's Law

And we can write

$$\bar{P}_{i,v} = H\, C_{i,L} \qquad (7.28)$$

Where, H is Henry's Law constant

Equation (26) can we have rewritten as:

$$N_i = Kv\left(HC_{i,L} - P_{i,v}\right) \qquad (7.29)$$

Total Flux

$$N = \sum_{i=1}^{4} N_i \qquad (7.30)$$

The different constants used in these equations can be determined by the following equations.

Reynolds Number

$$R_e = \frac{D_d V \rho}{\mu} \qquad (7.31)$$

Schmidt Number

$$s_C = \frac{\mu}{\rho D_{Lv}} \qquad (7.32)$$

Sherwood Number

$$s_h = \frac{k_v D_d}{D_{Lv}} \qquad (7.33)$$

$$s_h = 2 + 0 \cdot 552\left[Re^{0.5} Sc0.5\right] \qquad (7.34)$$

Where,

D_d is Droplet diameter

V Flow Speed

ρ Density of element

D_{Lv} is Mass diffusivity of element

7.3 Conclusions

The objective of developing a mathematical model for Cr(VI) in welding fumes was twofold. Firstly, to investigate the relationship between various process parameters, such as voltage, current, wire speed, and shielding gases, and the formation of Cr(VI) in welding fumes. This is due to the fact that these process parameters exert a significant influence on the forces that govern droplet formation, and therefore on the size of the droplets. As it is well established that a significant portion of welding fumes is generated from the droplets, a comprehensive understanding of this relationship is crucial. The second objective was to use the findings from the first objective to develop a chemical model that would study the interactions between the molten metal and the shielding gases at high temperatures. This model would be based on principles of chemical equilibria and heat and mass transfer kinetics, thereby enabling a more comprehensive understanding of the mechanisms involved in the formation of Cr(VI) in welding fumes. The end goal of this chemical model would be to quantify and determine the Cr(VI) concentration in welding fumes.

In this study, it can be concluded that the first objective was successfully achieved. The size and temperature of the droplets, as well as the heat and mass transfer from the droplet surface, can provide insight into the elements that are evaporated from the welding droplet over a specific period of time. This information can give an idea of the concentration of various elements, including total chromium, present in the fumes, but not specifically the concentration of Cr(VI). However, to fully realize the second objective, which is to model Cr(VI) concentrations, a deeper understanding of computational and chemical modelling, as well as proficiency in various modelling software, is required.

Chapter VIII : Summative and conclusive remarks

The research conducted on Cr(VI) in welding fumes has provided important insights into the mechanism of Cr(VI) generation and the identification of airborne Cr(VI) compounds. In this thesis, the main research gaps were identified during the literature review process and efforts were made to address .The most significant research gap was comprehending the mechanism of Cr(VI) formation in various welding techniques. To understand this, it was crucial to determine the different compounds present in welding fumes. This was achieved by utilizing FTIR to identify the various Cr(VI) species generated during welding.

In chapter IV , FTIR was used for arc welding fumes collected from Manual Metal Arc Welding (MMA), Flux Cored Arc Welding (FCAW) and Solid Wire Welding (Metal Inert/ Active Gas Welding [MIG/ MAG]). For MMA and FCAW samples, clear spectra corresponding to Na, K, dichromates was observed at wave number of around 725-740 cm^{-1} and at 890-900 cm^{-1}. Chromate species were also observed at around 850-855 cm^{-1}, as was evidence of CrO3 (chromium trioxide) too (950-970 cm^{-1}). The identification of these compounds was done by carefully identifying the Cr-O-Cr anti-symmetric vibrations, the symmetric stretching of the CrO4 tetrahedra, and the stretching vibrations of the planar CrO3 structure for the chromium trioxide. All the above compounds were volatile, and present as nanoparticles in welding fumes, thereby potentially causing significant harm to the welders. Additionally, crystalline phases (Fe-Mn spinels) were also observed through powder XRD, and the data was compared.

In Chapter V, the utilization of FTIR for quantifying Cr(VI) compounds in welding fumes was thoroughly explored as an alternative to the conventional wet chemistry ion chromatography method. The findings revealed that FTIR can be a prospective technique for quantification, provided appropriate attention is given to developing calibration samples. Despite being based on a distinct approach, the estimates obtained from FTIR were reasonably close to the actual values derived from ion chromatography, underscoring the potential of FTIR as an efficient means for measuring Cr(VI) compounds in welding fumes and offering advantages over traditional wet chemistry methods.

To maximize the accuracy and reliability of FTIR analysis for Cr(VI) measurements in welding fumes, further research on calibration samples is essential. Developing well-characterized calibration samples will enhance the precision of the method. Moreover, the establishment of

robust calibrations is crucial to ensure consistent and dependable results in Cr(VI) measurements. Operator training is another critical aspect to consider. Well-trained operators can effectively use FTIR to eliminate atmospheric interferences and optimize the analysis process, leading to more accurate measurements. While FTIR shows promise as an alternative method, it should be complemented with traditional wet chemistry approaches such as ICP and ion chromatography. By combining these techniques, a comprehensive understanding of welding fumes and their compound composition can be attained. In conclusion, by investing in research, establishing robust calibrations, providing operator training, and integrating FTIR with traditional methods, a more accurate and comprehensive analysis of welding fumes and their potential hazards can be achieved.

In Chapter V, the use of electrochemistry to create sensors for continuous monitoring of Cr(VI) in industries was evaluated, but it was found to be not practical. This was due to the complex nature of welding fumes, which consist of various compounds in different oxide and spinel forms, especially Cr, Mn, and Fe compounds. The results from cyclic voltammetry indicated that the oxidation of Fe, Mn, and Cr occurred at 0.6V in 0.5M ammonium hydroxide solution, making it challenging to quantify the mixed peak. However, this research opens the possibility for further exploration. If electrodes can be developed that are selective only to Cr(VI) compounds in welding fumes, this technique could be ground-breaking as it would enable real-time monitoring of Cr(VI).

Chapter VI study provides valuable insights into the mechanisms underlying Cr(VI) formation during various arc welding processes, with a particular focus on the influence of the oxygen index in different shielding gases. The research highlights the significance of the oxidation index in determining Cr(VI) production when using solid stainless-steel wires. Additionally, the stability of the welding arc and the ionization potential of the shielding gases were identified as key factors affecting Cr(VI) generation. The findings indicate that gas mixtures comprising carbon dioxide (CO_2) and oxygen (O_2) with Argon (Ar) result in the least formation of Cr(VI) compared to single gases of CO_2 or O_2 with Ar. Despite possessing the highest oxygen index, the CO_2 and O_2 mixture provides a more stable arc, leading to reduced Cr(VI) formation among oxidizing shielding gas mixtures. Furthermore, Flux Cored Wires (FCW) welding with Argon as the shielding gas showed the highest levels of Cr(VI) due to the presence of sodium (Na) and potassium (K) in the wires, promoting the oxidation of Cr(III) to Cr(VI). Conversely, using oxidizing shielding gases lessens Cr(VI) formation as Na and K react with oxygen to form their respective oxides, limiting their availability for chromate and dichromate formation. The

research also found no significant impact of shielding gases on the structure of welding fume particles, which consistently exhibited spinel structures across different shielding gas configurations. These comprehensive findings contribute to the advancement of knowledge in the field and offer valuable guidance for implementing appropriate measures to minimize welders' exposure to Cr(VI) in industrial settings

In Chapter VII, the focus was to gain insights into the mechanism of Cr(VI) formation through mathematical modelling. Although the results of the mathematical modelling were not conclusive, the work performed laid the foundation for future research in this field. In the future, the mathematical model worked upon in chapter VII, can be used using variables such as wire feed rate, voltage, and shielding gases into simulation software. This will allow for a better understanding of how these factors impact Cr(VI) formation on a macro level, which can be verified with experimental data. On the micro level the impact of these variables can also be studied in exploring their effect on the forces generated during arc welding and their impact on the arc physics, droplet size and temperature and this information can then be used in automation and developing welding machines modelled to reduce the Cr(VI) formation in welding fumes.

In conclusion, this PhD research addressed crucial aspects of the mechanism of Cr(VI) formation and advanced our understanding of Cr(VI) in welding fumes. It also laid the foundation for future technologies that can be developed for closely monitor Cr(VI) levels in industry and find solutions to protect welders and those affected by Cr(VI) in welding fumes.

Further work

FTIR analysis has demonstrated significant potential in identifying Cr(VI) compounds, but its application for quantitative analysis requires further research, particularly in accurately identifying silicates present in welding fumes. Accurate identification of silica compounds in welding fumes would greatly enhance the development of FTIR for quantification using the intensity ratio method, as discussed in Chapter V of this thesis. It is important to recognize that welding fumes contain not only Cr(VI), which adversely affects the health of welders, but also other compounds such as Mg and Si. Therefore, comprehensive studies on these compounds and their mechanisms of formation are also necessary.

To advance the development of electrochemical sensors, more research is needed on ion-selective membranes to enhance their capabilities. The mathematical model presented in this thesis lays the groundwork for further investigations, and its potential can be expanded by integrating thermodynamic and chemical modeling. This integrated approach can enable the prediction not only of Cr(VI) composition in welding fumes but also the quantities of other harmful substances present. This mathematical model, if developed accurately and precisely, has the potential to be groundbreaking, facilitating the creation of products that are less harmful to the health of welders. By combining cutting-edge research on FTIR analysis, the study of other compounds in welding fumes, and the development of advanced mathematical models, significant advancements can be made in occupational health safety for welders.

Recommendations for welders and industries from the research presented in this thesis:

(a) Welding fumes, including those generated during the welding of mild steel, are categorized as carcinogens, meaning they have the potential to cause cancer. To safeguard yourself from potential health risks, it is essential to take necessary precautions. Always use Personal Protective Equipment (PPE) kits, which may include respiratory protection, gloves, and eye protection, to minimize exposure to fumes and metal particles. Whenever possible, perform welding in well-ventilated areas to ensure adequate air circulation and reduce fume concentrations. Local exhaust ventilation systems (LEVs) can be employed to capture and remove fumes at the source, further reducing the inhalation of harmful substances. Prioritizing safety and adopting preventive measures will help protect your health and well-being when working with welding processes.

(b) While Cr(VI) is indeed a primary constituent of welding fumes that is associated with cancer risk, it is crucial to recognize that welding fumes contain other hazardous elements that can pose health risks to welders. Manganese (Mn) and Silicon (Si) are two such elements that are commonly present in welding fumes and can be dangerous to the health of welders. Manganese, found in certain welding processes and base metals, can lead to neurological effects, and cause a condition known as "manganese-induced Parkinsonism." Prolonged exposure to high levels of manganese can result in symptoms similar to Parkinson's disease. Silicon, which is commonly found in the base metal being welded, can produce fine particulates when subjected to the welding process. Inhalation of these particulates can lead to respiratory issues and irritation of the respiratory tract. It is, therefore, vital for welders to be aware of the potential

hazards associated with welding fumes and to take appropriate precautions to minimize exposure.

(c) Continual monitoring of exposure limits to welding fumes is highly recommended to ensure the safety and well-being of workers. It is essential to conduct monitoring regularly and, at a minimum, whenever there is a change in welding processes or techniques. Adhering to government safety guidelines and exposure limits is not only a legal requirement but also crucial for protecting the health of welders. By regularly monitoring exposure levels, potential hazards can be identified promptly, allowing for timely implementation of necessary control measures. Monitoring also helps in identifying trends and patterns in exposure, which can guide improvements in workplace safety practices and help create a healthier work environment for welders. By staying vigilant and proactive in monitoring exposure levels, employers can demonstrate their commitment to worker safety and ensure compliance with regulatory requirements.

Publications from this thesis:

(a) FTIR spectroscopy as a convenient tool for detection and identification of airborne Cr(VI) compounds arising from arc welding fumes.
https://www.sciencedirect.com/science/article/pii/S0304389423001449?via%3Dihub

Research Paper

FTIR spectroscopy as a convenient tool for detection and identification of airborne Cr(VI) compounds arising from arc welding fumes

Vishal Vats [a,c], Geoff Melton [b], Meez Islam [a], Venkatesan V. Krishnan [a,*]

[a] Teesside University, United Kingdom
[b] TWI, Cambridge, United Kingdom
[c] NSIRC, Cambridge, United Kingdom

HIGHLIGHTS

- Arc welding fumes (MMA, FCAW and MIG/MAG) were analyzed using FTIR.
- IR-active modes for Cr(VI) at 800–900 cm^{-1}, e.g., Cr-O-Cr, Cr-O, Cr=O, CrO_4.
- Cr(VI) speciates as Chromates, Di-chromates and CrO_3, and partly as spinels.
- Highest levels of Cr(VI) in MMA welding, compared to FCAW, and MIG/MAG.
- FTIR is facile, and augments Ion Chromatography, by identifying Cr(VI) species.

GRAPHICAL ABSTRACT

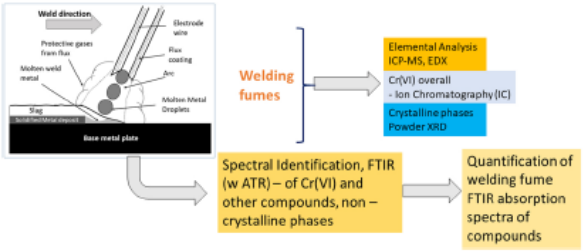

ARTICLE INFO

Editor: John D Atkinson

Keywords:
MMA
FCAW
MIG/MAG
FTIR
Ion chromatography (IC)

ABSTRACT

Given the significant presence of the carcinogenic Cr(VI) in arc welding fumes from stainless steels, it is also important, in addition to estimating the Cr(VI) levels, to identify Cr(VI) compounds, as it throws light on the mechanistic pathways towards fume formation. FTIR data is presented in this paper for arc welding fumes collected from Manual Metal Arc Welding (MMA), Flux Cored Arc Welding (FCAW) and Solid Wire Welding (Metal Inert/ Active Gas Welding [MIG/ MAG]). For MMA and FCAW samples, clear spectra corresponding to Na, K, dichromates was observed at wave number of around 725-740 cm^{-1} and at 890-900 cm^{-1}. Chromate species were also observed at around 850-855 cm^{-1}, as was evidence of CrO_3 (chromium trioxide) too (950-970 cm^{-1}). The identification of these compounds was done by carefully identifying the Cr-O-Cr anti-symmetric vibrations, the symmetric stretching of the CrO_4 tetrahedra, and the stretching vibrations of the planar CrO_3 structure for the chromium trioxide. All the above compounds were volatile, and present as nanoparticles in welding fumes, thereby potentially causing significant harm to the welders. Additionally, crystalline phases (Fe-Mn spinels) were also observed through powder XRD, and the data was compared with ion chromatography estimates for Cr(VI) and found to be consistent.

Abbreviations: Cr(VI), Hexavalent chromium; TWA, Time-Weighted Average; FTIR, Fourier Transform Infrared Spectroscopy; ATR, Attenuated Total Reflectance; MMA, Manual Metal Arc; FCAW, Flux Cored Arc welding; MIG/MAG, Metal Inert Gas welding/ Metal Active Gas; SEM, Scanning Electron Microscopy; EDX, Energy Dispersive X-ray spectroscopy; XRD, X-ray Diffraction; ICP-MS, Inductively Coupled Plasma – Mass Spectrometry; IC, Ion Chromatography.

* Corresponding author.
E-mail address: v.krishnan@tees.ac.uk (V.V. Krishnan).

https://doi.org/10.1016/j.jhazmat.2023.130862
Received 16 September 2022; Received in revised form 6 January 2023; Accepted 23 January 2023
Available online 24 January 2023

(b) Investigation into Cr(VI) generation in metal inert gas (MIG), metal active gas (MAG), and flux cored arc welding (FCAW) by varying the oxidation potential of the shielding gas

https://link.springer.com/article/10.1007/s40194-023-01563-x

Welding in the World
https://doi.org/10.1007/s40194-023-01563-x

RESEARCH PAPER

Investigation into Cr(VI) generation in metal inert gas (MIG), metal active gas (MAG), and flux cored arc welding (FCAW) by varying the oxidation potential of the shielding gas

Vishal Vats[1,2] · Geoff Melton[3] · Meez Islam[1] · Venkatesan V. Krishnan[1]

Received: 24 April 2023 / Accepted: 7 July 2023

Abstract

The presence of Cr(VI) in welding fumes classifies them as carcinogens, posing a health risk to welders. Therefore, it is crucial to minimize welders' exposure to Cr(VI) by understanding the role of shielding gases in the generation of Cr(VI) during welding. This article offers valuable insights into the impact of shielding gases' oxygen index on Cr(VI) production in welding fumes and highlights key variables that influence the Cr(VI) generation during welding. The study reveals that the behavior of shielding gases in Cr(VI) production varies between flux-cored arc welding (FCAW) and solid stainless-steel wires, with the oxidation index of the shielding gas playing a significant role in solid stainless-steel wires. Furthermore, the study indicates that the arc stability and ionization potential of shielding gases also affect the amount of Cr(VI) produced. Interestingly, the use of a CO_2 and O_2 mixture with Ar resulted in the lowest formation of Cr(VI). In FCAW, the highest levels of Cr(VI) were observed when argon was used as the shielding gas, primarily due to the presence of Na and K in the wires, which promote the oxidation of Cr(III) to Cr(VI). Conversely, the utilization of oxidizing shielding gases reduces the formation of Cr(VI) as Na and K react with oxygen to form their oxides, thereby reducing the availability of these elements to form chromates and dichromates.

Keywords Shielding gases · Oxidation index · Welding fumes · Cr(VI) · MIG/MAG welding · Arc welding

1 Introduction

Particulates and gases generated during the welding of metals can be hazardous to the health of the welders [1–3]. Hexavalent chromium is one among the many hazardous components generated during the welding of stainless steel [2, 4–7]. Welders, as an occupational group, show an increased risk of developing cancer later in life due to their exposure to hexavalent chromium, in contrast to individuals who are not employed as welders [7–9]. This risk can be reduced significantly if exposure to hexavalent chromium is reduced at the source. Hexavalent Cr and other undesirable components in welding fumes are inadequately controlled simply through local exhaust ventilation or personal respiratory protection because of high costs of implementation, and the burden of individual responsibility placed upon the workers themselves. Welding fumes are usually generated during the welding processes at high temperature by the processes of vaporisation, oxidation and condensation [10–13]. The main contributor to these fumes is the filler material in the welding electrodes which contributes about 90% of the welding fumes [14]. Welding wires used to weld stainless steel (SS) are rich in chromium and when the welding arc strikes, the chromium and alkali elements present in the fluxes of welding wires (in case of FCAW) react with each other to form the alkaline chromates and dichromates such as Na_2CrO_4, K_2CrO_4, $K_2Cr_2O_7$, $NaK_3(CrO_4)_2$ and $NaK_3(Cr_2O_7)_2$ [5, 6, 15, 16].

The above mechanisms have been verified, by usage of FTIR spectroscopy (Fourier transform infrared spectroscopy) [17], which provides a clear detection of chromates and dichromates, whereas ion chromatography (IC) is able

Recommended for publication by Commission VIII-Health, Safety, and Environment

✉ Venkatesan V. Krishnan
v.krishnan@tees.ac.uk

[1] Teesside University, Middlesbrough, UK
[2] NSIRC, Cambridge, UK
[3] TWI, Cambridge, UK

Published online: 16 July 2023

References

1. Khan, M.I., *Welding science and technology*. 2007: New Age International.
2. Hirst, A.A., *Fume formation in flux cored metal inert gas welding*. 1990, University of Bradford.
3. Milner, D., G. Salter, and J. Wilkinson, *Arc characteristics and their significance in welding.* British Welding Journal, 1960. **2**: p. 73-88.
4. Busz, G. and W. Finkelnburg, *Thermische Lichtbögen hoher Temperatur und niedriger Brennspannung.* Zeitschrift für Physik, 1954. **139**(2): p. 212-225.
5. Finkelnburg, W. and H. Maecker, *Electric arcs and thermal plasma*. 1956.
6. Glickstein, S., *Temperature measurements in a free burning arc.* Welding Journal, 1976. **55**(8): p. 222s-229s.
7. Acinger, K., L. Sipek, and E. Smars, *Temperature, Metal Vapour Density, and Energy Balance in an Argon Shielded Welding Arc with Iron Electrodes.* 1970.
8. Howden, D., *Mass transfer of metal vapor and anode temperatures in arc melting.* WELD J, 1969. **48**(3): p. 125.
9. Hultgren, R., et al., *Selected values of the thermodynamic properties of the elements*. 1973, National Standard Reference Data System.
10. Easterling, K., *Introduction to the physical metallurgy of welding*. 2013: Elsevier.
11. Needham, J., *Metal transfer in inert-gas shielded-arc welding*. 1960.
12. Sterjovski, Z., J. Norrish, and B.J. Monaghan, *The effect of voltage and metal transfer mode on particulate fume size during the GMAW of plain carbon steel.* Welding in the World, 2010. **54**(9): p. R249-R256.
13. Dean, G., J. Norrish, and C.D. Cook, *Evaluation of control techniques for dip transfer gas metal arc welding.* 2005.
14. RAPP, R.A., *Kinetics, microstructures and mechanism of internal oxidation-its effect and prevention in high temperature alloy oxidation.* Corrosion, 1965. **21**(12): p. 382-401.
15. Gourd, L., *Principles of welding technology*. 1986: E. Arnold.
16. Haidar, J. and J. Lowke, *Predictions of metal droplet formation in arc welding.* Journal of Physics D: Applied Physics, 1996. **29**(12): p. 2951.
17. Gray, C., P. Hewitt, and R. Hicks, *The prediction of fume compositions in stainless steel metal inert gas welding.* Weld pool chemistry and metallurgy, 1980: p. 197-203.
18. Palani, P. and N. Murugan, *Selection of parameters of pulsed current gas metal arc welding.* Journal of Materials Processing Technology, 2006. **172**(1): p. 1-10.
19. Guidotti, T., V. Lappi, and S. Langard, *Hazards of welding technologies.* Environment and Occupational Medicine, Rom NW (ed) 2nd Edition, Little Brown & Company, London, 1992: p. 831-840.

20. Records, R.E., *Primary care of ocular emergencies: 2. Thermal, chemical, and nontraumatic eye injuries.* Postgraduate Medicine, 1979. **65**(5): p. 157-163.
21. Ham, W.T., H.A. Mueller, and D.H. Sliney, *Retinal sensitivity to damage from short wavelength light.* Nature, 1976. **260**(5547): p. 153-155.
22. Wang, J., *Determination of hexavalent chromium in industrial hygiene samples using ultrasonic extraction and flow injection analysis.* Analyst, 1997. **122**(11): p. 1307-1312.
23. De Gruijl, F. and J. Van der Leun, *Estimate of the wavelength dependency of ultraviolet carcinogenesis in humans and its relevance to the risk assessment of a stratospheric ozone depletion.* Health physics, 1994. **67**(4): p. 319-325.
24. Loukzadeh, Z. and M. Torab Jahromi, *Occupational hazards in welding industry.* Occupational Medicine Quarterly Journal, 2013. **5**(3): p. 95-114.
25. Sullivan Jr, J.B., G.B. Krieger, and R.J. Thomas, *Hazardous materials toxicology: clinical principles of environmental health.* Journal of Occupational and Environmental Medicine, 1992. **34**(4): p. 365-371.
26. Stokinger, H.E., *Evaluation of the Hazards of Ozone and Oxides of Nitrogen. Factors modifying Toxocity.* Arch. Indust. Health, 1957. **15**(3): p. 181-90.
27. Loprieno, N., *International Agency for Research on Cancer (IARC) monographs on the evaluation of carcinogenic risk of chemicals to man:" relevance of data on mutagenicity".* Mutation research, 1975. **31**(3): p. 210.
28. Gibb, H.J., et al., *Lung cancer among workers in chromium chemical production.* American journal of industrial medicine, 2000. **38**(2): p. 115-126.
29. Prevention, H., *Control in the Work Environment: Airborne Dust WHO.* World Health Organization: Geneva, Switzerland, 1999.
30. Jenkins, N. and T. Eagar, *Chemical analysis of welding fume particles.* WELDING JOURNAL-NEW YORK-, 2005. **84**(6): p. 87.
31. Lehnert, M., et al., *Exposure to inhalable, respirable, and ultrafine particles in welding fume.* Annals of occupational hygiene, 2012. **56**(5): p. 557-567.
32. Dasch, J. and J. D'Arcy, *Physical and chemical characterization of airborne particles from welding operations in automotive plants.* Journal of Occupational and Environmental Hygiene, 2008. **5**(7): p. 444-454.
33. Elihn, K. and P. Berg, *Ultrafine particle characteristics in seven industrial plants.* Annals of Occupational Hygiene, 2009. **53**(5): p. 475-484.
34. Brouwer, D.H., J.H. Gijsbers, and M.W. Lurvink, *Personal exposure to ultrafine particles in the workplace: exploring sampling techniques and strategies.* Annals of Occupational Hygiene, 2004. **48**(5): p. 439-453.
35. Stephenson, D., G. Seshadri, and J.M. Veranth, *Workplace exposure to submicron particle mass and number concentrations from manual arc welding of carbon steel.* AIHA Journal, 2003. **64**(4): p. 516-521.

36. Voitkevich, V., *Welding fumes: formation, properties and biological effects*. 1995: Woodhead Publishing Limited.
37. Hewett, P., *Estimation of regional pulmonary deposition and exposure for fumes from SMAW and GMAW mild and stainless steel consumables.* American Industrial Hygiene Association Journal, 1995. **56**(2): p. 136-142.
38. Farrants, G., et al., *Characterization of the morphological properties of welding fume particles by transmission electron microscopy and digital image analysis.* American Industrial Hygiene Association Journal, 1989. **50**(9): p. 473-479.
39. Antonini, J.M., et al., *Pulmonary effects of welding fumes: review of worker and experimental animal studies.* American journal of industrial medicine, 2003. **43**(4): p. 350-360.
40. Faustman, E.M. and G. Omenn, *Risk assessment and the impact of ecogenetics.* Gene-environment Interactions: Fundamentals of Ecogenetics, 2006: p. 427-450.
41. Gordon, T., et al., *Pulmonary effects of inhaled zinc oxide in human subjects, guinea pigs, rats, and rabbits.* American Industrial Hygiene Association journal, 1992. **53**(8): p. 503-509.
42. Meredith, S., V. Taylor, and J. McDonald, *Occupational respiratory disease in the United Kingdom 1989: a report to the British Thoracic Society and the Society of Occupational Medicine by the SWORD project group.* Occupational and Environmental Medicine, 1991. **48**(5): p. 292-298.
43. Ross, D., B. Sallie, and J. McDonald, *SWORD'94: surveillance of work-related and occupational respiratory disease in the UK.* Occupational Medicine, 1995. **45**(4): p. 175-178.
44. Baur, X., P. Degens, and K. Weber, *Occupational obstructive airway diseases in Germany.* American journal of industrial medicine, 1998. **33**(5): p. 454-462.
45. Groth, M. and O. Lyngenbo, *Respiratory symptoms in Danish welders.* Scandinavian journal of social medicine, 1989. **17**(4): p. 271-276.
46. Yamamoto, Y., et al., *Arc-welders' pneumoconiosis with atypical radiological and bronchoalveolar lavage fluid findings: A case report.* Respiratory Medicine Case Reports, 2020. **29**: p. 101023.
47. Ebihara, I., *Lung carcinoma among workers exposed to dust. I. welders.* Journal of Science of Labour, 1988. **64**(12): p. 565-578.
48. Moulin, J.J., et al., *A mortality study among mild steel and stainless steel welders.* Occupational and Environmental Medicine, 1993. **50**(3): p. 234-243.
49. Sjögren, B., *Effects of gases and particles in welding and soldering.* Occupational Medicine. 3rd ed. Chicago, IL: Mosby-Year Book, 1994: p. 917-23.
50. Chromium, I., *nickel, and welding. IARC Monograph on the Evaluation of Carcinogenic Risks to Humans.* World Health Organization: Lyon, France, 1990.

51. Newman, D., *A case of adeno-carcinoma of the left inferior turbinated body and perforration of the nasal septum in the person of a worker in chromate pigment.* Glasgow MJ, 1890. **33**: p. 469.
52. Pfeil, E., *Lung tumors as an occupational disease in chromium plants.* Dtsch Ned Wochenschr, 1935. **61**: p. 1197-200.
53. Teleky, L., *Krebs bei chromarbeitern.* DMW-Deutsche Medizinische Wochenschrift, 1936. **62**(33): p. 1353-1353.
54. Mancuso, T.F., *Chromium as an industrial carcinogen: Part I.* American journal of industrial medicine, 1997. **31**(2): p. 129-139.
55. Mancuso, T.F., *Chromium as an industrial carcinogen: Part II. Chromium in human tissues.* American journal of industrial medicine, 1997. **31**(2): p. 140-147.
56. Hayes, R.B., A. Sheffet, and R. Spirtas, *Cancer mortality among a cohort of chromium pigment workers.* American Journal of Industrial Medicine, 1989. **16**(2): p. 127-133.
57. Sorahan, T., D. Burges, and J. Waterhouse, *A mortality study of nickel/chromium platers.* Occupational and Environmental Medicine, 1987. **44**(4): p. 250-258.
58. ATSDR, S., *Toxicological profile for chromium. Agency for toxic substances and disease registry.* Public Health Service, US Department of Health and Human Services. http://www. atsdr. cdc. gov/toxprofiles/tp. asp, 2012.
59. Hessel, E.V., et al., *Occupational exposure to hexavalent chromium. Part I. Hazard assessment of non-cancer health effects.* Regulatory Toxicology and Pharmacology, 2021. **126**: p. 105048.
60. den Braver-Sewradj, S.P., et al., *Occupational exposure to hexavalent chromium. Part II. Hazard assessment of carcinogenic effects.* Regulatory Toxicology and Pharmacology, 2021. **126**: p. 105045.
61. Brown, K., *Environmental aspects of fume in air and water.* Villepinte: International Institute of Welding Document, 1997: p. 1804-97.
62. Haidar, J., *An analysis of heat transfer and fume production in gas metal arc welding. III.* Journal of Applied Physics, 1999. **85**(7): p. 3448-3459.
63. Simpson, S. and P. Zhu, *Formation of molten droplets at a consumable anode in an electric welding arc.* Journal of Physics D: Applied Physics, 1995. **28**(8): p. 1594.
64. Jenkins, N.T., *Chemistry of airborne particles from metallurgical processing*. 2003, Massachusetts Institute of Technology.
65. Lin, C.-F., W.-T. Tseng, and M.S. Feng, *Formation and characteristics of silicon nanocrystals in plasma-enhanced chemical-vapor-deposited silicon-rich oxide.* Journal of Applied Physics, 2000. **87**(6): p. 2808-2815.
66. Dreizin, E., A. Suslov, and M. Trunov, *General trends in metal particles heterogeneous combustion.* Combustion science and technology, 1993. **90**(1-4): p. 79-99.
67. Gonser, M. and T. Hogan, *Arc welding health effects, fume formation mechanisms, and characterization methods.* Arc welding, 2011: p. 299-320.

68. Carpenter, K.R., B.J. Monaghan, and J. Norrish. *Influence of shielding gas on fume formation rate for gas metal arc welding (GMAW) of plain carbon steel*. in *Proceedings of the 8th international conference trends weld. Res*. 2009.
69. Stepanova, T., et al., *Processes of formation and physical--chemical properties of welding fumes.* Welding international, 2016. **30**(10): p. 786-793.
70. Ashley, K., et al., *Sampling and analysis considerations for the determination of hexavalent chromium in workplace air.* Journal of Environmental Monitoring, 2003. **5**(5): p. 707-716.
71. Dennis, J.H., et al., *Control of exposure to hexavalent chromium and ozone in gas metal arc welding of stainless steels by use of a secondary shield gas.* Annals of Occupational Hygiene, 2002. **46**(1): p. 43-48.
72. Madden, M., *Hexavalent chromium in aerosols evolved during a high temperature metallurgical process*. 1987, University of Bradford.
73. Yoon, C.S., N.W. Paik, and J.H. Kim, *Fume generation and content of total chromium and hexavalent chromium in flux-cored arc welding.* Annals of occupational hygiene, 2003. **47**(8): p. 671-680.
74. Heile, R. and D. Hill, *Particulate fume generation in arc welding processes.* Welding Journal, 1975. **54**(7): p. 201s-210s.
75. Vishnyakov, V., et al., *Effect of shielding gas temperature on the welding fume particle formation: Theoretical model.* Journal of Aerosol Science, 2018. **124**: p. 112-121.
76. Huang, X., et al., *Oxidation behavior of 316L austenitic stainless steel in high temperature air with long-term exposure.* Materials Research Express, 2020. **7**(6): p. 066517.
77. Dennis, J., et al., *Reduction of hexavalent chromium concentration in fumes from metal cored arc welding by addition of reactive metals.* The Annals of Occupational Hygiene, 1996. **40**(3): p. 339-344.
78. Vishnu, B., et al., *Cr6+ reduction in welding fumes by nano composite coatings on stainless steel manual metal arc welding electrodes.* Process Safety and Environmental Protection, 2018. **114**: p. 334-346.
79. Topham, N., et al., *Reducing Cr6+ emissions from gas tungsten arc welding using a silica precursor.* Journal of aerosol science, 2010. **41**(3): p. 326-330.
80. Ferrera, K. and D. Olson, *Performance of the MnO–SiO2–CaO system as a welding flux.* Welding Research Supplement, 1975. **54**: p. 211-215.
81. Sowards, J., et al., *A new chromium-free welding consumable for joining austenitic stainless steels.* Weld J, 2011. **90**: p. 63s-76s.
82. *EN ISO 15011-1 - Health and safety in welding and allied processes — Laboratory method for sampling fume and gases Part 1: Determination of fume emission rate during arc welding and collection of fume for analysis (2009), (Annex A, Design 2)*.
83. Shen, J., et al., *Microstructure and mechanical properties of gas metal arc welded CoCrFeMnNi joints using a 308 stainless steel filler metal.* Scripta Materialia, 2023. **222**: p. 115053.

84. Martin, A.C., J.P. Oliveira, and C. Fink, *Elemental effects on weld cracking susceptibility in AlxCoCrCuyFeNi high-entropy alloy.* Metallurgical and Materials Transactions A, 2020. **51**(2): p. 778-787.
85. Oberdörster, G., et al., *Role of the alveolar macrophage in lung injury: studies with ultrafine particles.* Environmental health perspectives, 1992. **97**: p. 193-199.
86. Hänninen, H., et al., *Internal load of aluminum and the central nervous system function of aluminum welders.* Scandinavian journal of work, environment & health, 1994: p. 279-285.
87. Hedenstedt, A., et al., *Mutagenicity of fume particles from stainless steel welding.* Scandinavian Journal of Work, Environment & Health, 1977: p. 203-211.
88. Mohan, S., et al., *Strategies for controlling welding fumes at the source-A review.* Applied Mechanics and Materials, 2014. **592**: p. 2539-2545.
89. Kirichenko, K.Y., et al., *Characterization of fume particles generated during arc welding with various covered electrodes.* Scientific reports, 2018. **8**(1): p. 1-9.
90. Sowards, J., et al., *Characterization of welding fume from SMAW electrodes-Part I.* WELDING JOURNAL-NEW YORK-, 2008. **87**(4): p. 106.
91. Donaldson, J., *The physiopathologic significance of manganese in brain: its relation to schizophrenia and neurodegenerative disorders.* Neurotoxicology, 1987. **8**(3): p. 451-462.
92. GOLBABAEI, F., et al., *Evaluation of parameters influencing hexavalent chromium mist sampling: a full factorial design.* 2007.
93. Pourbaix, M., *Atlas of electrochemical equilibria in aqueous solution.* NACE, 1974. **307**.
94. Reig, F.B., J.G. Adelantado, and M.M. Moreno, *FTIR quantitative analysis of calcium carbonate (calcite) and silica (quartz) mixtures using the constant ratio method. Application to geological samples.* Talanta, 2002. **58**(4): p. 811-821.
95. Mackie, D.M., et al., *Simple, fast, and accurate methodology for quantitative analysis using Fourier transform infrared spectroscopy, with bio-hybrid fuel cell examples.* MethodsX, 2016. **3**: p. 128-138.
96. Khalaji, A. and M. Ghorbani, *Mn2O3 nanoparticles synthesized from thermal decomposition of manganese (II) Schiff base complexes.* Acta Phys. Pol. A, 2018. **133**: p. 7-9.
97. Rahaman, H., et al., *Fabrication of Mn 2 O 3 nanorods: an efficient catalyst for selective transformation of alcohols to aldehydes.* RSC Advances, 2015. **5**(43): p. 33923-33929.
98. Ashoka, S., et al., *Synthesis and characterisation of microstructural α-Mn2O3 materials.* Journal of Experimental Nanoscience, 2010. **5**(4): p. 285-293.
99. Najjar, R., R. Awad, and A. Abdel-Gaber, *Physical properties of Mn2O3 nanoparticles synthesized by co-precipitation method at different pH*

values. Journal of Superconductivity and Novel Magnetism, 2019. **32**(4): p. 885-892.
100. Pugazhvadivu, K., K. Ramachandran, and K. Tamilarasan, *Synthesis and characterization of cobalt doped manganese oxide nanoparticles by chemical route.* Physics Procedia, 2013. **49**: p. 205-216.
101. Floros, N., *Welding fume main compounds and structure.* Welding in the World, 2018. **62**(2): p. 311-316.
102. Zheng, M., et al., *A simple additive-free approach for the synthesis of uniform manganese monoxide nanorods with large specific surface area.* Nanoscale Research Letters, 2013. **8**(1): p. 1-7.
103. Hoffmann, M.M., J.G. Darab, and J.L. Fulton, *An infrared and X-ray absorption study of the equilibria and structures of chromate, bichromate, and dichromate in ambient aqueous solutions.* The Journal of Physical Chemistry A, 2001. **105**(10): p. 1772-1782.
104. Azeez, H.S. and M.R. Mohammad, *Study the structure, morphology and vibration modes for K2CrO4 and K2Cr2O7.* Al-Nahrain Journal of Science, 2017. **20**(2).
105. Hedberg, Y.S., et al., *Welding fume nanoparticles from solid and flux-cored wires: Solubility, toxicity, and role of fluorides.* Journal of Hazardous Materials, 2021. **413**: p. 125273.
106. Muller, O., W.B. White, and R. Roy, *Infrared spectra of the chromates of magnesium, nickel and cadmium.* Spectrochimica Acta Part A: Molecular Spectroscopy, 1969. **25**(8): p. 1491-1499.
107. Stammreich, H., et al., *The vibrational spectrum of the dichromate ion.* Spectrochimica Acta, 1958. **13**(3): p. 192-196.
108. Rajeswari, V.B., et al., *Effect of substituting fine rutile of the flux with nano TiO2 on the improvement of mass transfer efficiency and the reduction of welding fumes in the stainless steel SMAW electrode.* High Temperature Materials and Processes, 2020. **39**(1): p. 117-123.
109. Mishra, M., *Fourier transform infrared spectrophotometry studies of chromium trioxide-phthalic acid complexes.* Chemical Science Transactions, 2016. **5**(3): p. 770-774.
110. Weckhuysen, B.M., I.E. Wachs, and R.A. Schoonheydt, *Surface chemistry and spectroscopy of chromium in inorganic oxides.* Chemical Reviews, 1996. **96**(8): p. 3327-3350.
111. Hill, W. and G. Öhlmann, *Thermal decomposition of chromium (VI)-oxide supported on silica.* Reaction Kinetics and Catalysis Letters, 1989. **38**(2): p. 289-294.
112. Datar, D. and S. Jatkar, *REACTIONS OF CHROMATES AT HIGH TEMPERATURES PART IX. THERMAL DECOMPOSITION OF CHROMIUM TRIOXIDE.* Journal of the Indian Institute of Science, 1939. **22**: p. 119.
113. Vats, V. and A. Singhal, *Effect of Ru substitution in La0. 85Sr0. 15CoO3 towards oxygen evolution reaction: Activity of ionic Ru.* Electroanalysis, 2021. **33**(3): p. 618-626.

114. Saravanan, S. and R. Dubey, *Synthesis of SiO2 nanoparticles by sol-gel method and their optical and structural properties.* Rom. J. Inf. Sci. Technol, 2020. **23**: p. 105-112.
115. Shokri, B., M.A. Firouzjah, and S.I. Hosseini. *FTIR analysis of silicon dioxide thin film deposited by metal organic-based PECVD*. in *Proceedings of 19th international symposium on plasma chemistry society*. 2009.
116. Correcher, V., et al., *Study of the thermoluminescence emission of a natural α-cristobalite.* Radiation Effects & Defects in Solids, 2009. **164**(1): p. 59-67.
117. Rajendran, S., *Influence of potassium dichromate-Zn2+ system on corrosion inhibition of rebar steel in simulated concrete pore solution.* JOURNAL OF ADVANCED APPLIED SCIENTIFIC RESEARCH, 2017. **1**(9).
118. Mayerhöfer, T.G., et al., *Consolidated silica glass from nanoparticles.* Journal of Solid State Chemistry, 2008. **181**(9): p. 2442-2447.
119. Mylarappa, M., et al. *A facile hydrothermal recovery of nano sealed MnO2 particle from waste batteries: An advanced material for electrochemical and environmental applications*. in *IOP Conference Series: Materials Science and Engineering*. 2016. IOP Publishing.
120. Vargas, M.A., J.E. Diosa, and E. Mosquera, *Data on study of hematite nanoparticles obtained from Iron (III) oxide by the Pechini method.* Data in brief, 2019. **25**: p. 104183.
121. Hwang, S., et al., *Synthesis and characterization of iron oxide nanoparticles for phenyl hydrazine sensor applications.* Sensor Letters, 2014. **12**(1): p. 97-101.
122. Ansari, M.S., et al., *Kinetic studies on the catalytic degradation of rhodamine b by hydrogen peroxide: Effect of surfactant coated and non-coated iron (III) oxide nanoparticles.* Polymers, 2020. **12**(10): p. 2246.
123. Alrehaily, L., et al., *Gamma-radiation induced formation of chromium oxide nanoparticles from dissolved dichromate.* Physical Chemistry Chemical Physics, 2013. **15**(1): p. 98-107.
124. Jaswal, V.S., et al., *Synthesis and characterization of chromium oxide nanoparticles.* Orient J Chem, 2014. **30**: p. 559-566.
125. Pesch, B., et al., *Exposure to hexavalent chromium in welders: Results of the WELDOX II field study.* Annals of Work Exposures and Health, 2018. **62**(3): p. 351-361.
126. Keane, M., et al., *Hexavalent chromium content in stainless steel welding fumes is dependent on the welding process and shield gas type.* Journal of Environmental Monitoring, 2009. **11**(2): p. 418-424.
127. Gomes, J.F.P., et al., *Determination of airborne nanoparticles from welding operations.* Journal of Toxicology and Environmental Health, Part A, 2012. **75**(13-15): p. 747-755.
128. Jenkins, N., W. Pierce, and T. Eagar, *Particle size distribution of gas metal and flux cored arc welding fumes.* Welding J, 2005. **84**(10): p. 156-163.

129. Gomes, J.F., et al., *Comparison of deposited surface area of airborne ultrafine particles generated from two welding processes.* Inhalation toxicology, 2012. **24**(11): p. 774-781.
130. Joni, I., L. Nulhakim, and C. Panatarani. *Characteristics of TiO2 particles prepared by simple solution method using TiCl3 precursor*. in *Journal of Physics: Conference Series*. 2018. IOP Publishing.
131. Xu, Y., et al., *Adsorptive stripping voltammetry determination of hexavalent chromium by a pyridine functionalized gold nanoparticles/three-dimensional graphene electrode.* Microchemical Journal, 2019. **149**: p. 104022.
132. Ramírez, M.L., et al., *Cysteine functionalized bio-nanomaterial for the affinity sensing of Pb (II) as an indicator of environmental damage.* Microchemical Journal, 2018. **141**: p. 271-278.
133. Bagheri, H., A.A. Asgharinezhad, and H. Ebrahimzadeh, *Determination of trace amounts of Cd (II), Cu (II), and Ni (II) in food samples using a novel functionalized magnetic nanosorbent.* Food Analytical Methods, 2016. **9**(4): p. 876-888.
134. Elgrishi, N., et al., *A practical beginner's guide to cyclic voltammetry.* Journal of chemical education, 2018. **95**(2): p. 197-206.
135. Yamada, H., et al., *Cyclic Voltammetry Part 1: Fundamentals.* Electrochemistry, 2022. **90**(10): p. 102005-102005.
136. Joshi, P. and D. Sutrave, *A brief study of cyclic voltammetry and electrochemical analysis.* International Journal of ChemTech Research, 2018. **11**(9): p. 77.
137. Velasco, G., et al., *The electrochemical reduction of Cr (VI) ions in acid solution at titanium and graphite electrodes.* Journal of environmental chemical engineering, 2016. **4**(3): p. 3610-3617.
138. Owlad, M., et al., *Removal of hexavalent chromium-contaminated water and wastewater: a review.* Water, air, and soil pollution, 2009. **200**(1): p. 59-77.
139. Rodriguez-Valadez, F., et al., *Electroreduction of Cr (VI) to Cr (III) on reticulated vitreous carbon electrodes in a parallel-plate reactor with recirculation.* Environmental science & technology, 2005. **39**(6): p. 1875-1879.
140. Lingane, J.J. and I. Kolthoff, *Polarographic study of the reduction of chromate ion at the dropping mercury electrode.* Journal of the American Chemical Society, 1940. **62**(4): p. 852-858.
141. Mvola, B. and P. Kah, *Effects of shielding gas control: welded joint properties in GMAW process optimization.* The International Journal of Advanced Manufacturing Technology, 2017. **88**(9): p. 2369-2387.
142. Shanping, L., F. Hidetoshi, and N. Kiyoshi, *Effects of CO2 shielding gas additions and welding speed on GTA weld shape.* Journal of materials science, 2005. **40**(9): p. 2481-2485.
143. Tanaka, M., et al., *Influence of shielding gas composition on arc properties in TIG welding.* Science and technology of welding and joining, 2008. **13**(3): p. 225-231.

144. Cena, L.G., et al., *Size distribution and estimated respiratory deposition of total chromium, hexavalent chromium, manganese, and nickel in gas metal arc welding fume aerosols.* Aerosol Science and Technology, 2014. **48**(12): p. 1254-1263.
145. McQueen, C., *Comprehensive toxicology*. 2017: Elsevier.
146. Smith, K., *Fundamentals of Momentum, Heat and Mass Transfer. By JR WELTY, CE WICKS and RE WILSON. Wiley, 1976. 789 pp. 50.00.* Journal of Fluid Mechanics, 1978. **89**(4): p. 793-794.
147. HALMOY, E., *Wire melting rate, droplet temperature and effective anode melting potential.* 1980.